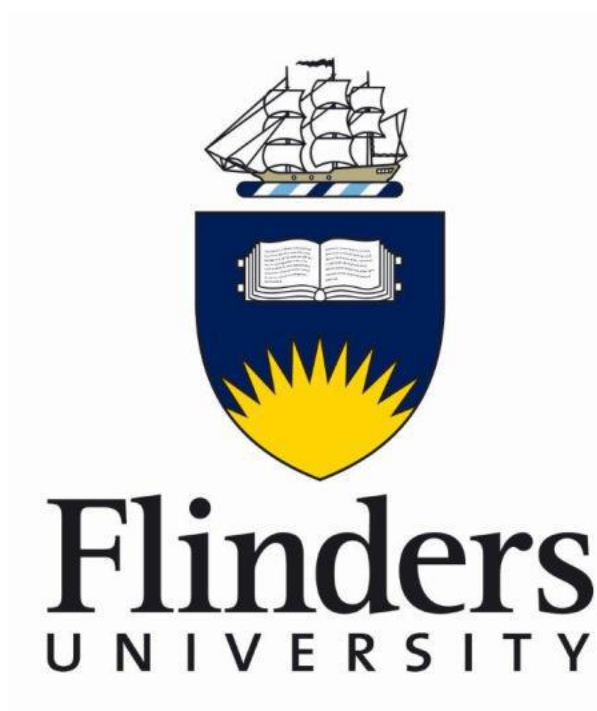# Investigating the Surface Structure of Liquids Containing Ionic Species

Christiaan Ridings

Thesis submitted to the School of Chemical and Physical Sciences,

Faculty of Science and Engineering

Flinders University

in fulfilment of the requirements for the degree of

Doctor of Philosophy

October 2014

Table of contents

Abstract

In this work liquid systems containing ionic species are investigated in order to further understand the forces that govern the surface structure of liquids. The distribution of ions along the surface normal, or charge distribution, is especially important in foam films (such as soap bubbles) where the electrostatic forces generated from the separation of charges at the liquid/air interfaces play a pivotal role in stopping the film from collapsing.

Many powerful techniques for investigating surfaces require the samples to be measured under ultra-high vacuum. The volatile nature of liquids makes their use in these instruments difficult, especially so in the case of foam films which are already in a fragile, metastable state. Specialised equipment and experimental techniques are developed for the investigation of foam films under vacuum. A glass film holder is used to generate and hold the film. This film holder is held inside an enclosed cell designed to minimise the evaporation of solvent from the film and aid film stability. Variations to the setup are designed and tested which allow for greater stability of the foam film, along with the means to measure the films under altering conditions.

Foam films of a cationic surfactant, hexadecyltrimethylphosphonium bromide, were investigated. A range of measurements were performed that demonstrated the thinning, and consequential surface rearrangement, of the foam film over time. These results also indicated a decrease in the surface potential upon foam film formation, partially owing to the reorientation of surfactant molecules at the surface.

Foam films containing a non-ionic surfactant, dodecyldimethyl phosphine oxide, were also investigated using the above technique. These films were studied with no added electrolyte as well as added salts, where the anion was varied. Comparing the concentration depth profiles of the foam films to the corresponding bulk liquid surfaces for the various systems studied allowed for the determination as to how the liquid surface changes upon foam film formation. It was found that the addition of salt increased the surfactant adsorption at the surface of both the foam film and bulk liquid. Additionally, it was seen that while iodide was detected as a surface excess at the bulk liquid, chloride was not. Both are detected as a surface excess at the foam film surface.

Surfaces of ionic liquids were also investigated, as they represent a unique situation of a liquid being comprised totally of charged species. Thus, the charge distribution is not mediated by an additional species, as is the case with aqueous solutions. The effect of small amounts of water as a surface impurity in $[C_6mim][Cl]$ was investigated. Increasing the water content lead to an increase in the amount of anion adsorbed at the surface, indicating how forces other than the electrostatic interaction between ions governs surface structure. It was seen that for both protic and aprotic ionic liquids that the cation aliphatic chain length had a significant influence on the surface structure. Increasing the chain length caused increased adsorption of the cation, with subsequent cation reorientation at the surface.

Declaration

I certify that this thesis does not incorporate without acknowledgement any material previously submitted for a degree or diploma in any university; and that to the best of my knowledge and belief it does not contain any material previously published or written by another person except where due reference is made in the text.

_____

Christiaan Ridings

Acknowledgements

This thesis, and the entire journey of my PhD, would not have been possible without many different people.

Firstly, I would like to deeply thank my supervisor, Gunther Andersson. Having worked in his group for the last 5 and a half years, I have become enormously grateful for the opportunity to learn from such a dedicated professional, and work alongside a truly good person. Gunther has always provided me with advice, encouragement, and enthusiasm which gave me faith in my abilities that I might not otherwise have had. His ability to be so professional and so personable at the same time is outstanding.

I would like to thank the awesome people around Flinders University who have made this time both informative and enjoyable. My research group in particular has been a highlight: Anirudh Sharma, Natalya Schmerl, Alex Sibley, Ben Chambers, Herri Trilaksana, and Rantej Kler, along with others who have drifted through over the years. Other academics around the university, Prof. Joe Shapter, Prof. Jamie Quinton, Prof. David Lewis, Dr. Chris Gibson, have been a great source of advice over the years, even with matters not related to this project. I would like to specifically thank Assoc. Prof. Martin Johnston as his knowledge of organic chemistry and all things related has been a huge help to me. Thanks also to the other PhD students who have made this time what it is: Daniel Gruszecki, Daniel Mangos, Daniel Tune, Sam Ogden. I would like to specifically thank my office mate, Ashley Slattery. Working in different groups on completely different projects has given me a wider outlook on science, and it has been great to chat about all things over the years.

The Technical Services Unit at the university have been invaluable throughout my project. They have provided countless hours of assistance for maintenance as well as unit design and construction for the various little projects and ideas I've had over the years. Thanks to Bill Drury, Chris Price, Andrew Dunn, and Mark Ellis. In particular thanks to Wayne Peacock and Bob Northeast who I ended up bugging for help the most, but have also been great to chat to over the last few years.

List of publications

Peer-reviewed journals

[1]   Ridings, C. & Andersson, G. Determining concentration depth profiles of thin foam films with neutral impact collision ion scattering spectroscopy. *Review of Scientific Instruments* **81**, 113907-113915 (2010).

[2]   Ridings, C., Lockett, V. & Andersson, G. Effect of the aliphatic chain length on electrical double layer formation at the liquid/vacuum interface in the $[C_n mim][BF4]$ ionic liquid series. *Physical Chemistry Chemical Physics* **13**, 17177-17184 (2011).

[3]   Ridings, C., Lockett, V. & Andersson, G. Significant changes of the charge distribution at the surface of an ionic liquid due to the presence of small amounts of water. *Physical Chemistry Chemical Physics* **13**, 21301-21307 (2011).

[4]   Wakeham, D., Niga, P., Ridings, C., Andersson, G., Nelson, A., Warr, G., Baldelli, S., Rutland, M., Atkin, R. Surface structure of a "non-amphiphilic" protic ionic liquid. *Physical Chemistry Chemical Physics* **14**, 5106-5114 (2012).

[5]   Ridings, C., Lockett, V. & Andersson, G. Comparing the charge distribution along the surface normal in the [C6mim]+ ionic liquid with different anions. *Colloids and Surfaces A: Physicochemical and Engineering Aspects* **413**, 149-153 (2012).

[6]   Ridings, C., Warr, G. G. & Andersson, G. G. Composition of the outermost layer and concentration depth profiles of ammonium nitrate ionic liquid surfaces. *Physical Chemistry Chemical Physics* **14**, 16088-16095 (2012).

[7]   Andersson, G. & Ridings, C. Ion Scattering Studies of Molecular Structure at Liquid Surfaces with Applications in Industrial and Biological Systems. *Chemical Reviews* **114**, 8361-8387 (2014).

[8]   Ridings, C. & Andersson, G. G. Deconvolution of NICISS profiles involving elements of similar masses. *Nuclear Instruments and Methods in Physics Research Section B: Beam Interactions with Materials and Atoms* **340**, 63-66 (2014).

[9]   Ridings, C., Stubenrauch, C. & Andersson, G. Effect of Sodium Halides on the Surface Structure of Foam Films Stabilized by a Nonionic Surfactant. *The Journal of Physical Chemistry C* **119**, 441-448 (2014).

[10]   Ridings, C. & Andersson, G. Change of Surface Structure upon Foam Film Formation. *ChemPhysChem* **Accepted for publication** (2014). DOI: 10.1002/cphc.201402821R1

Book chapters

Ridings, C. & Andersson, G. in Innovations in Nanomaterials, **Under review,** (Nova Science Publishers, Inc., 2014).

List of figures

List of tables

Abbreviations

Abbreviations	
AIL	Aprotic ionic liquid
CBF	Common black film
cmc	Critical micelle concentration
DLVO (theory)	Derjaguin Landau Verwey Overbeek (theory)
DRS	Direct recoil spectroscopy
EDL	Electrical double layer
FPDT	Foam pressure drop technique
FWHM	Full-width half-maximum
HOMO	Highest occupied molecular orbital
IL	Ionic liquid
IMFP	Inelastic mean free path
ISS	Ion scattering spectroscopy
LEIS	Low energy ion scattering
MD	Molecular dynamics
MIES	Metastable induced electron spectroscopy
MO	Molecular orbital
NBF	Newton black film
NICISS	Neutral impact collision ion scattering spectroscopy
NLO	Non-linear optical
NMR (spectroscopy)	Nuclear magnetic resonance (spectroscopy)
NR	Neutron reflectivity
PIL	Protic ionic liquid
QMS	Quadrupole mass spectrometer
RBS	Rutherford backscattering spectroscopy

RTIL	Room temperature ionic liquid
SFA	Surface force apparatus
SFG	Sum frequency generation vibrational spectroscopy
TFPB	Thin film pressure balance
TOF	Time of flight
UHV	Ultra high vacuum
UPS	Ultraviolet photoelectron spectroscopy
VSFS	Vibrational sum frequency spectroscopy
XPS	X-ray photoelectron spectroscopy
XR	X-ray reflectivity

Frequently discussed chemical abbreviations

C_nTAB	(alkyl)trimethylammonium bromide
C_nTPB	(alkyl)trimethylphosphonium bromide
$C_{12}DMPO$	(alkyl)dimethylphosphine oxide
$[C_nmim]^+$	1-(alkyl)-3-methylimidazolium$^+$
$[BF_4]^-$	tetrafluoroborate$^-$
POPC	1-palmitoyl-2-oleoylphosphatidylcholine
EAN	ethylammonium nitrate
PAN	propylammonium nitrate
EtAN	ethanolammonium nitrate

Contextual Statement

This thesis presents the investigations into the surface structure of liquids containing ionic species as performed as part of the author's PhD project. It also contains some grounding work from the author's preceding Honours project that directly flows onto the PhD project, which justifies its inclusion.

The Introduction chapter contains a literature review of the current field directly concerning the project, while the Experimental chapter contains the experimental details of the project, along with a discussion of the experimental methods used as part of the project. Given that such a large portion of the project was involving the NICISS technique, a particularly in-depth discussion and review of the method is given in that chapter.

The results chapters 3 – 7 are reformatted versions of the published peer-reviewed papers of the same title, while chapters 8 and 9 are reformatted versions of papers either under review or sent to journals for review.

The author of this thesis was the primary author of all papers used as results chapters. All experimental work was completed by the author. Exceptions involve: Dr. V. Lockett who carried out the Karl Fisher titration to determine the water content in the aprotic ILs; and Dr. E. Carey who performed TFPB measurements (in addition to those completed by the author) in order to test data reproducibility. The author also completed all data evaluation, but acknowledges the input of the respective co-authors in the final interpretation of results.

Chapter 1

Introduction

1.1   Overview

Understanding the structure and interactions of molecules at liquid surfaces is vital to understanding a vast role of processes. For example, it is now understood that the uptake of gasses in liquids is influenced by reactions at the air/water interface.[1] These reactions take place readily in water aerosols due to their high surface-to-volume ratio. This has direct impact on atmospheric chemistry given that these gas reactions take place in seawater aerosols (tiny droplets kicked from the ocean due to waves) that make their way into the atmosphere.[2,3] Additionally, there are new studies to show that the origins of life on Earth may have come about due to reactions only possible at the air/water interface, rather than in the bulk of water.[4] Part of the reason for this lies in the fact that amino acids need to be in a specific orientation relative to one another in order for peptide bond formation to occur. Amino acids have random orientations in the bulk of water, but take on a specific orientation at the air/water interface, which increases the probability of peptide bond formation.[5,6] However, the interest in liquid surfaces is not simply limited to reactions at the air/water interface. The properties of a liquid surface depend on the opposing phase: liquid, gas, or solid. Understanding the interactions at the solid/liquid interface is important in understanding the spreading of liquids over solid surfaces and the movement of liquids through capillaries,[7] while further understanding has led to the design of solid substrates that can switch between hydrophobic and hydrophilic surfaces under certain stimuli.[8] Surfactants are amphiphilic molecules whose name derives from their use as 'surface active agents'. Their amphiphilic nature allows them to adsorb at liquid interfaces and lower the interfacial tension, hence increasing the stability of the interface.[9] Surfactants are therefore widely used in the stabilisation of foams (liquid/air system) and emulsions (liquid/liquid system), and thorough understanding of these systems has led to applications such as switchable surfactants that can act as an emulsifier stabilising an oil/water emulsion, then change to a demulsifier to destabilise the emulsion under certain

conditions.[10] These systems could be useful in aiding oil recovery from oceans, where the emulsions can then be efficiently broken down after recovery.[11]

The case of ions at the liquid/vapour interface provides a particularly interesting field. The tendency for one type of ion to adsorb at the liquid surface over another type of ion leads to the separation of charges at the liquid/vapour interface. Additionally, the preference of some ions to be adsorbed at the liquid/vapour interface leads to them being present as a surface excess compared to normal bulk levels. This enhanced concentration of charges near the surface changes how the otherwise pure liquid surfaces would interact. This can be seen in the electrolyte dependent thickness of foam films,[12] or the ability of electrolyte to inhibit the coalescence of air bubbles in water.[13]

1.2   Liquid surfaces

Knowledge of the structure of liquid interfaces has been developed substantially over the past few decades. The traditional view of the salty air/water solution interfaces held that ions were depleted at the surface, followed by a monotonic increase to bulk concentrations, which was inferred from macroscopic property measurements.[14-16] Advancements in surface sensitive experimental techniques, along with the development of theoretical tools such as molecular dynamics simulations, have shed light on this topic to reveal the traditional view was not entirely accurate. Electrical charges at liquid interfaces are particularly influential on the physical chemistry of colloidal systems. The resulting forces play important roles in the formation of clays, the stability of nanoparticles, and the interaction of biological membranes.

1.2.1   Surface structure in liquids

Surface energy and surface tension

The existence of surface phenomena in liquids are often the result of the energy difference of molecules at the surface compared to those in the bulk. This can be conceptualised by considering the interactions of a particle in the bulk, surrounded by a sphere of neighbours. The energy per particle of type A, E_A, in a given phase can be expressed as the product of the interaction potential, v, between the particles and the number density of these particles in the shell of nearest neighbours, which can be given by:[9]

$$E_A \approx \frac{1}{2} z_{AA} v_{AA}(r)$$

Eq. 1-1

where z is the number of particles in the shell of nearest neighbours and r is the average distance of these particles from the central particle. Given that $z_{surface} \approx \frac{1}{2} z_{bulk}$ and that v is negative,[9] Eq. 1-1 shows that work needs to be done when moving a molecule from the bulk to the surface. This simplified example indicates that the interactions at the surface of a phase will be different from the bulk, and furthermore, that an increased surface energy (compared to the bulk) will lead to the system acting to minimise this energy. In the case of a simple, pure liquid this can lead to the system minimising its surface area, which is seen in the curved surfaces of water droplets. The surface energy for a pure liquid is equivalent to the surface tension.[9] Surface tensions are well known for a wide range of pure liquids and given the high degree of precision in most readily available lab-based setups, surface tension is often used as a means of determining the presence of surface active impurities.[11] Additionally, given that surface tension versus concentration curves are often unique to individual solutions, surface tension measurements are often used as a way of determining the purity of solutes, where a minimum in the curve indicates the presence of an impurity.[17]

The question arises as to what exact region the surface tension refers to. In order to understand this, Kirmse and Morgner investigate the surface of binary liquid mixtures using the perfectly surface sensitive technique, metastable induced electron spectroscopy.[18] Their technique probes the molecular orbitals of molecules at exclusively the outermost layer. The resulting spectrum can then be broken down into a linear combination of the spectra of both pure components, where the factor coefficients can be directly interpreted as the fraction of the surface covered by the respective species. Their study came up with two remarkable results: Firstly, that the outermost layer is solely responsible for the surface tension, and secondly that the systems studied could be separated into two categories: 1) binary mixtures where the surface tension was linearly dependent on surface fraction to high accuracy, and 2) surface tension being piecewise linearly dependent on surface fraction. The first result leads to the conclusion that the surface tension of a binary mixture is the sum of the surface tensions of the pure components weighted by the fraction of the surface covered by the respective components

$$\sigma = \sigma_A \alpha_A + \sigma_B \alpha_B \qquad \text{Eq. 1-2}$$

where σ is the surface tension, and α is the fraction of surface occupied by components A and B as denoted in subscript. This relation has also been seen in gas uptake experiments.[19] The second result is less obvious, but Kirmse and Morgner offer the explanation that phase separation at the surface could account for the piecewise linear relationship in an otherwise fully miscible system. Additionally, the difference in surface tension of the pure components for the mixtures that fall into the first category are less than 10 mN/m, while the mixtures in the second category have surface tension difference around 20 mN/m.

Surface excess and Gibbs dividing plane

Liquid surfaces are able to lower their surface energy though the adsorption of other species, which can lead to the adsorbed species being present at the surface in larger amounts than in the bulk. This species is then said to be present as a surface excess, which can be described quantitatively using the Gibbs dividing plane. In the idealised model of two bulk phases (α and β) in contact, the 'surface phase' separating the bulk phases has a thickness of zero. However, in real systems it is known that this surface phase has a finite thickness over which the concentration of components varies from the bulk concentration of α to the bulk concentration of β. In this case, it is possible to arbitrarily choose a dividing plane whereby the excess (or deficiency) in concentration of a component relative to its value in a bulk phase can be defined. The surface excess, Γ_i, is the amount per area of the component, i, in the surface area and is given by[20]

$$\Gamma_j x_i - \Gamma_i x_j = \text{constant} \qquad \text{Eq. 1-3}$$

where x is the mole fraction of the components i and j, and the constant gives that the sum is independent of the choice of dividing plane. Figure 1-1 gives a schematic illustration of the Gibbs dividing plane concept as adapted from Adamson in the case of varying density across the depth range.[20]
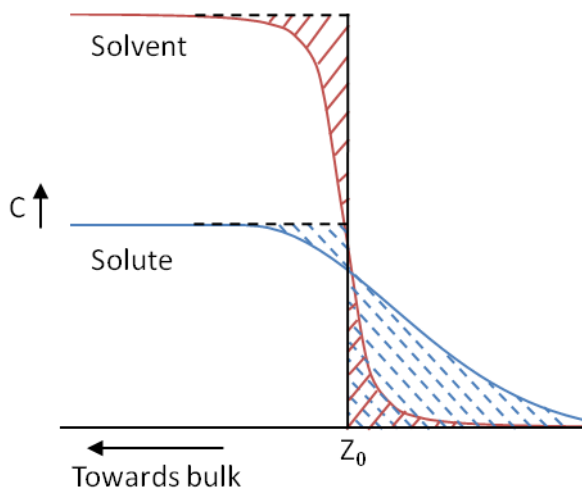
Figure 1-1. Schematic illustration of the Gibbs dividing plane as adapted from Adamson.[20] The dividing plane is chosen such that $\Gamma_{solvent}$ is equal to zero. For the solute (blue), the area to the right of the plane minus the area to the left gives a positive area, indicating a surface excess of solute.

The relationship between the chemical potential, μ, the surface tension, γ, and the surface excess is given via the Gibbs equation, which is derived by setting the excess of one component to zero in Eq. 1-3.[20]

$$\mathrm{d}\gamma = -\sum_{i=1}^{n} \Gamma_i \mu_i \qquad \textbf{Eq. 1-4}$$

Measuring the surface tension is a relatively straightforward process due to the array of techniques available. Hence knowing one of the chemical potential or surface excess will allow for the direct determination of the other quantity.

1.2.2 Surface charge of liquids

This section explains the presence and consequences of charges at liquid interfaces, in particular along the lines of the electrical double layer model. Even though the electrical double layer model was originally conceptualised through the development of statistical thermodynamics, the exact mathematical origins is beyond the scope of this thesis and as such will be approached as a conceptual model first, with a subsequent section describing the basic mathematical background.

Electrical double layer

Charging of a liquid surface can happen in two main ways[21]:

i. The ionization or dissociation of the liquid, such as the autodissociation of water into OH^- and H^+/H_3O^+

ii. The adsorption of ions from the bulk onto the (previously uncharged) surface, such as the binding of cations to zwitterionic headgroups of lipid bilayers, or the adsorption of ionic surfactants to the liquid surface.

The electrical double layer is a model that is used to describe the charge distribution in colloidal systems. It must be noted that as a model, the electrical double layer starts with the precursor of a charged interface and does not itself describe the phenomenon of surface charging (e.g. the chemical attraction of ions to an interface). The main principle of this model is that, regardless of the charging mechanism, the surface charge is balanced by the formation of a region containing oppositely charged counterions which are either bound to the surface or exist in a diffuse layer spanning away from the surface towards the bulk. This results in the so-called 'electrical double layer', which describes the charge separation in the surface-near region of liquids. The length of this region is dependent on the concentration of ions in solution, with increasing concentration leading to an increased 'screening' of charges and more compressed electrical double layers.[9,21] This characteristic length is known as the Debye length, κ_D^{-1} and is given by[22]

$$\kappa_D^{-1} = \sqrt{\frac{\varepsilon k T}{8\pi n^0 e^2}} \approx C^{-\frac{1}{2}} \qquad \textbf{Eq. 1-5}$$

where ε is the dielectric constant of the solvent, k is Boltzmann's constant, T is temperature, n^0 is the number density of ions in the bulk, e is the elementary charge, and C is the molar concentration of electrolyte. The extent of the double layer is gauged by the size of κ_D^{-1} where the region of variable potential in typical solutions is of the order of a few multiples of κ_D^{-1}, which is generally in the nanometre length range.[9] When the separation between two charged interfaces becomes less than the sum of the respective Debye lengths a net electrostatic potential arises which acts to repel the two interfaces.[22] Electrical double layers have been directly observed experimentally in a number of different systems, however quantitative measurements are still somewhat lacking.[23-26] In

the case of Lockett et al. angle-resolved and synchrotron x-ray photoelectron spectroscopy was used to investigate the surface of aprotic ionic liquids.[23] Their results show that there is an uneven distribution of cation and anion along the surface normal, however were not able to determine the exact depth range due to the unknown electron inelastic mean free path in the sample. Therefore while this was able to show the existence of the double layer, the exact structure was undetermined.

While the magnitude of the surface charge can be estimated with techniques such as the surface force apparatus (applying DLVO theory), it is determining the sign of the surface charge that can prove troublesome. In the case of electrolyte solutions, the surface charge can be inferred indirectly via techniques such as surface tension measurements. However one subject that is still a topic of debate is the sign of the surface charge at the bare water/air interface.[27-29] Molecular dynamics simulations have been carried out which observe the adsorption of hydrated protons to the surface,[27,30] which is also seen in non-linear optical experiments.[31] This is in disagreement with previously performed ζ-potential investigations as to the isoelectric point of air bubbles in pure water, which indicate that the bubbles only gain a positive charge at a pH of less than 4.[32-34] Additionally, von Klitzing et al. have performed investigations onto pure water wetting films, that have shown that the addition of negatively charged polyelectrolyte stabilises water films, with the opposite observed for positively charged polyelectrolyte.[35,36] Even though these studies do not directly observe any structure at the air/water interface they strongly promote the idea that the air/water interface is negatively charged.

Poisson-Boltzmann equation

Taking into account the thermodynamic equilibrium requirement that the chemical potential must be uniform throughout a solution, the Boltzmann distribution of counterions in the solution is given by[21]

$$\rho = \rho_0 e^{-\frac{ze\psi}{kT}} \qquad \text{Eq. 1-6}$$

where ρ is the number density of ions of valency z, and ψ is the electrostatic potential. In this case ρ_0 is the density at the midplane. The net excess charge density at a given point, x, is given by Poisson's equation:[21]

$$\frac{d^2\psi}{dx^2} = -\frac{ze\rho}{\varepsilon\varepsilon_0}$$

Eq. 1-7

Combining these two equations gives the Poisson-Boltzmann equation:

$$\frac{d^2\psi}{dx^2} = -\left(\frac{ze\rho_0}{\varepsilon\varepsilon_0}\right)\exp^{-\frac{ze\psi}{kT}}$$

Eq. 1-8

Various treatments for the Poisson-Bolztmann equation exist which describe the electrical double layer in terms of different regions,[37] however one of the best known treatments is that owing to Debye and Hückel. In the case that the exponent in Eq. 1-8 is much less than unity, the exponentials can be expanded to obtain the approximate form of the Debye-Hückel equation which gives the mathematical origins of the Debye length:[21,37]

$$\psi_x \approx \psi_0 \exp^{-\kappa_D x}$$

Eq. 1-9

Attard reviews some advancements in applying Poisson-Boltzmann theory to colloidal systems, noting the shortcomings in various treatments as well as extending theories.[38] In particular the need to correct for image charges, and the fact that continuum theories break down under small separation lengths (below a few nm) present shortcomings of this approach.[39-41] Interactions between ions and the solvent have been seen to play an important role in the electrical double layer formation, which is not treated by the 'classical' Poisson-Boltzmann theory.[42,43] It is known that ion correlation forces, i.e. the attractive interaction of electric layers, cause the ions to experience an increased pressure in the bulk, which results in an increased adsorption of the ions to the surface. This leads to an increased screening of the surface charge compared to what is predicted by the mean field Poisson-Boltzmann approximation, which neglects these ion correlation forces.[44] Additionally, Attard points out that fitting experimental data with Poisson-Boltzmann theory only gives the effective surface charge, and that relating this to the actual surface charge is not a trivial issue due to the uncertainties in the experimental procedures.[38] The surface charge can be determined by charge titration, while the surface potential is usually obtained using electrokinetic techniques such as streaming potential measurements.[44] Charge titration can be inexact when surface areas of the colloid are not well defined as well as the uncertainty in knowing where the charges are located, while the effect of counter-ion binding can also lead to underestimating the surface charge.[44,45]

1.2.3   DLVO theory

In the 1940s Derjaguin and Landau, and Verwey and Overbeek developed a theory for treating surface interactions in colloidal systems, which has gone on to be known as DLVO theory.[46,47] This theory combines the attractive van der Waals forces and repulsive electrical double layer repulsion to explain the stability and interaction of colloidal bodies/interfaces with separations on the order of a few to around 100 nanometres.

DLVO theory runs on the assumptions of treating ions as point charges, and treating the solvent as a continuum field with a dielectric constant.[21] DLVO theory accurately models systems that it was originally designed to describe, dilute symmetrical electrolyte solutions, but breaks down outside of these parameters where atomic and molecular interactions begin to have a more significant effect.[48] The treatment of ions as point charges has two main limitations in that it ignores the finite size of the ions, and also ignores the chemical nature of the ions. The latter problem is addressed in more detail in section 1.2.4, while the former problem is addressed somewhat in the Stern model of the double layer.[21] DLVO theory is also limited by its overly-simplified description of the solvent as a continuum with uniform dielectric profile. This description ignores the chemical nature of the solvent and thus does not describe the effect of ion solvation or the structure of the solvent at interfaces.[49]

Electrical double layer forces

The electrical double layer repulsive forces can be gained by solving the Poisson-Boltzmann equation. As a non-linear second order differential equation, the Poisson-Boltzmann equation can be solved by invoking two of a range of boundary conditions, which typically involve the assumption of relatively small surface charges.[22] The osmotic pressure exerted by the overlap of electrical double layers is given by[21]

$$\Pi_{\mathrm{elec}} = kT(n_+ + n_- - 2n^0)$$

Eq. 1-10

where n_+ and n_- are the concentration of the cation and anion in the midplane of the system, and n^0 is the bulk concentration of ions. In the case that the ion concentration profiles are not known, they can be modelled with the Boltzmann distribution to give[21]

$$\Pi_{\mathrm{elec}} = kT2n^0 \left[\cosh\left(\frac{ze\varphi_m}{kT}\right) - 1 \right]$$

Eq. 1-11

where φ_m is the midplane potential. This can then be solved in the case of constant surface charge, or more commonly constant surface potential, where the latter model can be further simplified under the constraints of large separation distances and small surface potentials to yield:[22]

$$\Pi_{el} = 64n^0 kT\gamma^2 \exp(-\kappa h)$$
Eq. 1-12

$$\gamma = \left(\frac{\exp\left(\frac{Z}{2}\right) - 1}{\exp\left(\frac{Z}{2}\right) + 1} \right) \quad \text{and:} \quad Z = \frac{e\psi_0}{kT}$$

where ψ_0 is the surface potential.

van der Waals forces

Electrostatic in nature, van der Waals forces describe the general attractive forces between atoms and molecules. The main contributor to this is the dispersion force which arises due to the interaction of instantaneous molecular multipoles.[21,37] The individual dipole-dipole interaction of molecules is relatively weak, acting over the course of less than one nm, however these forces are additive for multi-bodied systems. The van der Waals force between two macroscopic bodies can be gained (via the microscopic approach) by integrating the molecular interaction potentials which gives for two flat surfaces[21]

$$\Pi_{vdW} = -\frac{A_{12}}{6\pi h^3}$$
Eq. 1-13

where h is the local separation between bodies, A_{12} is known as the Hamaker constant, and the negative sign indicates that the interaction is an attractive one. When investigating the van der Waals interactions between macroscopic bodies a few complications need to be taken into account. Firstly, a more complex Hamaker constant needs to be employed to account for retardation effects. These retardation effects arise due to the increasing ratio of electromagnetic field propagation time to molecular dipole lifetime with increasing distance.[9] Secondly, the local separation needs to be used rather than mean separation, meaning that a non-uniform attraction may result from interaction of non-planar surfaces.[50] Alternatively, a macroscopic approach can be taken to account for van der Waals interactions which is known as the Lifshitz theory, named after the scientist who first proposed this approach.[22] This approach considers the interactions explicitly as

electromagnetic fields, but results in a more complex formula which is not required for simple applications.

Steric forces

At very small separations, entropic confinement forces become significant and give rise to steric repulsion (or hindrance) forces between two bodies. These steric forces are particularly prevalent in the stabilisation of ultra-thin films such as surfactant/lipid bilayers where the lack of liquid core and small surface separation negates the previously described forces.[51] Israelachvili and Wennerström group these interactions under general classifications, allowing for a semi-quantitative approach to evaluating these forces.[52]

1.2.4   Specific ion effects

Specific ion effects describe the unique chemical character of ions, which are otherwise not considered by simple theories treating ions as point charges. The well-known emergence of this phenomenon stems from Hofmeister's experiments on the ability of different salts of the same valency to salt-out proteins from solution to varying extents.[53] It is well known that the surface tension of water increases with increasing salt concentration. The Gibbs model describes this as there being a negative surface excess of ions, i.e. a depletion of ions at the surface.[54] This was originally interpreted as the surface being a sharp interface between two dielectric media, and the ions being repelled due to image charge repulsion, a result that is still predicted by continuum models.[20,21] More recently, theoretical simulations and highly surface sensitive experimental techniques have debunked this notion, observing that not only are ions adsorbed to the outermost layer, but that the affinity to adsorb to the surface varied for different ions even with the same charge.[15,55]

Jungwirth et al. have performed numerous molecular dynamics simulations and calculations that pioneered the view that the more polarisable ions had preference to adsorb at the water/air interface due to ion-water interactions.[3,15,56,57] This work was based on the tuning of polarisable force fields at the liquid surface which allowed for the accommodation of the more polarisable species.[58] Investigations into halide-containing salts are particularly relevant due to their abundance, where the more polarisable iodide and bromide have been seen to strongly compete for surface adsorption as opposed to the less polarisable fluoride, which is depleted from the surface.[15,55,56,59-61] Boström et al.

provides a theoretical argument for the preferential adsorption of ions based on surface tension results that describes the tendency for the more polarisable anions to adsorb due to increased dispersion forces, but also claims that this is only part of the picture.[62]

Craig et al. investigate a similar phenomenon of specific ion effects, in the ability of different salts to inhibit bubble coalescence, i.e. the ability of individual bubbles to merge and combine, to varying degrees.[13,63,64] The simplified example of this is having three beakers: one containing pure water, one containing an aqueous surfactant solution, and the final containing a salty water solution. Shaking all three beakers, one can observe three distinct behaviours for the resulting bubbles in the beakers. For pure water the bubbles will be very short lived, and disappear shortly after shaking is ceased. In the surfactant solution the bubbles are stabilised by the surfactant to form a foam. In the salty solution the bubbles are stabilised for a short time before coalescing and dispersing out of the liquid phase.[50] It was found that this coalescence inhibition depends on the type of inorganic salt used as electrolyte. Craig et al. formed an empirical rule of salt types where ions were divided into category α or β. Combination of like ions (α-α, or β-β) led to inhibition of bubble coalescence in aqueous solutions, while combination of unlike ions (α-β) did not exhibit this effect. This leads to the important conclusion that it is the ion pair choice that plays a role, rather than just the choice of anion or cation.

1.3 Surfactants and Foam Films

Liquid foams are liquid-in-air dispersions often seen in soapy water or at the top of a delicious, cold beverage. Foams are a continuous 3-dimensional network of foam films, with the individual films connecting at points known as Plateau borders.[22] While the solvent comprising the foam is free to flow throughout the foam, it is the films themselves that give the key as to how foams are stabilised against the surrounding atmospheric pressure. Foam films are thin liquid films with two opposing liquid/vapour interfaces, where the interfaces are covered (to varying extents) with surfactant molecules that initially act to stabilise the film by lowering the interfacial tension.[22,65] The external atmosphere applies a pressure onto the films which acts to drain the solvent from the film's core, and as the film thins it turns from a 'droplet' to 'film'. The film state is reached when the two opposing surfaces reach a separation such that they begin to interact and stabilise the film against the external pressure.[65] These surface interactions are at the heart of colloid and interface science and are an important factor in understanding other

fields such as emulsions,[66] nanoparticle stabilisation,[67] and surfactant-free bubble coalescence.[63]
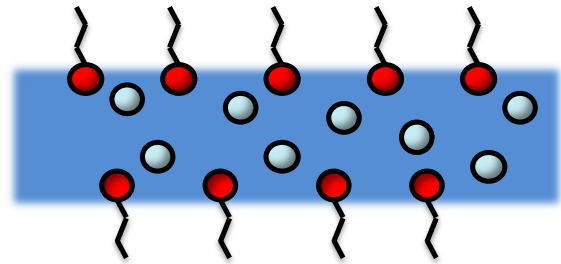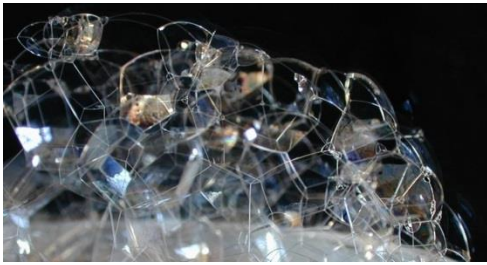
Figure 1-2. A picture of a typical liquid foam (left) along with a schematic illustration of an individual foam film (right).

1.3.1 Disjoining pressure

As a film drains the opposing surfaces reach a separation where they begin to interact, and the system is no longer characterised by hydrodynamic phenomena but via surface force interactions that maintain the film in a metastable state.[22,68] The sum of these forces are known as the disjoining pressure, Π, and is given by[22]

$$\Pi(h) = \Pi_{vdW} + \Pi_{edl} + \Pi_{steric} + \cdots$$

Eq. 1-14

where $\Pi(h)$ is the disjoining pressure given as a function of film thickness, and the subscripts representing: *vdW* the attractive van der Waals force, *edl* the repulsive force due to the electrical double layer, and *steric* the various structural forces dependent on the solvent and surfactant amongst others.[69] While there may be other forces that contribute to the disjoining pressure, they typically do not have the influence of the aforementioned forces and as such the general form of the thickness-dependent disjoining pressure is given as above. Mysels and Jones first designed an experimental setup capable of measuring film thickness as a function of applied external pressure.[70] This technique, now known as the thin film pressure balance (TFPB), is further discussed in section 2.3, but the basic principle is that at equilibrium thickness the disjoining pressure is equal to the external pressure, allowing for the measurement of a disjoining pressure versus thickness curve. Using this technique the value of the electric surface potential can be determined, but not the sign of the potential.[71] When ionic surfactants are used, the sign of the surface charge can be assumed to be the charge of the surfactant and this value increases with increasing

surfactant concentrations in the limit of small bulk concentrations.[72] This surface potential reaches saturation (calculated to be around 100 - 300 mV) at higher concentrations due to binding of the counterions to the surface, as determined from the adsorption isotherms of the surfactant and counterions.[73,74] The opposite trend is observed for non-ionic surfactants. At lower surfactant concentrations a surface charge of around 50 mV is observed, while the addition of surfactant reduces film thickness and eventually promotes a common black film to Newton black film transition, which is discussed further in section 1.3.3.[75,76] This effect is thought to be due to surfactant out-competing ions for surface adsorption.[65] The surface charge of non-ionic surfactant systems can come from the addition of electrolyte, or the dissociation of solvent molecules. In the latter case (i.e. salt-free, non-ionic surfactant systems) the surface potential is thought to be negative (relating to the inherent surface charge of pure water).[51] This has been observed with zeta potential measurements of the corresponding solutions resulting in a negative surface charge.[77] Additionally, the addition of cationic surfactant to these systems decreases the value of the surface potential, while addition of anionic surfactant increases the value of the surface potential.[78,79]

1.3.2   Foam film stability

Bergeron utilised the TFPB along with surface tension and neutron reflectivity to investigate the effect of the surfactant ordering at the surface on film stability.[80] Bergeron used the alkyltrimethylammonium bromide series (C_nTAB), n = 10, 12, 14, 16, and determined stability by the average rupture pressure of films formed in the TFPB. The results show that highly purified C_{10}TAB and C_{12}TAB have low stability (barely able to form films in the case of C_{10}TAB) with a sharp increase in film stability seen upon transition to the larger chain lengths. Additionally, small amounts of C_{12}OH 'impurity' increased the stability of C_{12}TAB to the level of C_{14}TAB. The study also included the addition of 11 mM KBr to C_{14}TAB films, in order to get films of the same ionic concentration as C_{12}TAB films. Interestingly, the stability of the C_{14}TAB/KBr films was not affected, even though the increased screening of the EDL lead to thinner films. The exact effect of the added salt on the surface forces in these films could not be discerned, due to the DLVO model used for fitting not being able to account for electrostatic effects beyond surface charge saturation. Stubenrauch and Khristov expanded on the investigation by using a similar technique, the foam pressure drop technique (FPDT), to correlate the

individual film stability in pure and impure films with that of the corresponding bulk foams, i.e. not just individual foam films.[81] The results show that the bulk foams behave in the same manner as the individual films, in that the influence of surfactant chain length and additional impurities have the same qualitative, and sometimes quantitative, influence on film/foam stability. This infers the dependence of bulk foam stability on the stability of the individual films. The comparison of symmetric (foam) and asymmetric (wetting) films has been able to shed light on the importance of the electrostatic contribution to film stability, in that above a critical electrolyte concentration both film types are governed by electrostatic forces rather than steric forces.[51,82] This has been seen with the stability range of foams relating to the charge reversal upon increasing surfactant concentration. Kristen et al. further investigated this with mixtures of a cationic surfactant ($C_{12}TAB$) and negatively charged polyelectrolyte.[83] They found a stability minimum for these mixtures around the isoelectric point, with stable films formed at a large range of concentrations either side of this.[84]

More recently techniques have been developed to study bulk foams with neutron reflectivity, in particular a technique for generating so-called 'bamboo foams'.[85-87] These have the potential to link information between the structure of foam films and their corresponding foams, but as of yet have not been refined to the point of gaining the necessary data.

1.3.3   Common black and Newton black films

Foam films are usually characterised as being in one of two states: a Newton black film (NBF), or common black film (CBF), with the former being named after Newton's historical first observations of film thinning.[88] CBFs are mainly stabilised by the electrostatic forces owing to the electrical double layers and as such have dynamic thicknesses, whereas NBFs are mainly stabilised by steric forces and consist mainly of a bilayer of the surfactant molecules, with film thicknesses on the order of twice the surfactant length (Figure 1-3).[65] In the case of non-ionic surfactants, CBF formation can often be achieved in concentrations below the cmc where there is sufficient area at the surface for adsorption of charge, while at and above the cmc, the surface becomes saturated with the surfactant and only a NBF can be formed.[75,89] The addition of electrolyte to the system enhances the prospect of CBF formation, however, increasing amounts of electrolyte screen the surface charge and decrease film thickness in accordance

with DLVO theory.[34,75,89,90] In some of these cases when the surface charge is sufficiently screened a CBF to NBF transition can occur.[12,91] In the case of ionic surfactants the intrinsic surface charge due to the adsorption of the charged surfactant leads to CBF formation, however a NBF transition is possible in some systems when the surfactant concentration is above the cmc, or in the case of added polyelectrolyte.[65,92,93] Kristen et al. performed extensive TFPB studies on $C_{14}TAB$/water with added polyelectrolyte of opposite charges.[94] Their results indicated that the reduction of net film charge with the addition of oppositely charged polyelectrolyte decreased the stability of the CBF, rather than inducing NBF formation. Additionally, at higher concentrations of oppositely charged polyelectrolyte they find that film stability increases. Surface tension measurements indicate a decrease in amount of material at the surface of the corresponding droplet systems, hence the authors propose that un-neutralised polyelectrolyte (not hydrophilic due to its charged nature) contributes to the electrostatic repulsion of surfaces, rather than a screening of charge. Similar effects for inorganic salts have not currently been observed.
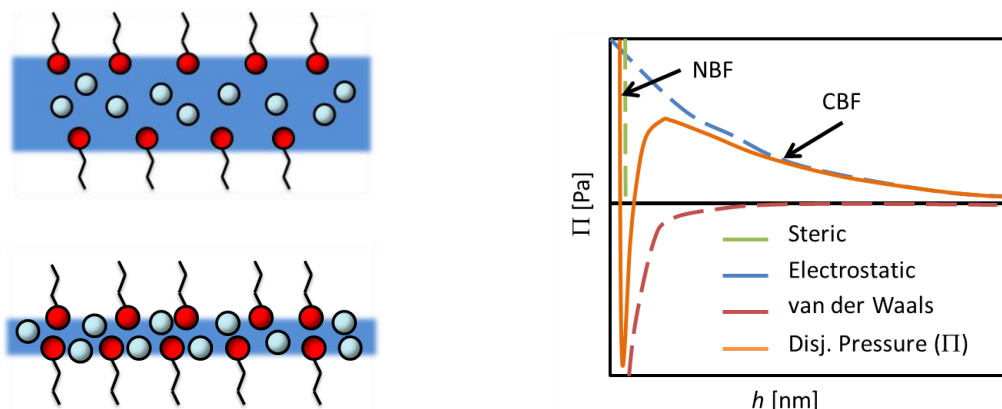
Figure 1-3. *Left*: an illustration of a CBF (top) and NBF (bottom). *Right*: Schematic representation of a disjoining pressure curve, highlighting the contribution of different forces and the regions of CBF and NBF formation.

Bélorgey and Benattar used x-ray reflectivity on foam films of the anionic surfactant sodium dodecylsulfate (SDS) in order to observe the structure of both a CBF and NBF of the same surfactant system.[88] They were able to determine the thickness and relative surface roughness of the films, and observed that the CBF had a definite liquid core (thickness = 27 ± 0.5 Å) while the NBF was much thinner with only a hydration layer of

liquid. Additionally, the surface roughness and surface area per surfactant molecule were equal, thus the defining factor between a CBF and NBF was indeed the liquid core thickness. However it must be noted that in this study it was not certain if the films were fully drained, due to the requirements of the experimental setup.

1.3.4 Thin foam film structure

As it had become apparent that DLVO models were not always adequate to describe the stability of foam films, Clunie et al. performed early studies on decyltrimethylammonium decyl sulphate ($C_{10}^+C_{10}^-$) in order to elucidate the structure of these films.[95] They used a combination of small angle X-ray scattering and reflected light measurements (assuming a three-layer optical model) to probe film thickness and structure. The x-ray scattering signal was too weak to determine any fine structure in the film, but the results from both methods regarding film thickness were in good agreement. They claim that these results give credit to the three-layer optical model used, consisting of a liquid core with a monolayer of the surfactant covering the opposing surfaces. However the disadvantage of this setup was that films were not measured in a fully drained, equilibrium state. Some years later, Thomas et al. produced the first results of neutron reflectivity on determining the structure of soap films.[96] They report from the beginning that the large size of the films needed for the measurements (10×2 cm^2) causes low film stability, which hinders the quality of measurement obtained. Their results were not detailed enough to propose a specific model for film thickness, however the shifting interference fringes in the reflectivity profiles allowed them to conclude that they were observing the film thinning over time, and in this circumstance gain the thickness of the film over time. Additionally this publication established the use of neutron reflectivity for determining foam film structure and investigating the adsorption of surfactants and other species at the surface of films. Thomas et al. later expand upon these studies by using neutron reflectivity to investigate the adsorption of C_nTAB surfactants at the air/water interface, where n is between 10 and 18.[97] Their results showed that the thickness of the alkyl chain layer was approximately constant across all chain lengths, with C_{10}TAB at lower surface coverage forming the thickest layer. These results were among the first that demonstrated the orientation of the surfactant molecules at the interface, as well as the extent of chain defects present in the longer chain surfactant molecules.

As discussed in section 1.2.1 – Surface excess and Gibbs dividing plane – knowing the surface tension and chemical potential allows for the determination of the surface excess. The chemical potential, or activity, can be determined from bulk properties, however these processes fail in the limit of small bulk concentrations where physical changes are too small for measurement.[98] Traditionally in these cases the activity is assumed to be constant.[99] However Strey et al. point out that this assumption is not valid, particularly for surfactants at concentrations less than but close to the cmc due to the non-negligible interactions of the molecules.[100] Andersson et al. approach the problem from the opposite angle, measuring the concentration depth profile of surfactants at the surface of solutions.[98,101] This allows for the direct determination of the surface excess of the surfactant, and thus the accurate determination of the activity and chemical potential of the surfactant once the surface tension of the solution is measured. In their investigation of an ionic surfactant solution, Andersson et al. conclude that the Gibbs equation itself is found to be valid, however the error in measuring the activity of certain systems lead to differences in results.[98]

Prosser and Franses provide a particularly in-depth review of the different methods and models for determining the adsorption of surfactants, and make point to note that ionic surfactants provide some difficulties in adhering to the standard Gibbs adsorption isotherm models.[99] Eastoe et al. utilise neutron reflection along with surface tension measurements to assess the validity of the Gibbs equation in determining the adsorption isotherm of ionic surfactants.[102] They give the Gibbs adsorption isotherm in terms of activity (rather than concentration)

$$\Gamma = -\frac{1}{mRT}\frac{d\gamma}{d\ln a}$$

<div align="right">**Eq. 1-15**</div>

and aim specifically to investigate the pre-factor, m, for the use of ionic surfactants and the impact of impurities on surfactant adsorption behaviour. Their results were able to confirm the validity of using surface tension methods to determine the adsorption behaviour of 1:1 ionic surfactants. The exact structure of the counterion profile was not able to be determined as the diffuse layer was not of sufficient density to be detected with their method. Li et al. performed a similar study on quaternary Gemini surfactants, highlighting the effect of the complex alkyl chains of the surfactant on the adsorption behaviour and measured Gibbs pre-factor.[103] Gilányi et al. took a different approach by neglecting the

standard adsorption models and instead determined the adsorption behaviour of cationic surfactants by a standard isotherm equation.[104] This approach calculates the equilibrium constant for surface coverage under an assumed surface saturation coverage, however the authors take care to note the recent studies that point out how this can be evaluated by taking into account the increased adsorption of surfactant past the cmc.[97] This approach revealed that the hydrophobic driving force for adsorption becomes independent of the surface excess beyond a certain coverage.

1.3.5   Specific ion effects in foams and foam films

Ingram was amongst the first to observe specific ion effects in foam films in investigations into the free energy and stability of foam films.[105] He observed varying equilibrium film thicknesses across a range of cations and anions of added inorganic electrolyte, and related this to the calculated surface potential for those species for inducing a CBF to NBF transition. However, he was not able to comment on what species had preferential adsorption at the surface. Angarska et al. later studied the effects of various salts at a specific concentration (24 mM) on the thinning of SDS foam films and stability of bulk foams.[106] They described their results along the lines of ion polarisability, with the weakly polarisable ions such as Cl^- and NO_3^- leading to relatively unstable films compared to the more polarisable ions such as PO_4^{3-} and CO_3^{2-}. The authors state that this film stability is related to the ions facilitating interconnection between the surfactant headgroups, which is further supported by the fact that changing from Na^+ to Mg^{2+} also increases film stability, an effect seen in another study.[107] For this system, in the case of the anions, it is thought that hydrogen bonding is the stabilising mechanism, while for the cations it is the direct electrostatic interactions of the cations with the negatively charged headgroups. A similar study was performed by Pandey et al. who investigated the effect of various cations on the foamability of dodecyl sulphate using the so-called 'shaking method', along with surface tension measurements.[108] They found that stability increased in the order $Li^+ < Na^+ < Cs^+$ for the monovalent cations, which they attribute to the varying ability of the cations to inhibit the micelle formation that stabilises these films.

Von Klitzing et al. have performed TFPB investigations into the role of specific ion effects in wettings films and foam films. In their investigation into the surface charge of pure water using wetting films, it was noticed that the choice of anion (F^-, Cl^-, I^-) in the added electrolyte had a significant effect of film thickness.[36] They offer the explanation

that with decreasing solvation shell size (I^- < Cl^- < F^-) that the halides are more likely to adsorb at the interface due to their more 'hydrophobic' nature. Interestingly the DLVO fits to the data indicate that the choice of anion had no significant effect on the Debye length of the electrical double layer. Von Klitzing et al. later performed TFPB along the lines of the original investigation of Pandey et al., investigating the effect of different cations on film thickness in dodecyl sulfate films.[109] They found that with increasing cation size, film thickness decreased, which can be explained with the increased adsorption of these cations shielding the negative surface charge and reducing electrostatic repulsion between surfaces. Further studies investigating both varying cation and anion in wetting films confirmed these findings, with the additional view that anion effects were more significant than cation effects.[110]

1.4 Ionic Liquids

Room temperature ionic liquids (RTILs) or simply, ionic liquids (ILs), are typically categorised as salts with a melting point below 100 °C. These ILs often consist of an organic cation along with an organic or inorganic anion, and have an unusual combination of properties, such as low vapour pressure, high electric and thermal stability, and the ability to dissolve a vast array of substances.[111] ILs differ from typical salts in that the mismatch of ions leads to a low lattice energy for crystallisation which results in their relatively low melting point,[85] while delocalisation of charge is thought to contribute also.[112] In this way ILs provide an interesting situation of a liquid comprised totally of charged species, as opposed to an ionic solution (such as those discussed in section 1.2.4) where the solvent dilutes the amount of charge in the liquid. ILs are typically separated into two main categories: protic ionic liquids (PILs) and aprotic ionic liquids (AILs). PILs are synthesised by the reaction of a Brønsted acid with a Brønsted base, where the proton transfer leads to hydrogen bond donor and acceptor sites.[87] AILs can be formed either by acid-base neutralisation or, more commonly, by salt metathesis reactions.[113] The immense range of ion combinations possible allow a large degree of freedom in tuning the properties of ILs which have seen them being used in applications such as: solvents,[111] gas-capture media,[114,115] electrolytes in solar cells,[116] and catalysis.[117] The structure of ILs at the liquid/vapour interface (a more general case of the liquid/air interface) is crucial to understanding the science behind many of these applications.

1.4.1 Liquid/vapour interface – Aprotic ionic liquids

A large range of powerful surface analytical techniques require experiments to be performed under high vacuum, causing difficulties in investigating surfaces of many common liquids, e.g. water. However the negligible vapour pressure of ILs allows them to be far more accessible to techniques requiring high vacuum conditions for operation. As such the liquid/vapour interface of ILs, particularly AILs, have been extensively investigated by a range of techniques, including: surface force apparatus,[118] sum frequency generation spectroscopy,[119-122] direct recoil spectroscopy,[123] x-ray photoelectron spectroscopy (including angle- and energy-resolved methods),[23,124-127] metastable induced electron spectroscopy,[128-130] and neutral impact collision ion scattering spectroscopy.[131] Santos and Baldelli present an in-depth review of the various methods used to investigate the liquid/vapour interface, and the corresponding results.[132]

Cation orientation at the surface is a topic of distinct interest given the large size of many cations used, along with other factors such as structural asymmetry and the inclusion of various functional groups as part of the cation. In particular, the effect of aliphatic chain length on the orientation of imidazolium-based cations was investigated across a number of different studies. The vast majority of studies indicate that both ions are present to some extent at the interface, however the cation orientation provides some insight into the hierarchy of forces at the liquid/vapour interface. When the cation alkyl chain is less than four carbon atoms in length, the cation ring orientation shows a dependence upon the anion,[121,128,133] while at longer cation chain lengths, the orientation shows little-to-no anion dependence.[120,122,125,128,134,135] These findings highlight the effect of the hydrophobic force between the alkyl chains overcoming electrostatic forces that would otherwise determine surface structure. This is supported by a variety of studies that demonstrate that increasing the cation alkyl chain length leads to a significant increase of the cation occupying the surface.[123,124,126-128,131] Although ion layering has been observed at the IL/solid interface,[118,136-138] this has not yet been explicitly observed at the vapour interface. This layering at the solid interface is dominated by the cation and provides further evidence to the hydrophobic forces dominating the electrostatic in this regard. Bresme et al. performed simulations which determined that ion size asymmetry is a significant factor in determining the charge structure at the IL/vapour interface.[139] Their results show that an increase in size asymmetry leads to an increased charge separation at the interface, with the larger ion being present in an increased amount at the interface compared to the

smaller ion. However, their simulations modelled the ions as charged sphered and as such the result would be difficult to observe experimentally due to the more complex chemical nature of ILs.

Investigations into the anion structure at the liquid/vapour interface are more scarce, due to the more 'popular' techniques used in these investigations unable to detect directly, or detect differences, between anions.[120,126,140-142] Freire et al. investigated the surface tension of imidazolium-based ILs with four molecular anions of various sizes and found that increasing the anion size led to a decrease in surface tension.[143] They comment that the increasing ion size leads to a decrease in hydrogen bonding, a conclusion that was also reached Deetlefs et al.[97] Hydrogen bonding was seen to be an important factor in ion interactions of imidazolium-based ILs by Jeon et al. who investigated the surface of $[C_4mim]^+$ with $[I]^-$ and $[BF_4]^-$ using infrared vibration spectroscopy.[144] By mixing the two ILs with D_2O they were able to observe the isotopic exchange to the most acidic carbon of the imidazolium ring (situated between the two nitrogens), and found that this exchange only took place for the $[I]^-$ IL and not with $[BF_4]^-$ even with prolonged D_2O exposure. Similar effects of hydrogen bonding factoring in AIL ion interactions have been seen experimentally and in molecular dynamics simulations.[145,146]

1.4.2 Liquid/vapour interface – Protic ionic liquids

The liquid/vapour interface of PILs has not been investigated nearly to the extent of AILs, however there have been a number of studies revealing details about this structure in recent years, pointing out in particular the importance of the hydrogen bonding network.[147,148] Kennedy and Drummond used electrospray ionisation mass spectrometry on a number of different PILs and found that these were prone to aggregating in clusters of the type $C_nA_{n-1}^+$ (with C being cation, A being anion), with $n = 8$ being by far the prevalent cluster.[149] This finding is in contrast to AILs which tend to aggregate in smaller clusters ($n = 2$ or 3).[86,102,150] Ludwig calculated that these clusters could be stable in the gas phase owing to its hydrogen bond network.[151] Wakeham et al. later proposed that these clusters exist at the IL/vapour interface.[152] Their x-ray reflectivity results showed a surface profile that was not consistent with a sharp liquid interface, and used the previous findings to justify that these clusters could exist in a diffuse layer at the interface. Additionally, they compare results between ethylammonium nitrate, propylammonium nitrate, and ethylammonium formate, the latter of which has a significantly reduced

hydrogen bonding network, and found that it had the least extensive interfacial region of the three ILs. Niga et al. investigated the IL/vapour interface of ethylammonium nitrate using a combination of X-ray reflectivity and vibrational sum frequency spectroscopy (VSFS).[153] They were able to observe surface ordering at the interface that extended 31 Å towards the bulk before decaying away, with the VSFS results observing a strong excess of the ethyl chains protruding towards the vapour phase.

1.4.3   Influence of water on IL structure

The sensitivity of ILs to impurities is a topic that has received significant attention over the last several years. Impurities such as halides, silicon, and water are known to affect both the bulk and surface physical properties of ILs, many of which need to be well defined for various applications.[154-156] The effect of water is a topic of particular interest given that the highly hygroscopic nature of many ILs leads them to quickly absorb water even from small exposure to atmosphere.[113] The interactions between water and ILs are heavily focussed on the hydrogen bonding network being accommodated or interrupted by the presence of either species. Even at very low mole fractions of IL the hydrogen bonding network in water becomes considerably interrupted,[157,158] however the bulk ionic network of ILs has been seen to be relatively unperturbed by the presence of water.[159] Molecular dynamics simulations of $[C_4mim][BF_4]$ with water indicate that water exists as linear chains in a nanoscale structure as opposed to a macroscopic phase separation even up to 0.5 mole fraction.[159,160] Molecular dynamics simulations by Bernades et al. indicate that ILs maintain bulk structure up to 0.95 mole fraction of water, while at mole fractions of 0.996, only 60% of the ions are isolated, indicating the significant barrier for solvation to overcome the electrostatic interaction between ions.[161]

The surface structure of IL/water mixtures has received some attention, mostly in the range of large water mole fractions.[162] It has been seen that ILs dominate for surface adsorption in a surfactant-like behaviour even up to very large water concentrations (Rivera-Rubero and Baldelli report that water only appears at mole fractions ≥ 0.98 mole fraction water[119]).[163] However, water does have an effect on the surface structure of ILs by influencing the orientation of the cation, and positioning of the anion which is seen to be dependent on both cation and anion type.[119,156-158,164,165] Interestingly water seems to have a more pronounced effect on more hydrophobic ILs compared to hydrophilic ILs.[143,165] Rivera-Rubero and Baldelli offer the explanation that in hydrophobic imidazolium-based

ILs, water is more likely to interact with the acidic proton of the imidazole ring via hydrogen bonding, having the effect of influencing the ring orientation at the surface. Additionally, in the case of the hydrophilic ILs, water is more likely to be accommodated in the bulk via ion solvation which is more favourable than surface adsorption.[165] This is in agreement with surface tension studies by Rilo et al. on mixtures of IL/water and IL/ethanol. They found that water has a rapidly decreasing effect on surface tension with increasing IL concentration, while ethanol has a more pronounced effect over a large concentration range, indicating that the more amphiphilic species can be accommodated at the surface.[163]

1.5   Thesis outline

The surface structure of liquids containing ionic species, in particular the charge distribution along the surface normal, is an area that lacks experimental investigation. While the models used for describing the surface structure and surface forces are accurate for a small range of conditions, the shortcoming of these models to account for the chemical nature of both ions and solvent cause them to be lacking in many situations. In these cases, knowing the concentration depth profiles of the species will shed significant light on this field.

Chapter 2 details the experimental methods used in this thesis, with particular attention to neutral impact collision ion scattering spectroscopy, due to the major role it plays in the research. Additionally, the design and implementation of methods for handling the samples, in particular the foam films, is discussed.

Chapters 3 to 6 focus on the studies of ionic liquids. Ionic liquids are an ideal candidate for investigation due to the large range of freedom in tuning the ions for various purposes, which allows for a large range of systematic studies to understand the hierarchy of forces governing ion adsorption at liquid surfaces.

Chapters 7 to 9 focus on the studies of foam films. There has been little experimental study into the surface structure of foam films, with the current understanding built either from comparison with the corresponding bulk liquid surfaces, or from estimations using models. Knowing the concentration depth profiles of the species in a foam film will allow for a greater understanding of how these films are formed and stabilised.

In the above chapters the discussion and subsequent conclusions are focussed only on that particular study, being treated independently of the other chapters. Chapter 10 gives a final summary of the work presented in this thesis.

1.6   **References**

1   Nathanson, G. M. Molecular beam studies of gas-liquid interfaces. *Annual Review of Physical Chemistry* **55**, 231-255 (2004).

2   Garrett, B. Ions at the air/water interface. *Science* **303**, 1146-1147 (2004).

3   Knipping, E. M. *et al.* Experiments and simulations of ion-enhanced interfacial chemistry on aqueous NaCl aerosols. *Science* **288**, 301-306 (2000).

4   Kunz, W., Lo Nostro, P. & Ninham, B. W. The present state of affairs with Hofmeister effects. *Current Opinion in Colloid & Interface Science* **9**, 1-18 (2004).

5   Griffith, E. C. & Vaida, V. In situ observation of peptide bond formation at the water–air interface. *Proceedings of the National Academy of Sciences* **109**, 15697-15701 (2012).

6   Dobson, C. M., Ellison, G. B., Tuck, A. F. & Vaida, V. Atmospheric aerosols as prebiotic chemical reactors. *Proceedings of the National Academy of Sciences* **97**, 11864-11868 (2000).

7   Thompson, P. A. & Troian, S. M. A general boundary condition for liquid flow at solid surfaces. *Nature* **389**, 360-362 (1997).

8   Wang, R. *et al.* Light-induced amphiphilic surfaces. *Nature* **388**, 431-432 (1997).

9   Hunter, R. J. *Foundations of Colloid Science*. Second edn, (Oxford University Press, 2001).

10   Liu, Y., Jessop, P. G., Cunningham, M., Eckert, C. A. & Liotta, C. L. Switchable Surfactants. *Science* **313**, 958-960 (2006).

11   Lide, D. R. *CRC Handbook of Chemistry And Physics*. (CRC Pr I Llc, 2006).

12   Todorov, R., Cohen, R. & Exerowa, D. Surface forces in foam films from DPPC and lung surfactant phospholipid fraction. *Colloids and Surfaces A: Physicochemical and Engineering Aspects* **310**, 32-38 (2007).

13   Henry, C. L. & Craig, V. S. J. Ion-Specific Influence of Electrolytes on Bubble Coalescence in Nonaqueous Solvents. *Langmuir* **24**, 7979-7985 (2008).

14   Adam, N. K. Physics and chemistry of surfaces. (1941).

15   Jungwirth, P. & Tobias, D. J. Ions at the Air/Water Interface. *J. Phys. Chem. B* **106**, 6361-6373 (2002).

16   Randles, J. E. B. Structure at the Free Surface of Water and Aqueous Electrolyte Solutions. *Physics and Chemistry of Liquids* **7**, 107-179 (1977).

17   Blunk, D., Tessendorf, R., Buchavzov, N., Strey, R. & Stubenrauch, C. Purification, Surface Tensions, and Miscibility Gaps of Alkyldimethyl and Alkyldiethylphosphine Oxides. *Journal of Surfactants and Detergents* **10**, 155-165 (2007).

18   Kirmse, K. & Morgner, H. Binary Liquid Mixtures. The Relation between Surface Tension and Surface Composition as Studied by MIES (Metastable Induced Electron Spectroscopy). *Langmuir* **22**, 2193-2199 (2006).

19   Li, Y. Q. *et al.* Uptake of HCl(g) and HBr(g) on Ethylene Glycol Surfaces as a Function of Relative Humidity and Temperature. *The Journal of Physical Chemistry A* **106**, 1220-1227 (2002).

20   Adamson, A. W. & Gast, A. P. *Physical chemistry of surfaces*. 6th edn, (Wiley-Interscience, 1997).

21   Israelachvili, J. N. *Intermolecular and Surface Forces*. Second edn, (Academic Press, 2000).

22   Bergeron, V. Forces and structure in thin liquid soap films. *Journal of Physics: Condensed Matter*, R215 (1999).

23   Lockett, V. *et al.* Orientation and mutual location of ions at the surface of ionic liquids. *Physical Chemistry Chemical Physics* **12**, 13816-13827 (2010).

24   Andersson, G. & Morgner, H. Investigations on solutions of tetrabutylonium salts in formamide with NICISS and ICISS: concentration depth profiles and composition of the outermost layer. *Surface Science* **445**, 89-99 (2000).

25   Schulze, K. D. & Morgner, H. Investigation of the electric charge structure and the dielectric permittivity at surfaces of solutions containing ionic surfactants. *Journal of Physics: Condensed Matter*, 9823 (2006).

26   Bökman, F., Bohman, O. & Siegbahn, H. O. G. Electric double layers at solution surfaces studied by means of electron spectroscopy: a comparison of potassium octanoate in formamide and ethylene glycol solution. *Chemical Physics Letters* **189**, 414-419 (1992).

27   Vacha, R., Buch, V., Milet, A., Devlin, J. P. & Jungwirth, P. Autoionization at the surface of neat water: is the top layer pH neutral, basic, or acidic? *Physical Chemistry Chemical Physics* **9**, 4736-4747 (2007).

28   Beattie, J. K. Comment on Autoionization at the surface of neat water: is the top layer pH neutral, basic, or acidic? by R. Va´ cha, V. Buch, A. Milet, J. P. Devlin and P. Jungwirth, Phys. Chem. Chem. Phys., 2007, 9, 4736. *Physical Chemistry Chemical Physics* **10**, 330-331 (2008).

29   Winter, B., Faubel, M., Vácha, R. & Jungwirth, P. Reply to comments on Frontiers Article [`]Behavior of hydroxide at the water/vapor interface'. *Chemical Physics Letters* **481**, 19-21 (2009).

30   Petersen, M. K., Iyengar, S. S., Day, T. J. F. & Voth, G. A. The Hydrated Proton at the Water Liquid/Vapor Interface. *The Journal of Physical Chemistry B* **108**, 14804-14806 (2004).

31   Petersen, P. B. & Saykally, R. J. Is the liquid water surface basic or acidic? Macroscopic vs. molecular-scale investigations. *Chemical Physics Letters* **458**, 255-261 (2008).

32   Takahashi, M. ζ Potential of Microbubbles in Aqueous Solutions: Electrical Properties of the Gas−Water Interface. *The Journal of Physical Chemistry B* **109**, 21858-21864 (2005).

33   Exerowa, D. Effect of adsorption, ionic strength and pH on the potential of the diffuse electric layer. *Kolloid-Z.u.Z.Polymere* **232**, 703-710 (1969).

34   Karraker, K. A. & Radke, C. J. Disjoining pressures, zeta potentials and surface tensions of aqueous non-ionic surfactant/electrolyte solutions: theory and comparison to experiment. *Advances in Colloid and Interface Science* **96**, 231-264 (2002).

35   Ciunel, K., Armélin, M., Findenegg, G. H. & von Klitzing, R. Evidence of Surface Charge at the Air/Water Interface from Thin-Film Studies on Polyelectrolyte-Coated Substrates. *Langmuir* **21**, 4790-4793 (2005).

36   Hanni-Ciunel, K., Schelero, N. & von Klitzling, R. Negative charges at the air/water interface and their consequences for aqueous wetting films containing surfactans. *Faraday Discuss.* **141**, 41-53 (2009).

37   Adamson, A. W. & Gast, A. P. *Physical Chemisty of Surfaces*. 6 edn, (John Wiley and Sons. Inc, 1997).

38   Attard, P. Recent advances in the electric double layer in colloid science. *Current Opinion in Colloid & Interface Science* **6**, 366-371 (2001).

39   Attard, P., Mitchell, D. J. & Ninham, B. W. Beyond Poisson--Boltzmann: Images and correlations in the electric double layer. II. Symmetric electrolyte. *The Journal of Chemical Physics* **89**, 4358-4367 (1988).

40   Attard, P., Mitchell, D. J. & Ninham, B. W. Beyond Poisson--Boltzmann: Images and correlations in the electric double layer. I. Counterions only. *The Journal of Chemical Physics* **88**, 4987-4996 (1988).

41   Attard, P. *Electrolytes and the Electric Double Layer*. (John Wiley & Sons, Inc., 2007).

42   Marčelja, S. Exact Description of Aqueous Electrical Double Layers. *Langmuir* **16**, 6081-6083 (2000).

43   Espinosa-Marzal, R. M., Drobek, T., Balmer, T. & Heuberger, M. P. Hydrated-ion ordering in electrical double layers. *Physical Chemistry Chemical Physics* (2012).

44   Attard, P., Antelmi, D. & Larson, I. Comparison of the Zeta Potential with the Diffuse Layer Potential from Charge Titration. *Langmuir* **16**, 1542-1552 (2000).

45   Beresford-Smith, B., Chan, D. Y. C. & Mitchell, D. J. The electrostatic interaction in colloidal systems with low added electrolyte. *Journal of Colloid and Interface Science* **105**, 216-234 (1985).

46   Derjaguin, B. V. & Landau, L. Theory of the stability of strongly charged lyophobic sols and of the adhesion of strongly charged particles in solution of electrolytes. *Acta Physicochim. URSS* **14**, 633-662 (1941).

47   Verwey, E. J. W. & Overbeek, J. T. G. *Theory of the Stability of Lyophobic Colloids: The interaction of sol particles having an electric double layer*. (Elsevier Pub. Co., 1948).

48   Ninham, B. W. & Yaminsky, V. Ion Binding and Ion Specificity: The Hofmeister Effect and Onsager and Lifshitz Theories. *Langmuir* **13**, 2097-2108 (1997).

49   Israelachvili, J. & Wennerstrom, H. Role of hydration and water structure in biological and colloidal interactions. *Nature* **379**, 219-225 (1996).

50   Henry, C. L. *Bubbles, Thin Films and Ion Specificity* PhD thesis, Australian National University, (2009).

51   Exerowa, D. *et al.* Foam and wetting films: electrostatic and steric stabilization. *Advances in Colloid and Interface Science* **104**, 1-24 (2003).

52   Israelachvili, J. N. & Wennerstroem, H. Entropic forces between amphiphilic surfaces in liquids. *The Journal of Physical Chemistry* **96**, 520-531 (1992).

53   Kunz, W., Henle, J. & Ninham, B. W. 'Zur Lehre von der Wirkung der Salze' (about the science of the effect of salts): Franz Hofmeister's historical papers. *Current Opinion in Colloid & Interface Science* **9**, 19-37 (2004).

54   Gibbs, J. W., Bumstead, H. A., Van Name, R. G. & Longley, W. R. *The collected works of J. Willard Gibbs*. (Longmans, Green and Co., 1902).

55   Petersen, P. B. & Saykally, R. J. Confirmation of enhanced anion concentration at the liquid water surface. *Chemical Physics Letters* **397**, 51-55 (2004).

56   Jungwirth, P. & Tobias, D. J. Surface Effects on Aqueous Ionic Solvation: A Molecular Dynamics Simulation Study of NaCl at the Air/Water Interface from Infinite Dilution to Saturation. *The Journal of Physical Chemistry B* **104**, 7702-7706 (2000).

57   Jungwirth, P. & Tobias, D. J. Molecular Structure of Salt Solutions: A New View of the Interface with Implications for Heterogeneous Atmospheric Chemistry. *The Journal of Physical Chemistry B* **105**, 10468-10472 (2001).

58   Perera, L. & Berkowitz, M. L. Many-body effects in molecular dynamics simulations of Na[sup +](H[sub 2]O)[sub n] and Cl[sup -](H[sub 2]O)[sub n] clusters. *The Journal of Chemical Physics* **95**, 1954-1963 (1991).

59   Brown, E. C., Mucha, M., Jungwirth, P. & Tobias, D. J. Structure and vibrational spectroscopy of salt water/air interfaces: predicitions from classical molecular dynamics simulations. *J. Phys. Chem. B* **109**, 7934-7940 (2005).

60   Cwiklik, L., Andersson, G., Dang, L. X. & Jungwirth, P. Segregation of inorganic ions at surfaces of polar nonaqeuous liquids. *ChemPhysChem* **8**, 1457-1463 (2007).

61   Andersson, G., Morgner, H., Cwiklik, L. & Jungwirth, P. Anions of Alkali Halide Salts at Surfaces of Formamide Solutions: Concentration Depth Profiles and Surface Topography. *The Journal of Physical Chemistry C* **111**, 4379-4387 (2007).

62   Boström, M., Williams, D. R. M. & Ninham, B. W. Surface Tension of Electrolytes: Specific Ion Effects Explained by Dispersion Forces. *Langmuir* **17**, 4475-4478 (2001).

63   Henry, C. L. & Craig, V. S. J. The link between ion specific bubble coalescence and Hofmeister effects is the partitioning of ions within the interface. *Langmuir* **26**, 6478-6483 (2010).

64   Henry, C. L., Dalton, C. N., Scruton, L. & Craig, V. S. J. Ion-Specific Coalescence of Bubbles in Mixed Electrolyte Solutions. *The Journal of Physical Chemistry C* **111**, 1015-1023 (2006).

65   Stubenrauch, C. & Klitzing, R. v. Disjoining pressure in thin liquid foam and emulsion films - new concepts and perspectives. *Journal of Physics: Condensed Matter*, R1197 (2003).

66   Karakashev, S. I., Manev, E. D., Tsekov, R. & Nguyen, A. V. Effect of ionic surfactants on drainage and equilibrium thickness of emulsion films. *Journal of Colloid and Interface Science* **318**, 358-364 (2008).

67   Nakashima, T. & Kimizuka, N. Water/Ionic Liquid Interfaces as Fluid Scaffolds for the Two-Dimensional Self-Assembly of Charged Nanospheres†. *Langmuir* **27**, 1281-1285 (2011).

68   Oolman, T. O. & Blanch, H. W. BUBBLE COALESCENCE IN STAGNANT LIQUIDS. *Chem. Eng. Commun.* **43**, 237-261 (1986).

69   Angarska, J. K. *et al.* Detection of the Hydrophobic Surface Force in Foam Films by Measurements of the Critical Thickness of the Film Rupture. *Langmuir* **20**, 1799-1806 (2004).

70   Mysels, K. J. & Jones, M. N. Direct measurement of the variation of double-layer repulsion with distance. *Discussions of the Faraday Society* **42**, 42-50 (1966).

71   v. Klitzing, R. Effect of interface modification on forces in foam films and wetting films. *Advances in Colloid and Interface Science* **114-115**, 253-266 (2005).

72   Exerowa, D., Zacharieva, M., Cohen, R. & Platikanov, D. Dependence of the equilibrium thickness and double layer potential of foam films on the surfactant concentration. *Colloid & Polymer Sci* **257**, 1089-1098 (1979).

73   Kralchevsky, P. A., Danov, K. D., Broze, G. & Mehreteab, A. Thermodynamics of Ionic Surfactant Adsorption with Account for the Counterion Binding: Effect of Salts of Various Valency. *Langmuir* **15**, 2351-2365 (1999).

74   Danov, K. D., Vlahovska, P. M., Kralchevsky, P. A., Broze, G. & Mehreteab, A. Adsorption kinetics of ionic surfactants with detailed account for the electrostatic interactions: effect of the added electrolyte. *Colloids and Surfaces A: Physicochemical and Engineering Aspects* **156**, 389-411 (1999).

75   Bergeron, V., Waltermo, A. & Claesson, P. M. Disjoining Pressure Measurements for Foam Films Stabilized by a Nonionic Sugar-Based Surfactant. *Langmuir* **12**, 1336-1342 (1996).

76   Stubenrauch, C., Schlarmann, J. & Strey, R. A disjoining pressure study of n-dodecyl-[small beta]-D-maltoside foam films. *Physical Chemistry Chemical Physics* **4**, 4504-4513 (2002).

77   Yoon, R.-H. & Yordan, J. L. Zeta-potential measurements on microbubbles generated using various surfactants. *Journal of Colloid and Interface Science* **113**, 430-438 (1986).

78   Balzer, D. Cloud point phenomena in the phase behavior of alkyl polyglucosides in water. *Langmuir* **9**, 3375-3384 (1993).

79   Aveyard, R. *et al.* Flocculation Transitions of Weakly Charged Oil-in-Water Emulsions Stabilized by Different Surfactants. *Langmuir* **18**, 3487-3494 (2002).

80   Bergeron, V. Disjoining Pressures and Film Stability of Alkyltrimethylammonium Bromide Foam Films. *Langmuir* **13**, 3474-3482 (1997).

81   Stubenrauch, C. & Khristov, K. Foams and foam films stabilized by CnTAB: Influence of the chain length and of impurities. *Journal of Colloid and Interface Science* **286**, 710-718 (2005).

82   Exerowa, D., Kolarov, T., Esipova, N. E., Yankov, R. & Zorin, Z. M. Foam and Wetting Films from Aqueous Cetyltrimethylammonium Bromide Solutions: Electrostatic Stability1. *Colloid Journal* **63**, 45-52 (2001).

83   Kristen, N., Vüllings, A., Laschewsky, A., Miller, R. & von Klitzing, R. Foam Films from Oppositely Charged Polyelectolyte/Surfactant Mixtures: Effect of Polyelectrolyte and Surfactant Hydrophobicity on Film Stability. *Langmuir* **26**, 9321-9327 (2010).

84   Kristen-Hochrein, N., Laschewsky, A., Miller, R. & von Klitzing, R. Stability of Foam Films of Oppositely Charged Polyelectrolyte/Surfactant Mixtures: Effect of Isoelectric Point. *The Journal of Physical Chemistry B* (2011).

85   Terriac, E. *et al.* Characterization of bamboo foam films by neutron and X-ray experiments. *Colloids and Surfaces A: Physicochemical and Engineering Aspects* **309**, 112-116 (2007).

86   Axelos, M. A. V. & Boué, F. Foams As Viewed by Small-Angle Neutron Scattering. *Langmuir* **19**, 6598-6604 (2003).

87   Etrillard, J. *et al.* In Situ Investigations on Organic Foam Films Using Neutron and Synchrotron Radiation. *Langmuir* **21**, 2229-2234 (2005).

88   Bélorgey, O. & Benattar, J. J. Structural properties of soap black films investigated by x-ray reflectivity. *Physical Review Letters* **66**, 313 (1991).

89   Márquez-Beltrán, C. & Langevin, D. Electrostatic effects in films stabilised by non-ionic surfactants. *Journal of Colloid and Interface Science* **312**, 47-51 (2007).

90   Cohen, R. *et al.* Direct measurement of molecular interaction forces in foam films from lung surfactant fraction. *Colloid & Polymer Science* **284**, 546-550 (2006).

91   Stubenrauch, C. & Strey, R. Phase Diagrams of Nonionic Foam Films: New Interpretation of Disjoining Pressure vs Thickness Curves. *Langmuir* **20**, 5185-5188 (2004).

92   Bergeron, V., Jimenez-Laguna, A. I. & Radke, C. J. Hole formation and sheeting in the drainage of thin liquid films. *Langmuir* **8**, 3027-3032 (1992).

93   Bergeron, V., Langevin, D. & Asnacios, A. Thin-Film Forces in Foam Films Containing Anionic Polyelectrolyte and Charged Surfactants. *Langmuir* **12**, 1550-1556 (1996).

94   Kristen, N. *et al.* No Charge Reversal at Foam Film Surfaces after Addition of Oppositely Charged Polyelectrolytes? *The Journal of Physical Chemistry B* **113**, 7986-7990 (2009).

95   Clunie, J. S., Corkill, J. M. & Goodman, J. F. Structure of black foam films. *Discussions of the Faraday Society* **42**, 34-41 (1966).

96   Thomas, R. K. *et al.* Critical reflection of neutrons from a soap film. *Journal of Colloid and Interface Science* **97** (1984).

97   Lyttle, D. J., Lu, J. R., Su, T. J., Thomas, R. K. & Penfold, J. Structure of a Dodecyltrimethylammonium Bromide Layer at the Air/Water Interface Determined by Neutron Reflection: Comparison of the Monolayer Structure of Cationic Surfactants with Different Chain Lengths. *Langmuir* **11**, 1001-1008 (1995).

98   Andersson, G., Krebs, T. & Morgner, H. Activity of surface active substances determined from their surface excess. *Physical Chemistry Chemical Physics* **7**, 136-142 (2005).

99   Prosser, A. J. & Franses, E. I. Adsorption and surface tension of ionic surfactants at the air-water interface: review and evaluation of equilibrium models. *Colloids and Surfaces A: Physicochemical and Engineering Aspects* **178**, 1-40 (2001).

100   Strey, R. *et al.* On the Necessity of Using Activities in the Gibbs Equation. *The Journal of Physical Chemistry B* **103**, 9112-9116 (1999).

101   Krebs, T., Andersson, G. & Morgner, H. Chemical Potential of a Nonionic Surfactant in Solution. *The Journal of Physical Chemistry B* **110**, 24015-24020 (2006).

102   Eastoe, J. *et al.* Adsorption of Ionic Surfactants at the Air−Solution Interface. *Langmuir* **16**, 4511-4518 (2000).

103   Li, P. X., Dong, C. C., Thomas, R. K., Penfold, J. & Wang, Y. Neutron Reflectometry of Quaternary Gemini Surfactants as a Function of Alkyl Chain Length: Anomalies Arising from Ion Association and Premicellar Aggregation. *Langmuir* **27**, 2575-2586 (2011).

104   Gilányi, T., Varga, I., Stubenrauch, C. & Mészáros, R. Adsorption of alkyl trimethylammonium bromides at the air/water interface. *Journal of Colloid and Interface Science* **317**, 395-401 (2008).

105   Ingram, B. T. Salt effects in foam films. *Journal of the Chemical Society, Faraday Transactions 1: Physical Chemistry in Condensed Phases* **68**, 2230-2238 (1972).

106   Angarska, J. K., Tachev, K. D., Kralchevsky, P. A., Mehreteab, A. & Broze, G. Effects of Counterions and Co-ions on the Drainage and Stability of Liquid Films and Foams. *Journal of Colloid and Interface Science* **200**, 31-45 (1998).

107   Micheau, C., Bauduin, P., Diat, O. & Faure, S. Specific Salt and pH Effects on Foam Film of a pH Sensitive Surfactant. *Langmuir* **29**, 8472-8481 (2013).

108   Pandey, S., Bagwe, R. P. & Shah, D. O. Effect of counterions on surface and foaming properties of dodecyl sulfate. *Journal of Colloid and Interface Science* **267**, 160-166 (2003).

109   Schelero, N., Hedicke, G., Linse, P. & Klitzing, R. v. Effects of Counterions and Co-ions on Foam Films Stabilized by Anionic Dodecyl Sulfate. *The Journal of Physical Chemistry B* **114**, 15523-15529 (2010).

110   Schelero, N. & von Klitzing, R. Correlation between specific ion adsorption at the air/water interface and long-range interactions in colloidal systems. *Soft Matter* **7**, 2936-2942 (2011).

111   Rogers, R. D. & Seddon, K. R. *Ionic Liquids IIIB: Fundamentals, Progress, Challenges, and Opportunities : Transformations and Processes*. (Oxford University Press, 2005).

112   Izgorodina, E. I., Forsyth, M. & MacFarlane, D. R. Towards a Better Understanding of 'Delocalized Charge' in Ionic Liquid Anions. *Australian Journal of Chemistry* **60**, 15-20 (2007).

113   Welton, T. Room-Temperature Ionic Liquids. Solvents for Synthesis and Catalysis. *Chemical Reviews* **99**, 2071-2084 (1999).

114   Scovazzo, P. Determination of the upper limits, benchmarks, and critical properties for gas separations using stabilized room temperature ionic liquid membranes (SILMs) for the purpose of guiding future research. *Journal of Membrane Science* **343**, 199-211 (2009).

115   Ren, W. & Scurto, A. M. Global phase behavior of imidazolium ionic liquids and compressed 1,1,1,2-tetrafluoroethane (R-134a). *AIChE Journal* **55**, 486-493 (2009).

116   Pinilla, C., Del Pópolo, M. G., Lynden-Bell, R. M. & Kohanoff, J. Structure and Dynamics of a Confined Ionic Liquid. Topics of Relevance to Dye-Sensitized Solar Cells. *The Journal of Physical Chemistry B* **109**, 17922-17927 (2005).

117   Itoh, T., Akasaki, E., Kudo, K. & Shirakami, S. Lipase-Catalyzed Enantioselective Acylation in the Ionic Liquid Solvent System: Reaction of Enzyme Anchored to the Solvent. *Chemistry Letters* **30**, 262-263 (2001).

118   Min, Y. *et al.* Measurement of Forces across Room Temperature Ionic Liquids between Mica Surfaces. *The Journal of Physical Chemistry C* **113**, 16445-16449 (2009).

119   Rivera-Rubero, S. & Baldelli, S. Influence of Water on the Surface of the Water-Miscible Ionic Liquid 1-Butyl-3-methylimidazolium Tetrafluoroborate: A Sum Frequency Generation Analysis. *The Journal of Physical Chemistry B* **110**, 15499-15505 (2006).

120   Rivera-Rubero, S. & Baldelli, S. Surface Characterization of 1-Butyl-3-methylimidazolium Br-, I-, PF6-, BF4-, (CF3SO2)2N-, SCN-, CH3SO3-, CH3SO4-, and (CN)2N- Ionic Liquids by Sum Frequency Generation. *The Journal of Physical Chemistry B* **110**, 4756-4765 (2006).

121   Santos, C. S. & Baldelli, S. Surface Orientation of 1-Methyl-, 1-Ethyl-, and 1-Butyl-3-methylimidazolium Methyl Sulfate as Probed by Sum-Frequency Generation Vibrational Spectroscopy†. *The Journal of Physical Chemistry B* **111**, 4715-4723 (2007).

122   Iimori, T. *et al.* Orientational ordering of alkyl chain at the air/liquid interface of ionic liquids studied by sum frequency vibrational spectroscopy. *Chemical Physics Letters* **389**, 321-326 (2004).

123   Law, G. & Watson, P. R. Surface orientation in ionic liquids. *Chemical Physics Letters* **345**, 1-4 (2001).

124   Lockett, V., Sedev, R., Bassell, C. & Ralston, J. Angle-resolved X-ray photoelectron spectroscopy of the surface of imidazolium ionic liquids. *Physical Chemistry Chemical Physics* **10**, 1330-1335 (2008).

125   Kolbeck, C. *et al.* Influence of Different Anions on the Surface Composition of Ionic Liquids Studied Using ARXPS. *The Journal of Physical Chemistry B* **113**, 8682-8688 (2009).

126   Maier, F. *et al.* Insights into the surface composition and enrichment effects of ionic liquids and ionic liquid mixtures. *Physical Chemistry Chemical Physics* **12**, 1905-1915 (2010).

127   Ikari, T. *et al.* Surface Electronic Structure of Imidazolium-Based Ionic Liquids Studied by Electron Spectroscopy. *e-Journal of Surface Science and Nanotechnology* **8**, 241-245 (2010).

128   Iwahashi, T. *et al.* Surface Structural Study on Ionic Liquids Using Metastable Atom Electron Spectroscopy. *The Journal of Physical Chemistry C* **113**, 19237-19243 (2009).

129   Krischok, S. *et al.* Temperature-Dependent Electronic and Vibrational Structure of the 1-Ethyl-3-methylimidazolium Bis(trifluoromethylsulfonyl)amide Room-Temperature Ionic Liquid Surface: A Study with XPS, UPS, MIES, and HREELS†. *The Journal of Physical Chemistry B* **111**, 4801-4806 (2007).

130   Höfft, O. *et al.* Electronic Structure of the Surface of the Ionic Liquid [EMIM][Tf2N] Studied by Metastable Impact Electron Spectroscopy (MIES), UPS, and XPS. *Langmuir* **22**, 7120-7123 (2006).

131   Hammer, T., Reichelt, M. & Morgner, H. Influence of the aliphatic chain length of imidazolium based ionic liquids on the surface structure. *Physical Chemistry Chemical Physics* **12**, 11070-11080 (2010).

132   Santos, C. S. & Baldelli, S. Gas-liquid interface of room-temperature ionic liquids. *Chemical Society Reviews* **39**, 2136-2145 (2010).

133   Santos, C. S. & Baldelli, S. Alkyl Chain Interaction at the Surface of Room Temperature Ionic Liquids: Systematic Variation of Alkyl Chain Length (R = C1−C4, C8) in both Cation and Anion of [RMIM][R−OSO3] by Sum Frequency Generation and Surface Tension. *The Journal of Physical Chemistry B* **113**, 923-933 (2009).

134   Gannon, T. J., Law, G., Watson, P. R., Carmichael, A. J. & Seddon, K. R. First Observation of Molecular Composition and Orientation at the Surface of a Room-Temperature Ionic Liquid. *Langmuir* **15**, 8429-8434 (1999).

135   Lovelock, K. R. J. *et al.* Influence of Different Substituents on the Surface Composition of Ionic Liquids Studied Using ARXPS. *The Journal of Physical Chemistry B* **113**, 2854-2864 (2009).

136   Endres, F. *et al.* Do solvation layers of ionic liquids influence electrochemical reactions? *Physical Chemistry Chemical Physics* **12**, 1724-1732 (2010).

137   Mezger, M. *et al.* Molecular Layering of Fluorinated Ionic Liquids at a Charged Sapphire (0001) Surface. *Science* **322**, 424-428 (2008).

138   Hayes, R., Warr, G. G. & Atkin, R. At the interface: solvation and designing ionic liquids. *Physical Chemistry Chemical Physics* **12**, 1709-1723 (2010).

139   Bresme, F. & et al. Influence of ion size asymmetry on the properties of ionic liquid–vapour interfaces. *Journal of Physics: Condensed Matter* **17**, S3301 (2005).

140   Law, G., Watson, P. R., Carmichael, A. J. & Seddon, K. R. Molecular composition and orientation at the surface of room-temperature ionic liquids: Effect of molecular structure. *Physical Chemistry Chemical Physics* **3**, 2879-2885 (2001).

141   Lynden-Bell, R. M. & Del Popolo, M. Simulation of the surface structure of butylmethylimidazolium ionic liquids. *Physical Chemistry Chemical Physics* **8**, 949-954 (2006).

142   Sloutskin, E. *et al.* Surface Layering in Ionic Liquids: An X-ray Reflectivity Study. *Journal of the American Chemical Society* **127**, 7796-7804 (2005).

143   Freire, M. G. *et al.* Surface tensions of imidazolium based ionic liquids: Anion, cation, temperature and water effect. *Journal of Colloid and Interface Science* **314**, 621-630 (2007).

144   Jeon, Y. *et al.* Structures of Ionic Liquids with Different Anions Studied by Infrared Vibration Spectroscopy. *The Journal of Physical Chemistry B* **112**, 4735-4740 (2008).

145   Restolho, J., Mata, J. L., Shimizu, K., Canongia Lopes, J. N. & Saramago, B. Wetting Films of Two Ionic Liquids: [C8mim][BF4] and [C2OHmim][BF4]. *The Journal of Physical Chemistry C*, null-null (2011).

146   Brussel, M. *et al.* On the ideality of binary mixtures of ionic liquids. *Physical Chemistry Chemical Physics* (2012).

147   Bodo, E. *et al.* Structure of the Molten Salt Methyl Ammonium Nitrate Explored by Experiments and Theory. *The Journal of Physical Chemistry B* (2011).

148   Fumino, K. *et al.* The influence of hydrogen bonding on the physical properties of ionic liquids. *Physical Chemistry Chemical Physics* (2011).

149   Kennedy, D. F. & Drummond, C. J. Large Aggregated Ions Found in Some Protic Ionic Liquids. *The Journal of Physical Chemistry B* **113**, 5690-5693 (2009).

150   Langevin, D. Polyelectrolyte and surfactant mixed solutions. Behavior at surfaces and in thin films. *Advances in Colloid and Interface Science* **89–90**, 467-484 (2001).

151   Ludwig, R. A Simple Geometrical Explanation for the Occurrence of Specific Large Aggregated Ions in Some Protic Ionic Liquids. *The Journal of Physical Chemistry B* **113**, 15419-15422 (2009).

152   Wakeham, D., Nelson, A., Warr, G. G. & Atkin, R. Probing the protic ionic liquid surface using X-ray reflectivity. *Physical Chemistry Chemical Physics* **13**, 20828-20835 (2011).

153   Niga, P. *et al.* Structure of the Ethylammonium Nitrate Surface: An X-ray Reflectivity and Vibrational Sum Frequency Spectroscopy Study. *Langmuir* **26**, 8282-8288 (2010).

154   Seddon, K. R., Stark, A. & Torres, M. J. Influence of chloride, water, and organic solvents on the physical properties of ionic liquids. *Pure Appl. Chem.* **72**, 2275-2287 (2000).

155   Smith, E. F., Rutten, F. J. M., Villar-Garcia, I. J., Briggs, D. & Licence, P. Ionic Liquids in Vacuo: Analysis of Liquid Surfaces Using Ultra-High-Vacuum Techniques. *Langmuir* **22**, 9386-9392 (2006).

156   Baldelli, S. Influence of Water on the Orientation of Cations at the Surface of a Room-Temperature Ionic Liquid: A Sum Frequency Generation Vibrational Spectroscopic Study. *The Journal of Physical Chemistry B* **107**, 6148-6152 (2003).

157   Singh, T. & Kumar, A. Cation-anion-water interactions in aqueous mixtures of imidazolium based ionic liquids. *Vibrational Spectroscopy* **55**, 119-125 (2011).

158   Jeon, Y. *et al.* Structural Change of 1-Butyl-3-methylimidazolium Tetrafluoroborate + Water Mixtures Studied by Infrared Vibrational Spectroscopy. *The Journal of Physical Chemistry B* **112**, 923-928 (2008).

159   Moreno, M., Castiglione, F., Mele, A., Pasqui, C. & Raos, G. Interaction of Water with the Model Ionic Liquid [bmim][BF4]: Molecular Dynamics Simulations and Comparison with NMR Data. *The Journal of Physical Chemistry B* **112**, 7826-7836 (2008).

160   Hanke, C. G. & Lynden-Bell, R. M. A Simulation Study of Water−Dialkylimidazolium Ionic Liquid Mixtures. *The Journal of Physical Chemistry B* **107**, 10873-10878 (2003).

161   Bernardes, C. E. S., Minas da Piedade, M. E. & Canongia Lopes, J. N. The Structure of Aqueous Solutions of a Hydrophilic Ionic Liquid: The Full Concentration Range of 1-Ethyl-3-methylimidazolium Ethylsulfate and Water. *The Journal of Physical Chemistry B* **115**, 2067-2074 (2011).

162   Reichelt, M., Hammer, T. & Morgner, H. Influence of water on the surface structure of 1-hexyl-3-methylimidazolium chloride. *Surface Science* **605**, 1402-1411 (2011).

163   Rilo, E., Pico, J., García-Garabal, S., Varela, L. M. & Cabeza, O. Density and surface tension in binary mixtures of CnMIM-BF4 ionic liquids with water and ethanol. *Fluid Phase Equilibria* **285**, 83-89 (2009).

164   Lauw, Y. *et al.* X-Ray reflectometry studies on the effect of water on the surface structure of [C4mpyr][NTf2] ionic liquid. *Physical Chemistry Chemical Physics* **11**, 11507-11514 (2009).

165   Rivera-Rubero, S. & Baldelli, S. Influence of Water on the Surface of Hydrophilic and Hydrophobic Room-Temperature Ionic Liquids. *Journal of the American Chemical Society* **126**, 11788-11789 (2004).

Chapter 2

Experimental

2.1   Neutral impact collision ion scattering spectroscopy

2.1.1   Background

Ion scattering spectroscopy (ISS, also known as low energy ion scattering, LEIS) is a technique that uses the interaction of ions with matter to gain structural and compositional information of the target. These interactions range from electronic interactions, to kinetic energy transfer, and removal of surface atoms via sputtering. A number of different ion scattering methods are listed in Table 2-1.

ISS was originally developed by Smith in 1967 with the purpose of obtaining compositional information of solid surfaces.[11] However the neutralisation probabilities of the rare gas ions used in an ISS experiment are sensitive to such a large range of conditions that they cannot be calculated to a sufficient degree of accuracy. Instead it was discovered that by analysing the recorded spectra in terms of the shadowing and blocking effects of the surface atoms on the projectiles, that qualitative structural information of solid surfaces could be obtained.[12] Aono et al. improved on the technique with impact collision ion scattering spectroscopy (ICISS).[5] While ISS detects scattered ions at an arbitrary angle, ICISS sets the angle of observation close to 180° which allows for the detection of ions that have made a head-on collision, thereby nullifying the previously unknown impact parameter and allowing for quantification. The high neutralisation probability in ISS and ICISS was overcome by Niehus and Cosma who modified the technique for the detection of backscattered neutrals (NICISS), significantly increasing the amount of signal. Additionally this change allowed information to be gained from the second layer of the target, further improving the structural information gained from the experiment.[4] A decade later Andersson and Morgner discovered that when used on soft-matter surfaces NICISS gave profiles similar to that seen in high energy and medium energy ion scattering (HEIS, MEIS) experiments, and discovered the ability of NICISS to determine the concentration depth profiles of the elements in soft-matter surfaces when no

Table 2-1. Different methods of ion scattering spectroscopy, which utilise differences in probing techniques and what they detect to gain different information about surfaces.

Method	Probe	Detection	Information
Low energy ion scattering (LEIS) [1,2]	Rare gas ions, kinetic energy 1 – 10 keV	Backscattered ions (between 90° and 180°)	Elemental composition of the outermost layer
Alkali ion impact collision ion scattering spectroscopy (ALICISS) [3,4]	Alkali ions, kinetic energy 1 – 10 keV	Backscattered ions	Elemental composition and structure of the outermost layer
Impact collision ion scattering spectroscopy (ICISS) [4,5]	Rare gas ions, kinetic energy 1 – 10 keV	Backscattered ions	Elemental composition of the outermost layer and structure of crystalline surfaces
Neutral impact collision ion scattering spectroscopy (NICISS) [4,6]	Rare gas ions, kinetic energy 1 – 10 keV	Backscattered neutrals	Concentration depth profiles of elements (soft matter) and structure of crystalline surfaces
Direct recoil spectroscopy (DRS) [7,8]	Rare gas ions, kinetic energy 1 – 10 keV	Recoil fragments ejected from the surface from projectile energy transfer	Composition of the outermost layer
Rutherford Backscattering (RBS) [9,10]	Ions (varying on type of experiment), kinetic energy 1 – 10 MeV	Backscattered ions	Concentration depth profiles of elements in crystalline and non-crystalline targets

longer range order exists in the sample.[6,13]

A brief overview of the NICISS technique for concentration depth profiling will be given here, with a more detailed explanation of processes to follow in chapter 2.1.2. A pulsed beam of ions is directed at the target. When inert gas ions are used, their high cross-section for neutralisation will lead to them being neutralised within a few Å of the surface. These projectiles then penetrate through the target until they collide with a target atom. If the mass of the target atom is greater than the mass of the projectile, the projectile may be backscattered (scattering angle, $\theta > 90^o$). The projectile experiences two modes of energy loss through its trajectory in the target: 1) a single energy loss due to the collision process which is proportional to the mass of the target atom and 2) a large number of small energy losses experienced on the projectile's trajectory to and from the target that can be treated as a continuous energy loss proportional to the length of the total trajectory (known as the stopping power). Therefore by knowing the initial energy of the projectiles (primary energy of the ion beam) and measuring the final energies of the backscattered projectiles, it is possible to determine what element the projectile collided with and how deep into the target this collision took place. NICISS utilises the detection of neutrals primarily to avoid complications related to the neutralisation of the projectiles. Helium is primarily used as the projectile as i) the requirement for the detection of neutrals leads to the necessity of using elements with high cross-sections for neutralisation (i.e. rare gasses), ii) the condition for backscattering means that heavier gasses (e.g. Ne) would result in no backscattering from lighter elements such as carbon, nitrogen and oxygen, and iii) the projectiles sputter hydrogen from the sample and heavier gasses increase the rate of sputtered hydrogen to the point where this signal dominates the spectra.

2.1.2 NICISS theory

Elastic energy loss in the backscattering process

The elastic component of the energy transfer between the projectile and target atoms can be approximated from the laws of conservation of momentum in a single collision system, where Figure 2-1 shows a basic schematic of the elastic scattering process for two particles.
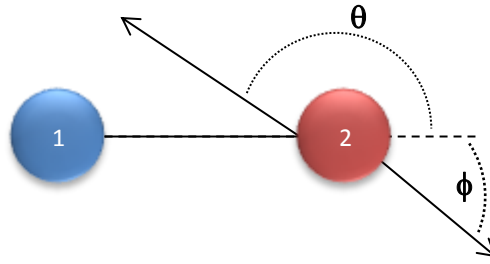
Figure 2-1. Schematic of the elastic scattering process.

For the interaction $1 + 2 \rightarrow 3 + 4$, where 1 and 3 have the same mass, m_1, and 2 and 4 have the same mass, m_2, and given momentum, $p = mv$, where v is velocity, conservation of momentum leads to the equations

$$p_1 = p_3 \cos\theta + p_4 \cos\phi$$

$$p_3 \sin\theta = p_4 \sin\phi$$

Eq. 2-2

where θ and ϕ denote the scattering angles of particle 1 and 2 respectively (as seen in Figure 2-1). These two equations simplify to

$$p_1^2 - 2p_1 \, p_3 \cos\theta + p_3^2 = p_4^2$$

Eq. 2-3

Given that kinetic energy, $E = \frac{1}{2}mv^2$, conservation of energy in the system gives

$$E_1 = E_3 + \frac{p_1^2 - 2p_1 \, p_3 \cos\theta + p_3^2}{2m_2}$$

Eq. 2-4

which can be simplified to a quadratic equation for $\sqrt{E_3}$, where the physically relevant solution for E_3 is given by

$$E_3 = E_1 K, \text{ where}$$

$$K = \frac{\left[\cos\theta + \sqrt{A - \sin^2\theta}\right]^2}{(1 + A)}$$

Eq. 2-5

where E_3 represents the final energy of the projectile, E_1 the initial energy of the projectile and A is m_2/m_1. Given that the initial energy is known, the mass of the projectile is known,

and the projectile scattering angle (θ) is known by setting the angle of the detector, once the final energy of the projectile is determined via the detector, the mass of the target atom is the only unknown and can hence be determined from equation Eq. 2-5.

Inelastic energy loss

During the close approach and collision of the projectile atoms with the atoms constituting the target, an amount of energy can be transferred between the kinetic energy of the projectile and the electrons in both the projectile and target. This energy loss is significant for both the collision/backscattering process and also the continuous energy loss experienced by the projectile on its trajectory in the target. The energy loss of He^+ scattered from solid surfaces has been measured experimentally and is seen as a peak of finite width whose area is skewed to the low energy side.[14] In terms of NICISS data evaluation the inelastic contribution to stopping power can be accounted for by measuring the energy loss of He^+ through layers of well-defined thickness, as discussed in the following section on 'stopping power and energy loss straggling'. The inelastic contribution to the collision process, caused mainly by electronic excitations between the projectile and target atoms,[15] leads to the energy loss from the elastic collision being convoluted by the range in inelastic energy losses and can be accounted for in the data evaluation with a modified equation Eq. 2-5.

$$E_f = E_0 K - Q_{in}$$

Eq. 2-6

where E_f is the final energy of the projectile, E_0 is the initial energy, K is the factor from equation Eq. 2-5, and Q_{in} is the mean inelastic energy loss from the collision process. Q_{in} (and the range in energy loss due to backscattering from a single element) can be measured experimentally by measuring the NICIS spectra of elements in a low density gas phase. If the density of the gas is low enough it can be safely assumed that the recorded spectrum from an element will not have any energy loss due to stopping power, and thus will contain a single peak for every element, where the mean position of the peak represents Q_{in} and the shape of the peak can be used to deconvolute the energy loss spectra. The setup for this experiment is discussed in section 2.1.4.

Stopping power and energy loss straggling

As mentioned previously the stopping power is a measure for how much energy a projectile loses while passing through matter. The stopping power has two contributors:

small angle scattering of the projectile from nuclei in the target, known as the nuclear stopping power; and electronic excitations (such as the neutralisation processes discussed in section 2.2.3), known as the electronic stopping power. The nuclear stopping power is the dominant contributor at low energies. While the stopping power consists of many different single events that can themselves be quantified, it is more common to treat these processes as a single, continuous energy loss per layer (of defined density) or per length of trajectory. Given the statistical probability of these events occurring there is a statistical spread to the stopping power, meaning that a stream of monoenergetic projectiles passing through a layer of constant density and composition will experience a range in their energy losses. This spread in stopping power energy loss is known as the energy loss straggling.[16]

Andersson and Morgner have experimentally determined the energy loss of He^{+} due to stopping power in organic samples by recording spectra of self-assembled alkanethiolate monolayers on silver and gold substrates.[17] By comparing the spectra of the bare substrate to that of the covered substrate allows for the quantification of the stopping power. Additionally, they altered the angle of observation and found that the stopping power was reduced when the angle of observation was approximately parallel to the orientation of the alkyl chain. They concluded that this was further proof of the nuclear contribution to the total stopping power being dominant at low energies.

Andersson et al. have also experimentally determined the range of energy loss straggling of He^{+} projectiles passing through organic samples at low energies.[18,19] In order to properly evaluate the straggling, a signal from an element must be measured where both the rising and falling edges of the signal can be observed. This is not the case with the monolayers on a solid substrate, where the signal of the substrate dominates the falling edge of the monolayer signal. Instead the energy loss straggling was determined by measuring spectra of surfactant solutions. In that case, the signal being measured comes from the surfactant (e.g. tetrabutylammonium iodide in their study), while the energy loss straggling comes from the energy loss of the projectiles passing through the vapour phase adjacent to the liquid phase. Controlling the temperature of the solution allows for control over the density of the vapour phase. Andersson proposed a method for accounting for the energy loss straggling that repetitively convoluted a spectrum from a lower vapour pressure measurement to fit a measurement from a higher vapour pressure.[19] Soon after Pezzi et al. proposed a method of accounting for the statistical fluctuations in the energy

losses in a medium energy ion scattering experiment, describing the statistical range with Poisson statistics.[20] Andersson et al. then proposed a similar treatment for use in deconvoluting NICIS spectra.[18] This approach is similar to the original, but is simplified practically making it preferable for use in deconvoluting NICIS spectra.

Data evaluation

Figure 2-2 shows the components of a NICIS spectrum as seen on the time-of-flight (TOF) scale for a sample of a surfactant (hexadecyltrimethylammonium bromide) in glycerol. NICIS spectra consist of three main components: i) backscattered projectiles of different energies that appear as the steps for each element, ii) a broad background due to the detection of sputtered hydrogen over a broad range of energies, and iii) a photon peak. The photon peak is the result of photons being generated as part of the interactions of the ion beam with matter,[21] and allows for the determination of the zero-mark on the TOF scale. The hydrogen background is a smooth curve and can be subtracted from the step of each element by fitting a low-order polynomial equation to both sides of a step.[6]

NICIS spectra are measured as TOF spectra of the backscattered neutrals, where the TOF is related to the energy loss of the projectiles by [6]
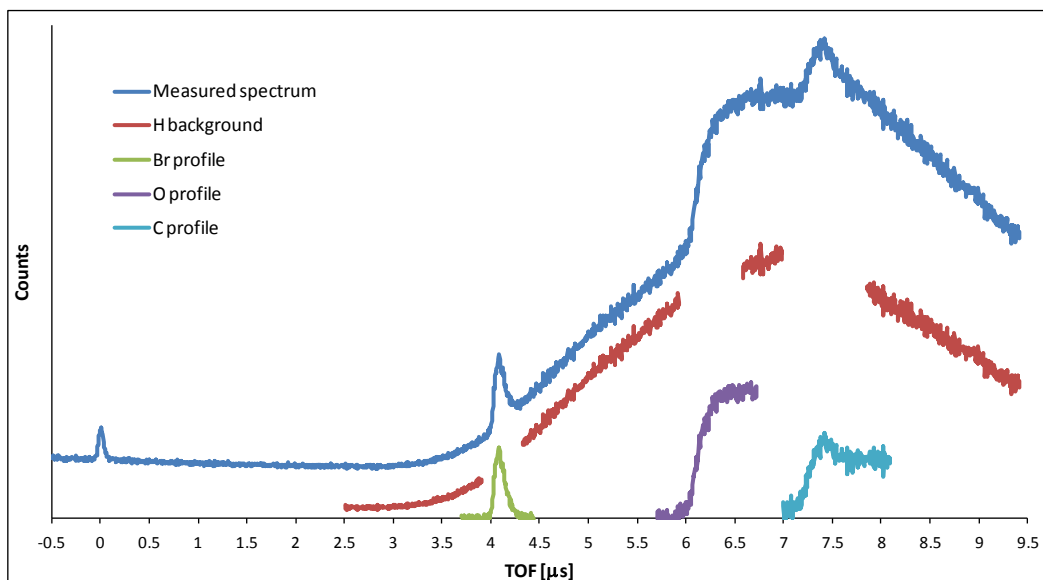
Figure 2-2. Data evaluation of a NICIS TOF spectrum where the measured spectrum, hydrogen background, photon peak, and individual steps of the elements are shown.

$$I(E) = I(t)\frac{dt}{dE}\frac{1}{d\sigma/d\Omega(E)}\frac{1}{\det(E)}$$ **Eq. 2-7**

where I represents the intensity of a spectrum, t is the TOF, E is the energy, $d\sigma/d\Omega(E)$ is the differential cross section, and $\det(E)$ is the detector sensitivity. The differential cross section indicates that the concentration depth profile for each element must be calculated separately, while the factor dt/dE indicates the non-linear relationship between TOF and energy loss. The energy loss spectrum can then be converted into a concentration depth profile for an element by

$$I(d) = I(E)\frac{dE}{dz}f_c$$ **Eq. 2-8**

where z is the depth, and f_c is a factor for converting the amount of detected projectiles to a concentration value, which can be determined knowing the molar mass and density of the sample. The ratio between the energy scale and depth scale is calculated by [6,17]

(1)
$$E_{i,in} = E_{i-1,in} - \frac{\Delta z}{\cos(\alpha + \psi)S_P(E_{i,in})}$$

For i = 1 ... n, with $z = n\Delta z$ and $E_{0,in} = E_0$

----

(2) $$E_{0,out} = E_{n,in}K - Q_{in}$$ **Eq. 2-9**

----

(3)
$$E_{j-1,out} = E_{j,out} - \frac{\Delta z}{\cos(\alpha)S_P(E_{i,in})}$$

For j = n ... 1

where $E_{i,in}$ is the energy in layer i on the ingoing trajectory (with layer $n = 1$ being the outermost layer), Δz is an increment on the depth scale, α is the angle between the surface normal and the detector, ψ is the angle between the ion beam and the detector, S_P is the stopping power, K is the factor from equation Eq. 2-5, and Q_{in} is the inelastic energy loss in the collision process (Eq. 2-6). The depth scale is therefore calculated from 3 energy loss processes: (1) the energy lost via stopping power on the ingoing trajectory, (2) the energy loss from the collision/backscattering, and (3) the energy loss on the outgoing trajectory. The stopping power of a compound is calculated from the stopping power of

elements using Bragg's rule.[22] A NICIS spectrum is therefore converted to concentration depth profiles of the elements by:

1. Isolating the step of an individual element from the total TOF spectrum. E.g. Figure 2-2 shows the isolation of the iodide step between 3.7 and 4.5 μs.

2. Subtraction of the hydrogen background by fitting a low-order polynomial to both sides of the element's step on the measured spectrum.

3. Converting the TOF step for each element for a concentration depth profile using equations Eq. 2-7, Eq. 2-8, and Eq. 2-9.

Deconvolution of measured spectra

In the case where exact details of the concentration depth profiles are needed, a further step can be taken in the data evaluation which involves deconvoluting the concentration depth profiles. Apart from the concentration depth profile itself, the shape of the step for a given element is influenced by: i) the finite time length and spread in primary energies of each ion beam pulse, ii) the spread in inelastic energy losses during the backscattering event, iii) thermal broadening due to the thermal motion of atoms, iv) the energy loss and straggling of the projectiles on their way towards the target atom, and v) energy loss and straggling of the projectiles after backscattering, on their way out from the surface. The influence of thermal broadening can be calculated if the masses of the projectile and target atoms are known and the energy of the projectiles are known, and this broadening is small compared to the spread in inelastic energies in the backscattering process.[23] The first two influences are independent of depth at which the backscattering occurs and can be considered as a single function, E_{gas}, while the last two influences are similar influences and can be considered together in a single function, E_{strg}. A NICIS spectrum for an element on the energy scale can be considered as a convolution, F_{conv}, of the gas phase spectrum of that element with a hypothetical spectrum where E_{gas} is neglected. Additionally, the influence of E_{strg} can be considered as a convolution, F_{strg}, where this convolution is dependent on the energy loss and therefore depth from which the projectile was backscattered. Convoluting F_{gas} with F_{strg} therefore gives the function, $F_{E\text{-Loss}}$, which takes into account the spread in inelastic energies in the backscattering process, but also how the straggling affects the spread in energies as a function of depth. The practical method of deconvoluting a spectrum involves fitting a function, F_{decon}, to the measured spectrum by convoluting F_{decon} with $F_{E\text{-Loss}}$. The genetic algorithm is used as a fitting

procedure which allows for a large number of starting parameters to be taken into account, where the standard deviation of the convoluted F_{decon} functions from the measured spectrum gives the uncertainty of the final fit.[18]

2.1.3   Experimental setup

A schematic illustration of the NICISS setup is shown in Figure 2-3, and pictured in Figure 2-4. The ion source is a Leybold-Heraeus 12/38 that contains the ionisation chamber, deflections plates (1) and focussing elements. A Wien filter (SPECS, Berlin) is added for mass selection of ions, while an additional set of electrostatic deflection plates (2) were made at the electronic and mechanical workshops at Flinders University. Gas is
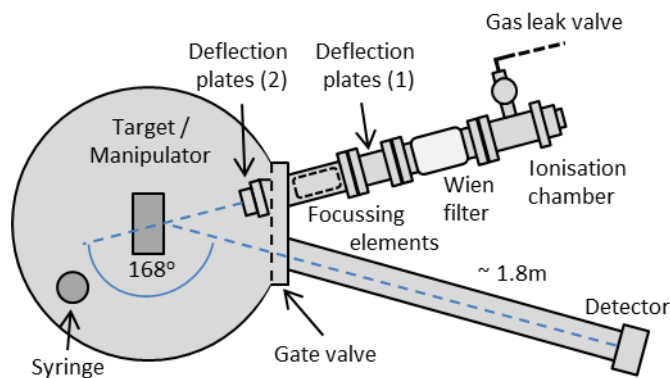
Figure 2-3. NICISS schematic (top down view).
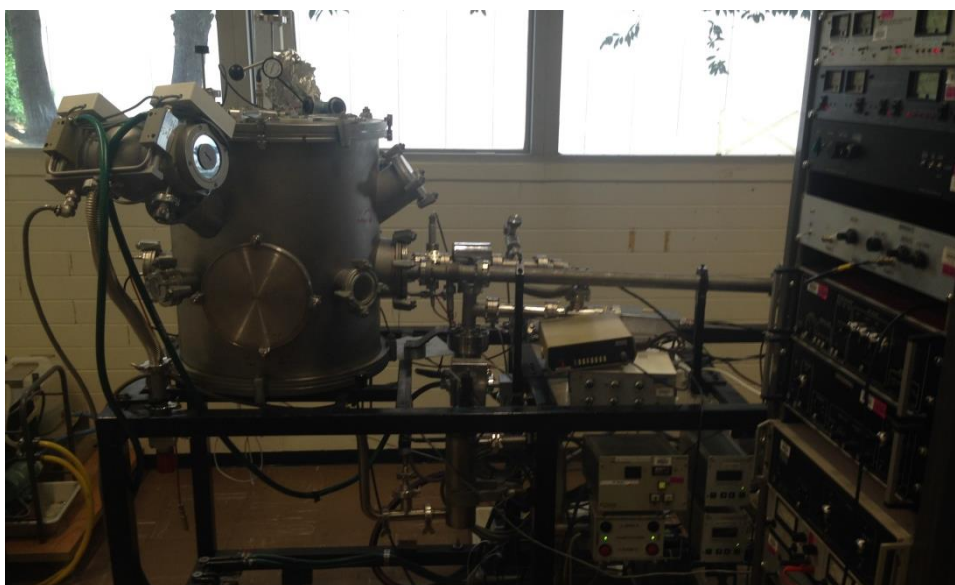
Figure 2-4. Picture of the NICISS setup at Flinders University (taken circa January 2013).

introduced into the ionisation chamber via a leak valve, where it is ionised via electron impact. The ions are then driven out of the ion source and into the Wien filter, which uses a constant magnetic field and variable electrostatic field to selectively pass ions of a chosen mass to ensure purity of the ion beam. The Wien filter also contains a pair of electrostatic deflection plates (stigmator) that allows for the correction of any astigmatism in the beam. The focussing elements consist of two pairs of semi-cylindrical plates that allow for focussing of the ion beam. The original deflection plates (1) allow for the scanning of the ion beam in the vertical (Y) and horizontal (X) plane of the sample, whose normal is in the same plane as the trajectory of the ion beam.

Pulsing of the ion beam was originally achieved by adding a pulsed voltage supply to the Wien filter (Y) and stigmator (X) which drove the beam in a rectangle, where one long side (Y) of the rectangle passed over a small aperture (approximately 1 mm diameter). The duration of the ion beam pulses were therefore governed by the rising time of the Y pulse. This lead to some practical problems during operation and eventually a new design for pulsing was implemented. This involved using the original electrostatic deflection plates (1) for the pulsing of the ion beam. A new set of electrostatic deflection plates (2) were then installed to allow for the scanning of the pulsed or un-pulsed ion beam over the target. The current setup uses a pulse width of approximately 20 ns and a repetition rate of approximately 56 kHz.

A target was needed for the observation of the ion beam for focussing purposes, and it was noted that potassium bromide could be suitable for this purpose.[24] A saturated aqueous solution of KBr was prepared, and then a few drops of this solution placed on the roughened surface of a stainless steel plate (approximately 15x15 mm, 1 mm thick). The plate was placed on a heating mantle and heated up to allow the water to evaporate, leaving a crust of KBr stuck to the surface of the plate. The plate was placed onto the solid sample holder (as described in section 2.1.4) in the NICISS main chamber, which is electrically isolated save for a monitor to observe the current on the sample. It was discovered that if the KBr layer was thicker than approximately a mm that it would be prone to charging, causing the beam to become misdirected at the surface. However, scraping the KBr off the surface, leaving a fine powder on the plate, was sufficient to observe the beam while avoiding charging. Later on a powder of unknown composition was acquired which was previously used to tune the spot size in an XPS setup. This powder proved to be more luminescent under ion beam excitation and less prone to

charging than the KBr, and was therefore used for all subsequent focussing of the ion beam.

2.1.4 Targets

A few different target units were necessary to perform measurements on a variety of different sample types. All these units were designed and constructed with the assistance of the Flinders University CAPS mechanical and electronics workshop, unless otherwise specified.

(A)   **(B)**   **(C)**
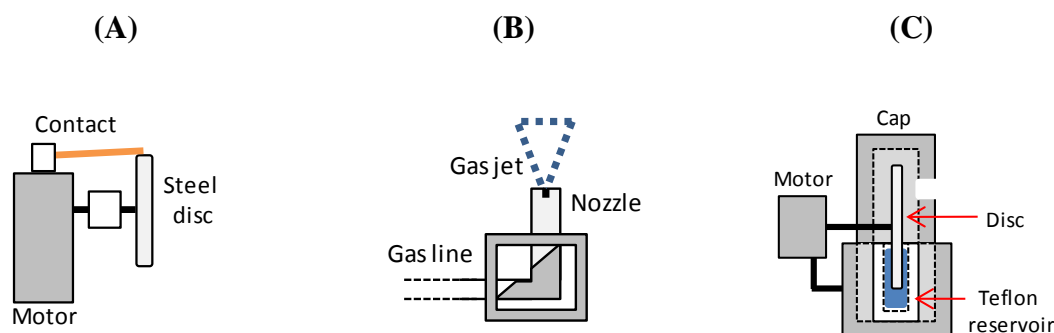
Figure 2-5. NICISS sample targets (side view). (A) Solid sample holder consisting of an electrically isolated, rotating steel disc; (B) Gas phase target where a gas can be introduced into the chamber via a leak vale; and (C) Liquid sample target where the rotating steel disc is immersed into a reservoir containing the liquid.

Manipulator unit

The NICISS main chamber contains a manipulator unit with a sample stage that allows for various targets to be attached. The manipulator unit can move along the horizontal axis for approximately 50 mm and the vertical axis for approximately 100 mm.

Solid sample holder

The solid sample holder (Figure 2-5 (A)) consists of a flat, steel disc 40mm in diameter. The disc is connected to a stepper motor allowing for rotation of the disc at a variety of different speeds as set by an external control unit. The disc is connected to the motor via a ceramic cylinder, such that the disc itself is electrically isolated. An external picoammeter is connected to the disc via a copper contact, allowing for the observation of current (due to the incident ion beam) on the disc. Solid samples can be attached to the disc via screws or the use of vacuum-safe adhesive tape (e.g. Copper tape). Although damage from the

incident ion beam is small, this effect can be further minimised by targeting the ion beam in the centre of the disc/sample, with the disc rotating. After an amount of time, the manipulator can be raised (~ 1-2 mm) allowing the beam to scan over a different 'ring' of the sample that had not previously been targeted with the ion beam.

Liquid target

The liquid target used in the NICISS experiments (Figure 2-5 (c)) is similar to the one used by Andersson and Morgner in the original NICISS investigations of concentration depth profiles.[6] It involves a flat, steel disc which is partly immersed into a reservoir containing the liquid under investigation. The disc is connected to a stepper motor allowing for the rotation of the disc at various speeds. As the disc rotates through the reservoir, a thin film of the liquid (several tenths of a millimetre) is left on the disc allowing for the investigations of a continuously refreshed liquid surface. Additionally, this unit can be encased in an air-tight cell, with the only opening being a small aperture (diameter 3 mm) in front of the disc, allowing for the access of the ion beam and exit of backscattered projectiles. The reason for encapsulation is such that as the chamber becomes evacuated for measurement, the inside of the cell becomes saturated at the vapour pressure of the solvent, where the loss of vapour to the outside of the cell is minimised by the small size of the aperture. This minimises liquid loss, due to evaporation of liquids with a vapour pressure higher than the base pressure of the evacuated chamber, while also protecting the chamber from any splashing of liquids experienced during evaporation.

Gas phase target

The gas phase target consists of a metal nozzle with a small opening (0.75 mm) for the exit of the gas. The gas is generally generated by exposing an amount of the suitable liquid with a high vapour pressure to vacuum, allowing it to vaporise. A small amount of the liquid is placed into a beaker, which is stored in a small chamber that is connected to the main chamber via a leak valve. A Teflon hose then connects the leak valve to the nozzle. The valve is opened slightly to allow for evacuation of the chamber, and then can be opened more for an appropriate level of gas flow from the sample. It is important in the measuring of the gas phase spectra that the distance between the detector and the target atom is known to within a few mm, hence it is necessary to restrict the gas flow such that the solid angle of the 'gas cone' escaping the nozzle is kept to a minimum, which allows

for the distance of the detector to the nozzle aperture to be used as the detector-target distance. The position of the nozzle is calibrated by use of the non-pulsed ion beam (to maximise backscattered intensity) to find the position immediately above the nozzle aperture. The manipulator is scanned horizontally to find the middle of the nozzle (given that the intensity either side of the nozzle will be dark counts, a few counts/second compared to a few thousand counts/second from the metal nozzle). Once the middle of the nozzle is found, the manipulator is lowered until the count rate drops to around 10% of the signal from when the beam is incident on the metal nozzle. This indicates that the vast majority of the beam is above the nozzle aperture, but not so far above that the expansion of escaping gas can significantly influence the target-detector distance. The width of the gas jet can be investigated by scanning the manipulator horizontally and monitoring the count rate.

Foam film target

The foam film target for NICISS uses a similar principle for generation and measurements of films as used in the thin film pressure balance (TFPB) discussed in section 2.3. A film holder (Figure 2-6) consists of a microporous glass disc (usually porosity 4) with an open glass capillary fused to the back, and a small aperture drilled through the disc away from the capillary. The film holder is placed in a beaker containing the solution such that the porous disc is fully submerged. The solution soaks through the disc and fills into the attached glass capillary. When the film holder is removed, a film of the solution remains, spanning the aperture. The film holder is then placed inside an enclosed pressure cell (Figure 2-7) where the only opening is an aperture on the front cover of the cell. A small amount of the solution is coated on the inside walls of the cell, so that when the main chamber is evacuated, this solvent evaporates, saturating the inside of the cell with the vapour of the solution, minimising evaporation from the foam film itself.[25]

Figure 2-6. Picture of a film holder used in the NICISS foam film experiments.
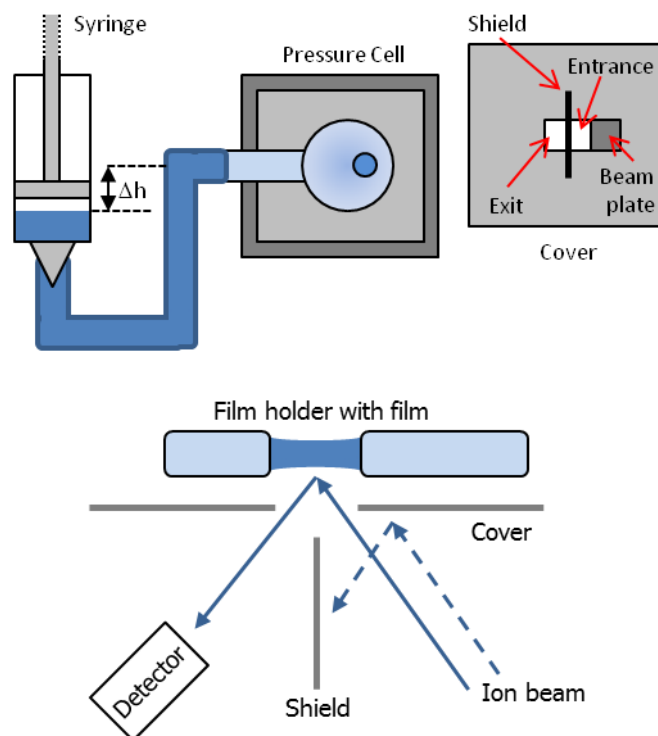
Figure 2-7. Schematic illustration of the latest foam film target (top). The film holder is connected to the reserve solution in the syringe by tubing. The cover attaches to the pressure cell and once the film holder is aligned, only the film over the aperture is seen through the front cover slit. Top down view of the foam film target (bottom) which displays the alignment with the ion beam.

For a source of an infinite supply of gas, the Knudsen flow can be used to calculate the pressure along a straight line through the axis, which is given by [26]

$$P(z') = (0.5P_0)\left(1 - \frac{z'}{(1 + z'^2)^{0.5}}\right)$$ **Eq. 2-10**

Figure 2-8 shows the pressure along the axis through the aperture as given by the Knudsen flow. Given that the normalised pressure returns to unity at 10mm, this is the distance that the film holder sits back from the front cover, which ensures that the local film environment is held at the vapour pressure of the solvent.
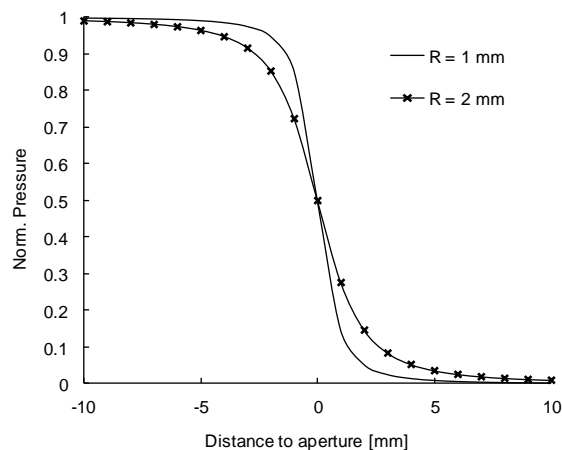
Figure 2-8. Normalized pressure through the aperture. Negative values of z indicate the inside of the pressure cell, i.e., towards the target.

The condition regarding the infinite supply of gas can be checked by comparing the volumetric flow through the aperture with the evaporation rate of glycerol. The volumetric flow, S_A, is given by [26]

$$S_A = R^2\sqrt{\pi kT/2M}$$ **Eq. 2-11**

where R is the aperture radius, k is the Boltzmann constant, T is the temperature, and M is the molecular mass. The evaporation rate of glycerol (the main solvent used for the NICISS foam film investigations) was measured by exposing a known mass of glycerol, with a known surface area, to vacuum for a controlled amount of time. From these measurements it was determined that at the vapour pressure of glycerol, the evaporation from the film is 2.0×10^{-10} mol/sec, while the flow given by Eq. 2-11 is 1.9×10^{-11} mol/sec. Hence the supply of glycerol vapour is greater than what is lost as flow through the aperture, validating the condition of an infinite supply of gas in the Knudsen equation.[25]

One result of the film holders sitting 10mm back from the apertures is that the He projectiles must travel through the vapour of the solvent before hitting the film, resulting in signal from projectiles backscattered from the solvent in the vapour phase, as well as an additional energy loss of the projectiles as they travel in and out of the vapour phase on their way to the film. Using the ideal gas law the molar densities for the liquid and gas phases are given by [25]

$$D_{gas} = \frac{n}{V} = \frac{P_{vap}}{RT} \quad \text{and} \quad D_{liq} = \frac{n}{V} = \frac{\rho}{M} \qquad \textbf{Eq. 2-12}$$

where D is the molar density, n is the molar amount, V is volume, P_{vap} is the solvent's vapour pressure, R is the universal gas constant, T is the temperature, ρ is the density of the solvent, and M is the molar mass. From these equations, the amount of vapour the projectiles pass through can be given as an equivalent liquid layer thickness, L, by [25]

$$L = \frac{D_{gas}}{D_{liq}} z \qquad \textbf{Eq. 2-13}$$

where z is the distance from the surface of the film to the aperture on the pressure cell cover. Table 2-2 gives the equivalent liquid layer thicknesses for two solvents that are suitable for use in NICISS experiments.

Table 2-2. Equivalent liquid layer thicknesses for two solvents given a path length of 10mm and temperature of 293K. P_{vap} is the vapour pressure and ρ_{liquid} is the liquid density.[25]

Liquid	P_{vap} @ 293K [Pa]	ρ_{liquid} [g/cm^3]	Thickness [Å]
Formamide	2.50	1.133	4.08
Glycerol	0.0114	1.261	0.034

The pressure cell is designed such that the vast majority of detected projectiles are backscattered from the film itself. This is achieved by having the entrance and exit apertures on the front cover of the cell being slightly smaller than the radius of the ion beam, ensuring that very little (or none) of the surrounding film holder is hit with the ion beam. This results in the part of the cover (around the aperture) being seen by the ion beam, however any signal received from this can be blocked by the use of a shield that essentially bisects the aperture on the front cover of the pressure cell, as shown in Figure 2-7 (bottom).

The length of the shield was calculated trigonometrically given the distances and angle between the ion beam and TOF viewing path.[25] The effectiveness of the shield was tested by placing a solid target in the pressure cell (in most cases, a dry film holder covered in aluminium foil) then monitoring the count rate while moving the manipulator unit up and

down, which has the effect of scanning over the aperture vertically. It was seen that the when the beam was incident only a few mm above the aperture that the count rate drops to only around 1% of the value when the beam is fully incident over the aperture. In order to position the film holder (containing a surfactant solution) correctly, a wetted film holder is placed inside the cell with no film spanning the aperture. The count rate is observed as the film holder is moved inside the pressure cell, such that when the film holder aperture is aligned with the aperture on the cell's cover, the count rate is a minimum as all projectiles pass through both apertures and do not hit a target. Once the optimum position has been found, a film is generated over the film holder's aperture by placing a drop of the surfactant solution on the aperture using a pipette. If the film does not collapse during the evacuation of the chamber, the ion beam will be incident upon the surface of the film and the count rate will be significantly increased from the previous situation. It can be further confirmed that a film is being measured as the count rate will drop back to the dark count rate upon collapse of the film. Film collapse can occur randomly during measurement, or in the case of a film that is stable for the lifetime of the measurement, can be broken afterwards using a fine needle. The return to the dark count rate of the chamber (a few orders of magnitude less than the count rate of a film) indicates that only the film itself, and none (or only a negligible portion) of the surrounding film holder is detected in these experiments.[25]

Another feature of the foam film target is the ability to apply a pressure on to the film to control its thickness. This is achieved by connecting the solution in the film holder to a solution in a reservoir, where the height difference between the level of the film and the level of the liquid in the reservoir will apply a pressure, ΔP, as given by

$$\Delta P = \rho g \Delta h$$

Eq. 2-14

where ρ is the density of the solution, g is acceleration due to gravity, and Δh is the height difference. The reserve liquid level being lower than the level of the film applies a negative pressure, or underpressure, which acts to drain liquid from the film, decreasing its thickness. The original design of the foam film target (as described by the author in reference [25]) utilised a bended-joint at the end of the film holder's glass capillary that stuck into a beaker containing the solution, where the height of the beaker could be adjusted to change the pressure. This setup was used in early experiments, however, the open system tended to generate a lot of splashing of the liquid within the main chamber

and was prone to getting bubbles form in the beaker and capillary system. An updated setup was designed where the beaker was replaced with a 20 mL syringe, where the plunger of the syringe can be controlled outside of the chamber (shown in Figure 2-7). The syringe is filled with the surfactant solution and connected via silicon tubing to the end of the film holder's capillary. The syringe allows for the solution to be pushed through the film holder, removing any bubbles and ensuring a continuous flow to the reserve solution while also allowing for height adjustment of the reserve liquid level for the application of pressure on to the film. The syringe setup can apply an underpressure on the film of up to 2 kPa.

2.2 Electron spectroscopy methods

2.2.1 X-ray photoelectron spectroscopy

X-ray photoelectron spectroscopy (XPS) is a surface sensitive technique for chemical analysis. The underlying theory is based on the principles of the photoelectric effect, originally proposed by Heinrich Hertz [27] and further explored by Albert Einstein who received the Nobel Prize in 1921 for this work.[28] The photoelectric effect describes the phenomenon of materials emitting electrons when irradiated by photons of sufficient energy, where the kinetic energy of an emitted electron is determined by the difference in energy between the incident photon and the binding energy of the material from which it was emitted. In an XPS experiment, samples are irradiated with high energy photons (in the x-ray region of the electromagnetic spectrum) of specific energy, typically using either Mg or Al Kα radiation (1253 and 1486.7 eV, respectively). This radiation is of sufficient energy to eject electrons from the core shells of the elements composing the sample, where the kinetic energy of these electrons, E_k, is given by

$$E_k = hv - E_b - \Phi_{sp} \qquad \textbf{Eq. 2-15}$$

where hv is the energy of the photon, E_b is the binding energy of the electron and Φ_{sp} is the spectrometer work function, which accounts for the work function of the detector. The chemical sensitivity of XPS is due to the fact that the binding energy of an electron is unique to the element, but also sensitive to the chemical state it is in. Therefore a scan over a range of kinetic energies will yield a spectrum consisting of a series of peaks which can be used to identify the elements in a sample along with information regarding their

chemical state. The surface sensitivity of this method is achieved due to the limited escape depth an electron can achieve at this range of excitement energies. This escape depth can be quantified by the inelastic mean free path (IMFP, also denoted λ) of the electron, which is a measure of the distance that an electron can travel without losing energy due to collisions, and is of the order of several nanometres in an organic sample.[29]

2.2.2   Ultra-violet photoelectron spectroscopy

Ultra-violet photoelectron spectroscopy (UPS) is analogous to XPS in that it utilises photons of known energy to probe chemical information of surfaces. The photons in a UPS experiment are typically from the He I line (21.2 eV) or He II line (40.8 eV). The lower energies of the photons utilised in UPS compared to XPS has two main consequences which are: i) a shorter escape depth for electrons (of only around 10 – 20 Å) and ii) only electrons of valence electron orbitals are now probed instead of the atomic core electrons as in XPS. The second consequence is the main point of utility in UPS in that it can probe molecular orbitals, i.e. the valence electrons contributing to bonds, hence its original name of 'molecular photoelectron spectroscopy' as given by its inventor, David Turner.[30,31]

2.2.3   Meta-stable induced electron spectroscopy

Meta-stable induced electron spectroscopy (MIES) is another technique capable of probing valence electrons, however, its advantage derives from probing only the outermost layer of a sample. This is achieved by replacing the photon as a probe (as in XPS and UPS) by a helium atom in the metastable (He*) state. The vast majority are in the $^3S_1$ state, which has an excitement energy of 19.8 eV. The relatively large cross sections for the deexcitation processes cause them to happen when the He* is within a few Å of the surface.[32] Figure 2-9 displays the two deexcitation processes of metastable atoms approaching a surface, namely resonance ionisation with subsequent Auger neutralisation, and Auger deexcitation, where the first process applies for metal surfaces and the latter for organic and semiconductor surfaces.[32,33] Auger neutralisation is the process that typically occurs with Auger deexcitation occurring when the former process is not possible.

(a_1) RI (a_2) AN   (b) AD
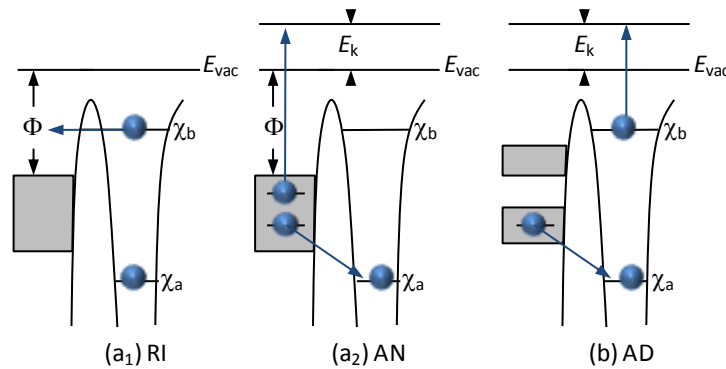
Figure 2-9. Deexcitation mechanisms of a metastable atom via resonance ionisation (a_1) followed by Auger neutralisation (a_2) and via Auger deexciation (b) on an insulator surface. Modified from Harada et al.[33]

In resonance ionisation (a_1) an electron tunnels from the excited level of the metastable atom (χ_b) to an empty level on the surface. This charge state is then neutralised via a process known as Auger neutralisation (a_2), where an electron in the surface loses energy and transitions to the empty state (χ_a) of the incoming atom. This energy is then used by another electron to be ejected from the surface with kinetic energy, E_k, given by

$$E_k = E^* - E_{bind} \qquad \textbf{Eq. 2-16}$$

where E^* is the excitation energy of the metastable atom, and E_{bind} is the binding energy of the ejected electron.[32]

2.2.4 Experimental setup

The aforementioned techniques of XPS, UPS and MIES are all housed in an ultra-high vacuum (UHV) rig designed and manufactured by SPECS, Berlin, and was commissioned in 2010. The UHV rig (pictured in Figure 2-10) consists of several different components: i) the analysis chamber, where samples are probed and analysed; ii) the detector, consisting of a hemispherical analyser (Phoibos 100, SPECS) and 6 sets of channeltrons for the kinetic energy determination of detected electrons; iii) a quadrupole mass spectrometer (QMS), for the analysis of residual gasses/contaminants in the analysis chamber; iv) a solid sample introduction chamber, which can be sealed off from the analysis chamber for separate venting; and v) a liquid sample introduction chamber, which can be sealed off from the analysis chamber. There are three probing sources: an IQE 12/38 rare gas ion source (SPECS, Berlin) for ion scattering spectroscopy or sample
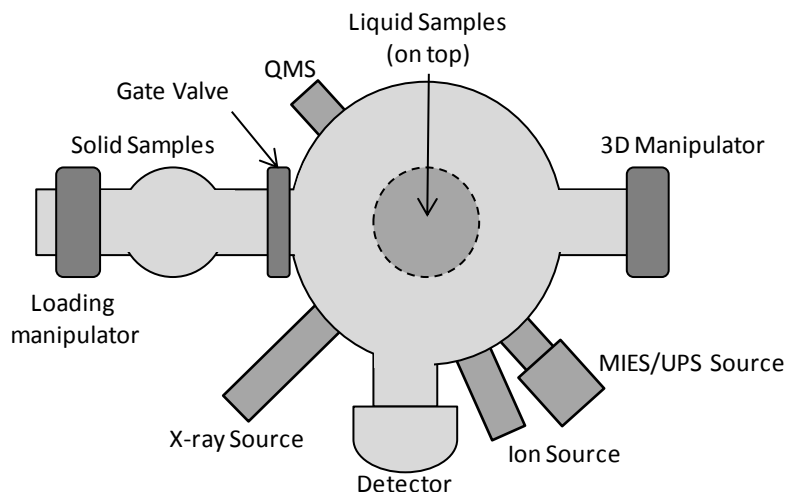
Figure 2-10. Top-down schematic of the MIES rig at Flinders University. Some additional components that were not used in this thesis are not shown.

sputtering, a non-monochromatic x-ray source (SPECS, Berlin) for Mg and Al Kα radiation, and the MIES/UPS source (MFS, Clausthal-Zellerfeld, Germany). The MIES/UPS source uses a two stage cold cathode gas discharge to simultaneously generate metastable helium (He$*^3$S$_1$) and UV light (He I line).

Solid samples (of size up to 10x10 mm) can be transferred from the solid sample loading chamber onto a 3-dimensional sample manipulator unit, which is equipped with an electrical probe to record any incident electrical current on the sample, as well as a heating unit capable of heating specifically designed molybdenum sample holders up to a few hundred degrees Celsius. The liquid sample loading chamber contains a target for liquid surfaces, similar to the rotating disc setup described in chapter 2.1.4, which was designed by SPECS (Berlin), contains a thermocouple and liquid level sensor and can hold up to 5mL of liquid. This target is mounted on a manipulator that is lowered into the analysis chamber and can be manipulated for a few centimetres in 3-dimensions as well as approximately 270° rotational manipulation around the vertical axis. Measurements are recorded using the software package, SpecsLab (SPECS, Berlin). The measurements can then be exported to commercially available software packages for further analysis or exported as simple text files that can be imported into and evaluated manually using spreadsheet software.

2.3   **Thin film pressure balance**

The thin film pressure balance (TFPB) is a technique designed for measuring surface forces in liquid films. In general, the technique involves measuring the thickness of liquid films as a function of a pressure applied on to them. If the film does not collapse at a given pressure, but instead reaches an equilibrium thickness, it can be safely assumed that the internal disjoining pressure of the film is equal to the external applied pressure. Plotting the internal disjoining pressure as a function of film thickness yields the so-called disjoining pressure curve [34,35] for a system, which can be evaluated to give various physical information about the forces that stabilise the film. The TFPB can be used to study pure liquids in the form of wetting films on a solid substrate[36], or foam films (free-standing)[37] stabilised by surfactant. The former case represents a system with liquid/solid and liquid/air interfaces interacting while the latter case represents two liquid/air interfaces.

2.3.1   TFPB theory

External pressure (such as atmospheric pressure) applied onto liquid films causes drainage of the liquid from the film and therefore a thinning of the film. This thinning of the film is eventually hindered when the two surfaces of the film are close enough to interact, where this interaction between surfaces gives rise to an internal disjoining pressure, Π, as discussed in section 1.3.1.[34,35] In a TFPB experiment, the disjoining pressure is generally given to be the sum of three main components: short-range repulsive static forces, long-range repulsive electrostatic forces, and long-range attractive van der Waals forces.[35] The contribution of these forces to the disjoining pressure is mathematically represented by:

$$\Pi(h) = \Pi_{el} + \Pi_{vdW} + \Pi_{st}$$ **Eq. 2-17**

The disjoining pressure curve shows two separate regions: one region where the disjoining pressure varies with thickness, and another region at the minimum thickness that shows a range of disjoining pressures for a single thickness. These two regions represent two types of films where the former case is known as a common black film (CBF) and the latter as a Newton black film (NBF) as discussed in section 1.3.3.[34] Electrostatic and van der Waals forces are negligible in NBFs while steric (and other short-range structural forces) forces dominate. Therefore while a CBF will change in thickness depending on the disjoining pressure, a NBF will have a set thickness for a given system. The electrostatic and van der

Waals forces are typically treated using DLVO theory, whereby the van der Waals forces are approximated for a layered system by [35]

$$\Pi_{vdW} = -\frac{A}{6\pi h^3}$$

Eq. 2-18

where h is the film thickness, and A is the non-retarded Hamaker constant which accounts for the interaction potential between the two surfaces and is known for a wide range of systems.[38] The electrostatic forces are given by [38]

$$\Pi_{el} = 64RTc \tanh^2\left(\frac{F\psi_0}{4RT}\right)\exp(-\kappa h)$$

Eq. 2-19

where R is the universal gas constant, T is the temperature, c is the concentration of charges, F is the Faraday constant, ψ_0 is the surface potential, and κ^{-1} is the Debye length. The disjoining pressure curves are typically fitted using this DLVO approach, where the concentration of charge (e.g. electrolyte) and the Hamaker constant are constant in the system, and the surface potential is used as the fitting parameter. The charge distribution in the film (and Debye length by association) is based on the electric double layer model and as such is subject to any limitations of the model itself.[39-41]

2.3.2 Experimental setup
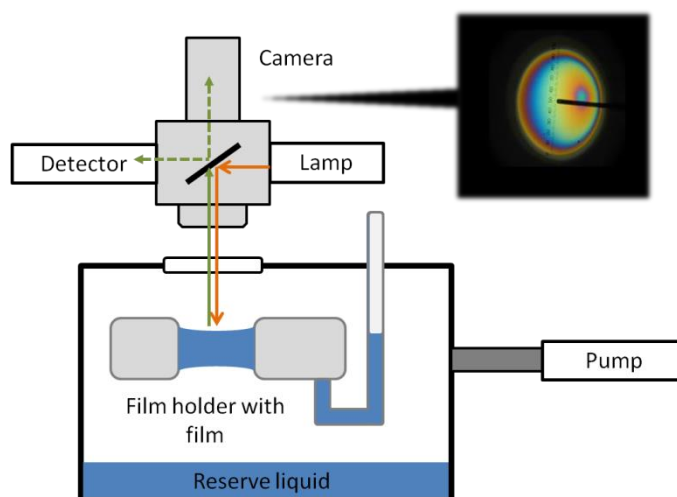
Figure 2-11. Schematic illustration of the TFPB setup.

The TFPB uses a porous glass film holder (similar to the one described in section 2.1.4 'Foam film target') to generate a film. The film holder is placed inside a cell where the gas pressure can be controlled via a pump. A small reserve of the solution is placed inside the cell to ensure a saturated atmosphere of the solvent vapour. The film that is formed over the aperture of the film holder can be viewed through a window on the top of the cell. White light of known intensity is directed at the film, and the intensity of reflected light is recorded by a spectrophotometer while the visual image of the reflected light from the film can be captured using a camera. When a positive pressure is applied onto the film, it begins to decrease in thickness, leaving a profile of varying thickness across the film. As these thicknesses are of the order of a few hundred nanometres or less the thinning of the film can be viewed as interference patterns of light that demonstrate the varying thicknesses by the range of colours observed. Eventually the film reaches an equilibrium thickness (across the whole film) which is typically 100 nm or less for films studied using this technique. A schematic illustration of the typical TFPB setup is shown in Figure 2-11.

Given a film with a refractive index of solution, n_s, and consisting of two interfacial layers of adsorbed surfactant of known thickness (h_{tail}, h_{head}) and refractive index (n_{tail}, n_{head}) the reflected light intensity can be converted to a film thickness by [34]

$$h = h_{eq} - 2h_{tail}\left(\frac{n_{tail}^2 - n_s^2}{n_s^2 - 1}\right) - 2h_{head}\left(\frac{n_{head}^2 - n_s^2}{n_s^2 - 1}\right) \qquad \textbf{Eq. 2-20}$$

where h_{eq} is the equivalent film thickness, which is a measure for the reflected light intensity and is given by [34]

$$h_{eq} = \frac{\lambda}{2\pi n_s}\arcsin\left(\frac{\Delta}{1 + (4R(1 - \Delta)/(1 - R)^2}\right) \qquad \textbf{Eq. 2-21}$$

where λ is the wavelength of the measured light, $\Delta = (I - I_{min})/(I_{max} - I_{min})$, $R = (n_s - 1)^2/(n_s + 1)^2$, where I is the instantaneous intensity of reflected light, and I_{max} and I_{min} are the maximum and minimum intensities in the experiment. The equivalent film thickness only considers the one refractive index (of the solution) while the true film consists of the two interfacial surfactant layers as well as the solution in the core of the film, which is considered in Eq. 2-20.

2.4   **Surface tension**

2.4.1   Theory

Materials gain a surface energy due to the difference in physical properties between two interfaces which can lead to consequences such as the unsaturated 'bonds' of surface molecules.[42] Therefore the amount of work, δw, that is needed to create a new surface is proportional to the amount of molecules moved from the bulk to the surface, which in turn increases the surface area, δA, giving the relationship [42]

$$\delta w = \gamma \delta A$$

<div align="right">**Eq. 2-22**</div>

where γ is the proportionality constant and is defined as the surface energy, which for a pure, single component liquid is equal (numerically) to the surface tension.[42] This also shows that a liquid is able to minimise its surface energy by minimising its surface area.

2.4.2   Experimental setup

Profile analysis tensiometer PAT 1

The surface tension instrument used at Flinders University is the Profile Analysis Tensiometer PAT 1 (Sinterface, Germany) that utilises the hanging drop technique for measuring surface tension. It measures the shape of a hanging drop of the solution and relates this to the surface tension by the Young-Laplace equation [43,44]

$$\gamma \left(\frac{1}{R_1} + \frac{1}{R_2} \right) = \Delta P_0 + \Delta \rho g h$$

<div align="right">**Eq. 2-23**</div>

where γ is the surface tension, R_1 and R_2 are the radii of curvature, ΔP_0 is the pressure difference between phases, $\Delta \rho$ is the density difference, g is acceleration due to gravity, and h is the vertical height of the drop. A camera is used to obtain an image of the droplet and the surface tension is obtained by fitting Eq. 2-23 to the image, where the surface tension is the fitting parameter. This technique boasts an accuracy of $\pm\, 0.1$ mN/m.

Du Noüy ring method

The surface tension instrument used at Universität Stuttgart The Du Noüy ring method,[45] using an STA1 tensiometer (Sinterface, Germany). This method measures the force

required to pull a ring (often platinum) of known radius out of a liquid which is then related to the work needed to re-create the surface and thus the surface tension, as given in Eq. 2-22.

2.5   Molecular orbital calculations

In order to gain an increased (and sometimes quantitative) understanding of MIES and UPS results it was necessary to perform molecular orbital (MO) calculations of the molecules being studied. MO calculations enable the calculation of MO energies, as well as the visual representation of each MO. Given that MIES/UPS probes the MOs of a sample, the calculated MOs can be used to assign regions of the electron spectra to the molecules/moieties present in the sample, thus gaining an increased understanding of the measured spectra.

2.5.1   Calculations

Original MO calculations were performed for the ILs ethylammonium nitrate, propylammonium nitrate, and ethanolammonium nitrate, with the calculations being performed on an ion pair as is common for ILs as seen in literature.[46,47] Calculations were originally performed with the 6-31G** basis set with B3-LYP functional, however this resulted in the transfer of a proton from the cation to the anion resulting in two neutral molecules, an effect which has been noted previously.[46] The aug-cc-pVTZ basis set (HF theory) was tested and found not to replicate the hydrogen jumping issue and was therefore used for calculations on the ILs. The calculations were performed using the Gaussian 09 package, with geometry optimisation performed. The ion pairs were created, and MOs were visualised using the GaussView 5.0 package. The above calculations were used in the preliminary analysis of the MIES/UPS spectra of protic ILs.[48]

The calculated MOs required a shift of several eV to fit to the electron spectra. This has previously been attributed to the change in electronic environment between an ion pair in vacuum (calculation) and in a liquid (experiment).[49] In order to more fully understand, and be able to account for, the nature of these shifts discussions were held with Dr. Ekaterina Pas at Monash University, who specialises in computational chemistry of ILs.

2.6 Sample preparation

2.6.1 Materials

Imidazolium-based ILs

1-C_n-3-methylimidazolium ($C_n$mim, n = 6, 8, 10) based ILs with anions bromide and chloride were purchased from Merck and purified by [50]: 1) dissolution in ultra-pure water, adsorption with ultra-high purity charcoal (Sigma-Aldrich), and filtration through 0.2 μm Teflon filters (Whatman); 2) extraction with acetyl acetate (Chemsupply, HPLC); 3) water and other volatile substances were removed by evaporation under moderate vacuum (10^{-2} Torr). The purified ILs were tested with XPS and NMR and found to contain no impurities, while the elemental compositions were equal to theoretical values. To decrease the amount of residual water in the ILs, they were left under vacuum (approximately 10^{-5} Torr) overnight prior to measurement. The water content was measured with Karl Fisher titration after experiments and was found to be 600 ppm for [C_4mim][BF_4], 1500 ppm for [C_6mim][BF_4], and 2200 ppm for [C_{10}mim][BF_4]. Water content in the [$C_n$mim][Cl] ILs were controlled for the purposes of the experiments, and as such their water contents are discussed in the chapter regarding these ILs (Section 4.2).

Protic ILs

Protic ILs were prepared using the method of Wakeham et al.[51] This is done by the dropwise addition of an acid (Nitric acid, hydrochloric acid, hydrobromic acid, hydroiodic acid, sulphuric acid; Sigma-Aldrich) to an amine base (ethylamine, Aldrich; propylamine, Fluka; ethanolamine, Sigma-Aldrich) in equimolar amounts, and in an excess of water. The solution is thoroughly stirred and kept below 10 °C during mixing. Excess water is removed by rotary evaporation at elevated temperatures (50 – 70 °C). Water content was then measured using Karl Fisher titration and was found to be < 0.1 wt% for all ILs. At laboratory pressure and temperature (approximately 1 atm, and 25 °C) only the nitrate ILs are liquid, while the chloride, bromide, and iodide were solid, and the sulfate ILs were in a slurry-like state. Prior to measurement, all IL samples were left under vacuum (approximately 10^{-5} Torr) overnight to minimise residual water content.

Surfactant solutions

Measurements on surfactant solutions were performed in three different solvents: ultra-pure water, glycerol (≥99%, Sigma-Aldrich), and formamide (>99.5%, Sigma-Aldrich). Formamide of this grade has been found previously to contain no impurities that affect surface investigations, and therefore needs no further purification.[52] Pure glycerol was analysed using NICISS and was found to contain only the elements carbon, oxygen, and nitrogen. Furthermore these elements were found to be in correct stoichiometric amounts for glycerol. The cationic surfactant hexadecyltrimethylammonium bromide (C_{16}TAB, >96%) was purchased from Fluka. This surfactant was used without further purification as it has been found that purification is not needed for this surfactant.[53] The cation surfactant hexadecyltrimethylphosphonium bromide was prepared using 1-bromohexadecane, 2-propanol, and trimethylphosphine (Sigma-Aldrich). The resulting surfactant was re-crystalised (by Dr. Leonid Lerner) and HNMR results conformed with literature.[54] The non-ionic surfactant 1-palmitoyl-2-oleoyl-sn-glycero-3-phosphocholine (POPC) was purchased from Avanti Polar Lipids Inc., was checked for purity using surface tension and was used without further purification. The non-ionic surfactant dodecyldimethyl phosphineoxide (C_{12}DMPO) was purchased from ABCR Chemicals (Germany) and re-crystallised twice from n-hexane prior to usage. In order to speed the solvation of surfactants in glycerol, these solutions were often sonicated at 30 °C for approximately 30 minutes which allowed for full solvation.

Gas-phase

Diiodo methane (>99%), bromoform (>99%), trimethylphosphite (>99%), trifluoroethanol (>99%), and chloroform (>99%) were purchased from Sigma-Aldrich and used without further purification.

2.6.2   Foam film holders

The original set of film holders for use in the NICISS instrument were produced by purchasing filter discs from Labglass Pty. Ltd. The filter discs were of a similar variety used in TFPB experiments, with a diameter of 40 mm and a porosity of 4. A glass capillary with inner diameter, ID = 3 mm, is fused to the back of the filter disc in such a way that solution is free to flow between capillary and disc, and this was done by Monash

Scientific Glass Blowing. Additional film holders were made in a similar way, but were purchased as entire units from Robu Sintered Glassfilters.

To prepare for a foam film experiment in the NICISS, a beaker containing a few tens of millilitres of the surfactant solution was placed inside the NICISS main chamber. The film holder and the silicon tube attached to the syringe were immersed into the solution. The chamber is then evacuated down to the low 10^{-5} mbar range and kept under vacuum for at least 2 hours to allow for evaporation of any residual water as well as promoting the solution to soak through the film holder. The chamber is then vented, and the plunger on the syringe pulled up to suck up an appropriate amount of solution (depending on the pressure to be applied to the film). Extra solution is pipetted into the film holder to fill the glass capillary. The film holder is then placed inside the pressure cell, with the film aperture aligned with the aperture on the cover of the pressure cell, and the silicon tube from the syringe is attached to the film holder, ensuring no bubbles and thus a continuous flow of liquid between the syringe and the film holder.

The high surface area of the porous discs leave the film holders vulnerable to contamination by foreign surfactants and other impurities and as such need to be sufficiently cleaned prior to measurements with each new system being investigated. Cleaning is done by soaking the film holders in hot ultra-pure water for around 30 minutes, then soaking in hot diluted hydrochloric acid for another 30 minutes. The film holders are then heated to around 400 °C for 2-3 hours, then allowed to cool. After cooling, around 0.5 L of hot ultra-pure water is sucked through the discs, then the discs are sucked dry and immersed in solution. The effectiveness of this cleaning procedure has been checked by immersing the film holders into ultra-pure water overnight, then measuring the surface tension of the water to check for any surface-active impurities.

2.7 References

1 Niehus, H., Heiland, W. & Taglauer, E. Low-energy ion scattering at surfaces. *Surface Science Reports* **17**, 213-303 (1993).

2 Aono, M. & Souda, R. Inelastic processes in ion scattering spectroscopy of solid surfaces. *Nuclear Instruments and Methods in Physics Research Section B: Beam Interactions with Materials and Atoms* **27**, 55-64 (1987).

3 Niehus, H. Surface structure determination using alkali and noble gas ion scattering. *Journal of Vacuum Science & Technology A: Vacuum, Surfaces, and Films* **5**, 751-756 (1987).

4 Niehus, H. & Comsa, G. Ion scattering spectroscopy in the impact collision mode (ICISS): Surface structure information from noble gas and alkali-ion scattering. *Nuclear Instruments and Methods in Physics Research Section B: Beam Interactions with Materials and Atoms* **15**, 122-125 (1986).

5 Aono, M., Oshima, C., Zaima, S., Otani, S. & Ishizawa, Y. Quantitative Surface Atomic Geometry and Two-Dimensional Surface Electron Distribution Analysis by a New Technique in Low-Energy Ion Scattering. *Japanese Journal of Applied Physics* **20**, L829 (1981).

6 Andersson, G. & Morgner, H. Impact collision ion scattering spectroscopy (ICISS) and neutral impact collision ion scattering spectroscopy (NICISS) at surfaces of organic liquids. *Surface Science* **405**, 138-151 (1998).

7 Rabalais, J. W. Direct recoil spectrometry. *Critical Reviews in Solid State and Materials Sciences* **14**, 319-376 (1988).

8 Masson, F., Sass, C. S., Grizzi, O. & Rabalais, J. W. Application of direct recoil spectrometry to determination of the saturation coverage of ethylene on Pt(111). *Surface Science* **221**, 299-316 (1989).

9 Hobbs, C. P., McMillan, J. W. & Palmer, D. W. The effects of surface topography in nuclear microprobe Rutherford backscattering analysis. *Nuclear Instruments and Methods in Physics Research Section B: Beam Interactions with Materials and Atoms* **30**, 342-348 (1988).

10 Kimura, K., Joumori, S., Oota, Y., Nakajima, K. & Suzuki, M. High-resolution RBS: a powerful tool for atomic level characterization. *Nuclear Instruments and Methods in Physics Research Section B: Beam Interactions with Materials and Atoms* **219–220**, 351-357 (2004).

11 Smith, D. P. Scattering of Low-Energy Noble Gas Ions from Metal Surfaces. *Journal of Applied Physics* **38**, 340-347 (1967).

12 Aono, M. *et al.* Recent developments in low-energy ion scattering spectroscopy (ISS) for surface structural analysis. *Nuclear Instruments and Methods in Physics Research Section B: Beam Interactions with Materials and Atoms* **37–38**, 264-269 (1989).

13 Andersson, G. & Morgner, H. Investigations on solutions of tetrabutylonium salts in formamide with NICISS and ICISS: concentration depth profiles and composition of the outermost layer. *Surface Science* **445**, 89-99 (2000).

14 Souda, R., Aizawa, T., Oshima, C., Otani, S. & Ishizawa, Y. Electronic excitation in impact scattering of low-energy He+ from solid surfaces. *Physical Review B* **40**, 4119 (1989).

15 Brongersma, H. H., Draxler, M., de Ridder, M. & Bauer, P. Surface composition analysis by low-energy ion scattering. *Surface Science Reports* **62**, 63-109 (2007).

16   Kührt, E. & Wedell, R. Energy-loss straggling and higher-order moments of energy-loss distributions for protons. *Physics Letters A* **96**, 347-349 (1983).

17   Andersson, G. & Morgner, H. Determining the stopping power of low energy helium in alkanethiolates with Neutral Impact Collision Ion Scattering Spectroscopy (NICISS). *Nuclear Instruments and Methods in Physics Research Section B: Beam Interactions with Materials and Atoms* **155**, 357-368 (1999).

18   Andersson, G., Morgner, H. & Pohl, H. Energy-loss straggling of helium projectiles at low kinetic energies: Deconvolution of concentration depth profiles of inorganic salt solutes in aqueous solutions. *Physical Review A (Atomic, Molecular, and Optical Physics)* **78**, 032904 (2008).

19   Andersson, G. Energy-loss straggling of helium projectiles at low kinetic energies. *Physical Review A* **75**, 032901 (2007).

20   Pezzi, R. P. *et al.* Advanced ion energy loss models: Applications to subnanometric resolution elemental depth profiling. *Surface Science* **601**, 5559-5570 (2007).

21   White, C. W., Thomas, E. W., Van der Weg, W. F. & Tolk, N. H. in *Inelastic Ion–Surface Collisions*   (eds N. H. Tolk & J. C. Tullyw Heilandc W. White) 201-252 (Academic Press, 1977).

22   Bragg, W. H. & Kleeman, R. XXXIX. On the α particles of radium, and their loss of range in passing through various atoms and molecules. *Philosophical Magazine Series 6* **10**, 318-340 (1905).

23   Hulpke, E. Scattering of Li+ from LEED characterized W(110) and Si (111) surfaces at energies between 2 and 20 eV. *Surface Science* **52**, 615-640 (1975).

24   Popeskov, B., Milivojevic, M., Cvetic, J., Nedeljkovic, T. & Draganic, I. Highly charged ion beam diagnostics at the mVINIS Ion Source. *Journal of Physics: Conference Series*, 423 (2007).

25   Ridings, C. & Andersson, G. Determining concentration depth profiles of thin foam films with neutral impact collision ion scattering spectroscopy. *Review of Scientific Instruments* **81**, 113907-113915 (2010).

26   Ogletree, D. F. *et al.* A differentially pumped electrostatic lens system for photoemission studies in the millibar range. *Review of Scientific Instruments* **73**, 3872-3877 (2002).

27   Hertz, H. Ueber einen Einfluss des ultravioletten Lichtes auf die electrische Entladung. *Annalen der Physik* **267**, 983-1000 (1887).

28   L.R. Nobel lectures, Physics: 1901–1921 (Elsevier Publishing Company, Amsterdam, 1967. 500 p. 80 guilders). *Nuclear Physics A* **130**, 696 (1969).

29   Seah, M. P. & Dench, W. A. Quantitative electron spectroscopy of surfaces: A standard data base for electron inelastic mean free paths in solids. *Surface and Interface Analysis* **1**, 2-11 (1979).

30   Turner, D. W. & Jobory, M. I. A. Determination of Ionization Potentials by Photoelectron Energy Measurement. *The Journal of Chemical Physics* **37**, 3007-3008 (1962).

31   Turner, D. W. & May, D. P. Franck---Condon Factors in Ionization: Experimental Measurement Using Molecular Photoelectron Spectroscopy. *The Journal of Chemical Physics* **45**, 471-476 (1966).

32   Morgner, H. in *Advances In Atomic, Molecular, and Optical Physics* Vol. Volume 42 (eds Bederson Benjamin & Walther Herbert) 387-488 (Academic Press, 2000).

33   Harada, Y., Masuda, S. & Ozaki, H. Electron Spectroscopy Using Metastable Atoms as Probes for Solid Surfaces. *Chemical Reviews* **97**, 1897-1952 (1997).

34   Stubenrauch, C. & Klitzing, R. v. Disjoining pressure in thin liquid foam and emulsion films - new concepts and perspectives. *Journal of Physics: Condensed Matter*, R1197 (2003).

35   Bergeron, V. Forces and structure in thin liquid soap films. *Journal of Physics: Condensed Matter*, R215 (1999).

36   Ciunel, K., Armélin, M., Findenegg, G. H. & von Klitzing, R. Evidence of Surface Charge at the Air/Water Interface from Thin-Film Studies on Polyelectrolyte-Coated Substrates. *Langmuir* **21**, 4790-4793 (2005).

37   Bergeron, V., Waltermo, A. & Claesson, P. M. Disjoining Pressure Measurements for Foam Films Stabilized by a Nonionic Sugar-Based Surfactant. *Langmuir* **12**, 1336-1342 (1996).

38   Israelachvili, J. N. *Intermolecular and Surface Forces*. Second edn, (Academic Press, 2000).

39   Attard, P. Recent advances in the electric double layer in colloid science. *Current Opinion in Colloid & Interface Science* **6**, 366-371 (2001).

40   Ibarra-Armenta, J. G., Martin-Molina, A. & Quesada-Perez, M. Influence of monovalent ion size on colloidal forces probed by Monte Carlo simulations. *Physical Chemistry Chemical Physics* (2011).

41   Marčelja, S. Exact Description of Aqueous Electrical Double Layers. *Langmuir* **16**, 6081-6083 (2000).

42   Hunter, R. J. *Foundations of Colloid Science*. Second edn, (Oxford University Press, 2001).

43   Young, T. An Essay on the Cohesion of Fluids. *Philosophical Transactions of the Royal Society of London* **95**, 65-87 (1805).

44   Laplace, P. On capillary attraction. *Supplement to the tenth book of the Mechanic Celeste. Translated with a commentary by Nathaniel Bowditch, LL. D* **4** (1806).

45   du Noüy, P. L. AN INTERFACIAL TENSIOMETER FOR UNIVERSAL USE. *The Journal of General Physiology* **7**, 625-631 (1925).

46   Lehmann, S. B. C., Roatsch, M., Schoppke, M. & Kirchner, B. On the physical origin of the cation-anion intermediate bond in ionic liquids Part I. Placing a (weak) hydrogen bond between two charges. *Physical Chemistry Chemical Physics* **12**, 7473-7486 (2010).

47   Reinmoller, M. *et al.* Theoretical reconstruction and elementwise analysis of photoelectron spectra for imidazolium-based ionic liquids. *Physical Chemistry Chemical Physics* (2011).

48   Ridings, C., Warr, G. G. & Andersson, G. G. Composition of the outermost layer and concentration depth profiles of ammonium nitrate ionic liquid surfaces. *Physical Chemistry Chemical Physics* **14**, 16088-16095 (2012).

49   Yoshimura, D. *et al.* Electronic structure of ionic liquids at the surface studied by UV photoemission. *Journal of Electron Spectroscopy and Related Phenomena* **144-147**, 319-322 (2005).

50   Lockett, V., Sedev, R., Ralston, J., Horne, M. & Rodopoulos, T. Differential Capacitance of the Electrical Double Layer in Imidazolium-Based Ionic Liquids: Influence of Potential, Cation Size, and Temperature. *The Journal of Physical Chemistry C* **112**, 7486-7495 (2008).

51   Wakeham, D., Nelson, A., Warr, G. G. & Atkin, R. Probing the protic ionic liquid surface using X-ray reflectivity. *Physical Chemistry Chemical Physics* **13**, 20828-20835 (2011).

52   Andersson, G., Krebs, T. & Morgner, H. Activity of surface active substances determined from their surface excess. *Physical Chemistry Chemical Physics* **7**, 136-142 (2005).

53   Stubenrauch, C. & Khristov, K. Foams and foam films stabilized by CnTAB: Influence of the chain length and of impurities. *Journal of Colloid and Interface Science* **286**, 710-718 (2005).

54   Pindzola, B. A. & Gin, D. L. Lyotropic Liquid-Crystalline Phase Behavior of Some Alkyltrimethylphosphonium Bromides. *Langmuir* **16**, 6750-6753 (2000).

Chapter 3

Effect of the aliphatic chain length on electrical double layer formation at the IL/vacuum interface

3.1   Introduction

Room temperature ionic liquids (ILs) are organic molten salts with a melting point below 100 °C, which can have an unusual combination of properties such as low vapour pressure, high electric- and thermo-stability, the ability to dissolve many substances, and high tunability for applications due to the great variety of ion combinations possible.[1] Not surprisingly, ILs have great practical potential in many chemistry-based applications including those that involve their free surface: biphasic catalysis, heterogeneous reactions, etc.[1] For example, recent research showed that ILs outperform standard techniques for acidic gas capture and separation, and refrigerant gas adsorption.[2-4] For these applications it is beneficial to understand the surface orientation of ions and surface charge distribution along the surface normal.

As ILs consist entirely of charged species, it is of interest to see how the surface charge distribution compares to a more dilute solution of charges, e.g. an aqueous electrolyte solution. The results of Min et al. point out the discrepancy in the Debye length as calculated from the traditional Poisson–Boltzmann equation with that measured via a surface force apparatus (SFA),[5] highlighting the knowledge gap in this area. Progress in this field has been made with a number of spectroscopic techniques which are well equipped for investigating molecular orientation exclusively at the surface.[6-20] Among these techniques are both non-vacuum based techniques such as sum frequency generation vibrational spectroscopy (SFG) (which was also performed under moderate vacuum to eliminate atmospheric contaminants),[21-23] and vacuum based techniques such as direct recoil spectroscopy (DRS),[24] angle resolved and energy resolved X-ray photoelectron

spectroscopy,[7-9,25,26] and metastable induced electron spectroscopy (MIES)[11-13] (for a comprehensive review, see ref. [6]). Through these studies it has become widely accepted that the aliphatic chains of 1,3-alkylsubstituted imidazolium and 1,1 substituted pyrrolidinium cations and alkylsulfate anions are oriented towards the gas phase and tilted at some angle to the surface normal, and that neither the cation nor the anion occupies the surface exclusively. Surface orientation of non-spherical organic ions and aromatic rings has also been discussed with the exact structure being dependent on the IL composition.[10,22,27]

Significantly less attention has been paid to the investigation of the distribution of ions and charges along the surface normal in ILs. Due to increasing interest in their electrochemical applications, a wide range of studies are being carried out on the charge structure at IL/solid interfaces (both charged and uncharged solids).[5,19,20,28] The results show that a multilayered charge structure forms at this interface. Molecular dynamics (MD) simulations show that this effect exists also for the IL/vapour interface and varies with variation in ion size asymmetry.[29-34] X-Ray and neutron reflectivity[18,35-37] first indicated the presence of such ordering at the IL/vapour interface. Additionally, angle resolved and energy resolved X-ray photoelectron spectroscopy showed how cation and anion profiles are not uniformly distributed along the surface normal, thus implying a local separation of charges.[8,26] Such charge separation can be described as an electrical double layer (EDL). The charge separation can be considered as a competition between the propensity of the specific ions to adsorb at the surface and the Coulomb forces opposing the charge separation. Even though the screening length in an ionic liquid is very short, the separation of charges requires a non-negligible amount of energy as locally there would be no charge neutrality and the screening length in the region of the charge separation will be different from regions with charge neutrality. However, the exact details of the charge distribution and the existence of an electrical double layer at the surface of ILs still remain to be explicitly answered.

One technique that is well equipped to address the question of EDL presence is neutral impact collision ion scattering spectroscopy (NICISS). NICISS has a depth range of about 20 nm and a resolution of a few Å close to the surface, and has already been used to investigate ion profiles at liquid surfaces.[38-41] NICISS is able to determine the

concentration depth profiles of the elements directly, thus circumventing the need for fitting models. Therefore, information about the charge distribution in a NICISS experiment can be gained by comparing the concentration depth profiles of the different elements, while this information is only implied via other techniques.[8,18,35-37] The concentration depth profiles of the ions show directly the charge distribution at the liquid surface which can furthermore be used to derive information regarding the sign of the surface charge and—provided the dielectric constant at the surface is known—the electrostatic potential along the surface normal. NICISS has recently been used for the investigations of IL surfaces,[42] however, Hammer et al. focus on molecular orientation and surface topography whereas this study focuses explicitly on the surface charge and EDL structure.

The aim of this present work is to measure directly with NICISS the concentration depth profiles of the cation and the anion of the ILs, 1-hexyl-3-methylimidazolium [C_6mim], 1-octyl-3-methylimidazolium [C_8mim], and 1-decyl-3-methylimidazolium [C_{10}mim] tetrafluoroborates [BF_4]. The charge distribution along the surface normal is then determined directly from the concentration depth profiles.

3.2   **Results and Discussion**

3.2.1   **NICIS spectra**

A detailed description of the data evaluation procedure is given in [43], but a brief summary is as follows. Photons are generated as part of the ion beam interaction with matter, and these photons are able to be detected by the micro channel plates. Knowing the TOF length and the speed of the photons allows the zero mark of the TOF spectrum to be gauged. As the condition for backscattering (scattering angle $>90^o$) is that the target mass must be greater than the projectile mass, the use of He^+ as the projectiles results in not finding backscattered projectiles from hydrogen. Instead, hydrogen is found as sputtered hydrogen with a broad background over a wide range of energies.[44] Apart from the signal due to the photons and the hydrogen background, the only other feature of a NICIS spectrum is the signal due to the backscattering of projectiles from the elements in the target. The profile due to an element can be separated from the total spectrum by fitting a
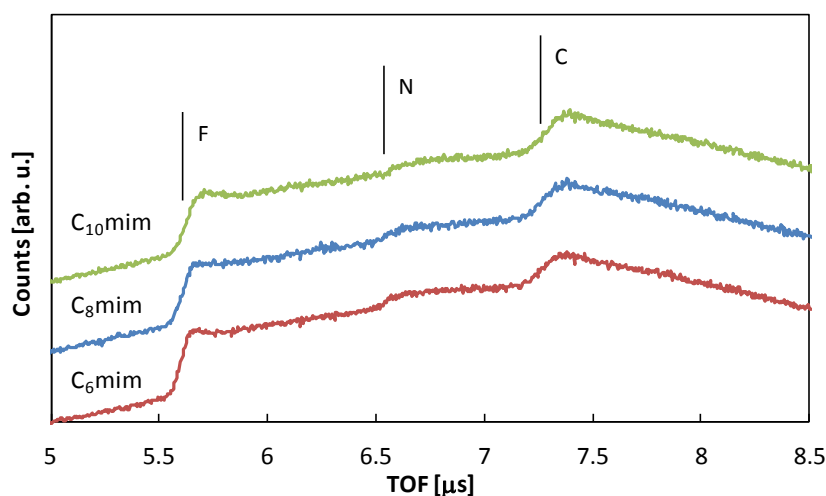
Figure 3-1. NICISS TOF spectra of the ILs [C_6mim] [BF_4], [C_8mim] [BF_4], and [C_{10}mim] [BF_4]. The spectra are offset for clarity. The vertical lines show the onsets for the elements in the TOF spectra, as indicated.

low-order polynomial to account for the background. The depth scale for each element is then calculated from the final energy scale of each element, with the zero mark of depth being calibrated using the gas phase spectra, as described above. The accuracy of the gauging procedure depends in first instance on determining the TOF position for the gas phase peak maxima. The accuracy of the zero mark for both nitrogen and fluorine is about 2 Å. However, as the uncertainty affects all profiles in the same way, it does not affect the accuracy in comparing the profiles Therefore while the absolute position of anion and cation has an uncertainty, the change in the position of the cation relative to that of the anion investigated is unambiguous when comparing the different ILs.

Figure 3-1 shows the TOF spectra for the three ILs as measured by NICISS. Steps due to the elements constituting the sample, namely fluorine, nitrogen and carbon, can be seen. No signal due to the presence of water can be identified. Even though the water content is low (for quantification, see section 2.6.1) it cannot be excluded that the residual water content influences the surface structure of the ILs.

Projectiles backscattered from heavier elements have higher kinetic energies and are thus detected at a lower TOF. A calibration factor, determined from the composition of the target, is then used to convert count rate to concentration. In the concentration depth

profiles, zero depth marks the outermost layer of the target, with increasing depth indicating the direction towards the bulk. It is important to note that signal in the measured profiles can be seen at negative depth; however this is not due to a 'concentration' above the surface, but rather due to the finite FWHM of the energy distribution in the

backscattering process. As the distance on the depth scale between two data point of the measured carbon and nitrogen profiles corresponds to less than 0.5 Å, the profiles displayed for carbon and nitrogen are averaged in a way such that every three data points are summed up to a single value. Figure 3-2a shows the concentration depth profiles for carbon. The bulk concentration of carbon increases with increasing aliphatic chain length (n = 6, 8, 10) due to the increasing number of carbon atoms in the cations. Figure 3-2b and
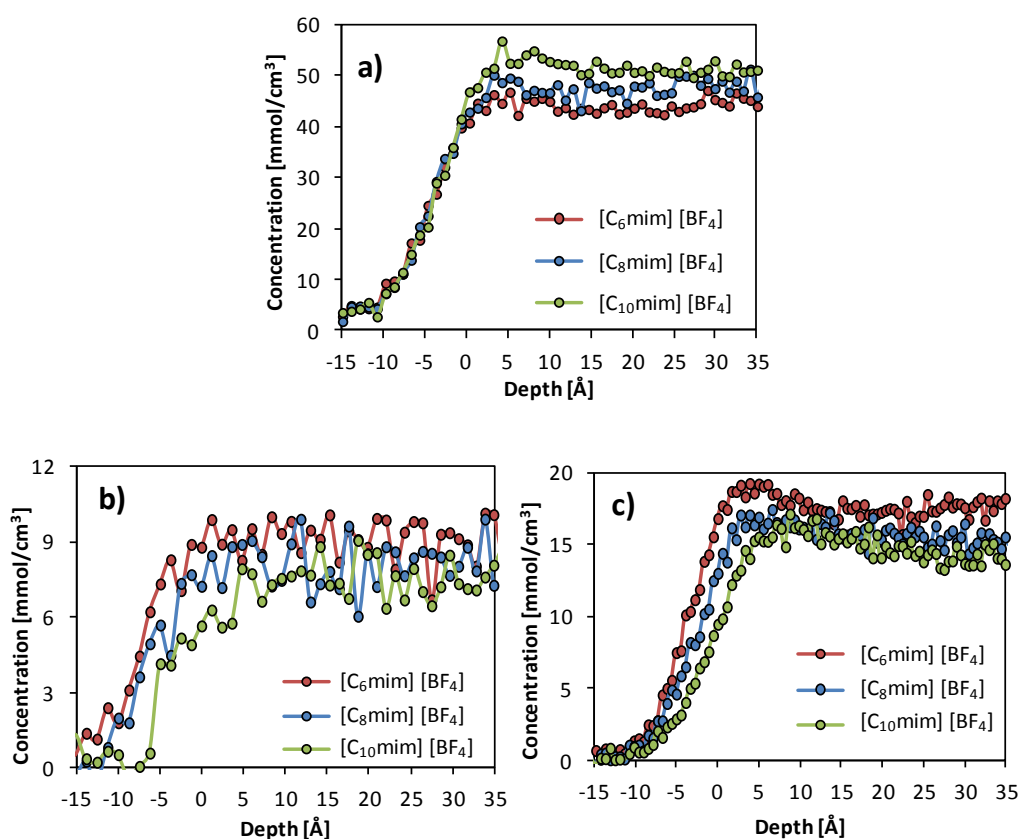
Figure 3-2. Comparing the measured concentration depth profiles of: (a) carbon, (b) nitrogen, and (c) fluorine in the three ILs. Increasing depth values indicates the direction further towards the bulk, with zero being the outermost layer.

Figure 3-2c show the concentration depth profiles of nitrogen and fluorine respectively. As nitrogen is only part of the cation and fluorine only part of the anion, these two elements represent the profiles of cation and anion respectively. The concentration depth profiles show that both ions are moving towards the bulk, i.e. greater depths, with increasing alkyl chain length. In contrast, all carbon profiles have the same onset close to 0 Å, thus showing that carbon is not depleted from the surface at all chain lengths. This result is similar to the result gained by Iwahasi et al. who used MIES to investigate the composition of the outermost layer of the liquid/vapour interface of $[C_nmim]$ $[BF_4]$ ILs with various aliphatic chain lengths.[11] Their results show that both cation and anion can be seen in the outermost layer of $[C_4mim]$ $[BF_4]$ but not in case of the C_8 or C_{10} cations. It is important to note that all fluorine profiles show a maximum in the top few Å before levelling off to bulk levels, as can be seen in Figure 3-2c.

3.2.2 Deconvolution
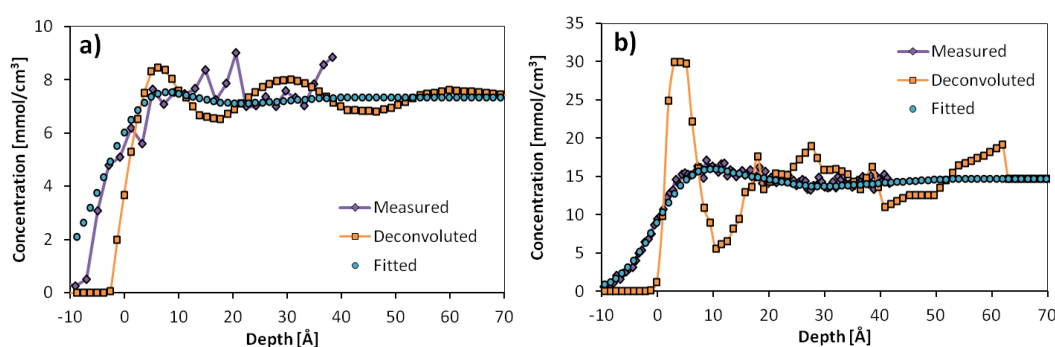
Figure 3-3. Measured, deconvoluted and fit to the measured concentration depth profiles of (a) nitrogen and (b) fluorine in the $[C_{10}mim][BF_4]$ IL. The data points shown in (a) are a sum of five measured data points.

Figure 3-3a and b show the measured, the deconvoluted and the fitted profiles (the convolution of the deconvoluted profiles) for nitrogen and fluorine, respectively, in $[C_{10}mim][BF_4]$. Comparing the fit to the measured profile gives a qualitative indication of the accuracy of the deconvolution of the measurements. The carbon concentration depth profiles have not been deconvoluted as the onset of the profiles coincides with the maximum of the hydrogen background. The level of accuracy achieved in the deconvolution of the carbon profile would be less than for the profiles of fluorine and
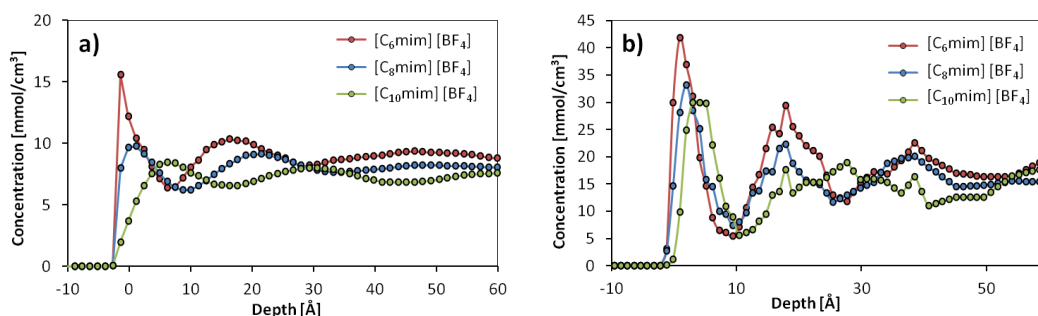
Figure 3-4. Comparing the deconvoluted profiles of (a) nitrogen and (b) fluorine for all three ILs investigated.

nitrogen. Thus the deconvolution would not add more information in the present case. However concentration depth profiles for both cation and anion can be gained via the profiles of nitrogen and fluorine alone. The data scattering for nitrogen is stronger than for fluorine, and as such the fit to the measured profile of nitrogen is slightly less accurate than the fit to those of fluorine.

As can be seen in Figure 3-3a, the rising edge of the nitrogen profile is fitted with a reasonable degree of precision, which shows that deconvolution fits the onset of the nitrogen concentration depth profile well, while it is the structure at greater depths that has some uncertainty. The data scattering around the onset of nitrogen has a width of no more than 3 Å, meaning that the fitted onset has a depth uncertainty of ± 1.5 Å. In comparing the surface charge for the ILs, it is the location of the cation and anion at the IL/vacuum interface that is important, hence it is the position of the onset for nitrogen and fluorine that is of the most relevance. As the onsets of both the nitrogen and fluorine profiles are fitted well, this allows for conclusions regarding surface charge to be made with a high degree of confidence. Figure 3-4 compares the nitrogen and fluorine profiles for the three ILs studied. For the deconvolution, the measured profiles have been considered up to a depth of 40 Å and set to the bulk concentration of the respective element at great depth. The reason is in the case of nitrogen that the accessible depth range is limited by the onset of the carbon depth profile to 40 Å and in case of the fluorine that no variation in the profile can be seen in the measured profile at a depth greater than 40 Å. This procedure, however, does not influence the interpretation of the deconvolution as only the depth up to

20 Å is of interest in the present case. The data shows that both nitrogen and fluorine are pushed towards the bulk with increasing chain length of the cation. Fluorine does not occupy the outermost layer of the surface at any of the three aliphatic chain lengths, but instead sits just below, and is pushed further to the bulk with increasing chain length. The data explicitly shows that in the case of the two shorter chain lengths (C_6 and C_8) the imidazolium cation (as given by nitrogen) is present close to the surface, whereas it is pushed below the surface in the case of the longest alkyl chain length. The concentration depth profiles also show that from [C_6mim] to [C_{10}mim] [BF$_4$] the nitrogen is pushed towards the bulk by a larger distance than the fluorine.

3.2.3 Surface charge and electrical double layer

Table 3-1. Depth of maximum concentration for fluorine (F, anion) and nitrogen (N, cation). The error for each position falls within the given range but is the same for both elements in all ILs measured. Additionally, the depth of maximum concentration for nitrogen in [C_6mim][BF$_4$] was determined as -1 Å in the deconvoluted profile. However as this has no physical meaning, the value is set to 0 Å (outermost layer). This change is less than the error in determining the zero mark.

	Max. concentration of F [Å]	Max. concentration of N [Å]
[C_6mim][BF$_4$]	1 ± 2	0 ± 2
[C_8mim][BF$_4$]	2 ± 2	1 ± 2
[C_{10}mim][BF$_4$]	4 ± 2	7 ± 2

The deconvoluted nitrogen and fluorine profiles show that there is some separation between cation and anion in all three ILs and that the separation is affected by the change in the aliphatic chain length with the imidazolium ring moving a larger distance towards the bulk than the anion. As this change in cation and anion position is unambiguous, the existence of an EDL and its change with the length of the alkyl chain in the IL series is evident. However there is some statistical fluctuation in the data due to the deconvolution procedure that give some uncertainty into the exact depth and thickness of the EDL.

Without the deconvoluted carbon profiles it is still possible to gain through the profiles of nitrogen and fluorine information on the aliphatic chain orientation at the liquid surface. The profiles in Figure 3-5 show that nitrogen experiences a greater shift towards the bulk than fluorine (also shown in Table 3-1). As the aliphatic chain length increases, both cation and anion are pushed towards the bulk indicating that the chains are occupying more of the liquid/vacuum interface. The change in position of the maximum in the nitrogen profile from [C_6mim] to [C_{10}mim] is ~ 7 Å, while the change in length from C_6 to C_{10} is ~ 5 Å as given by Tanford in ref. [45].

Taking into account the effect of Gauche defects on decreasing the end-to-end length of the aliphatic chain, the shift in nitrogen can be explained by the aliphatic chains becoming aligned more parallel to the surface normal. A schematic illustration of the orientation and position of cations and anions at the IL/vacuum interface is given in Figure. 3-6. This chain orientation agrees with other existing results.[6,7,21-23,26,46,47]
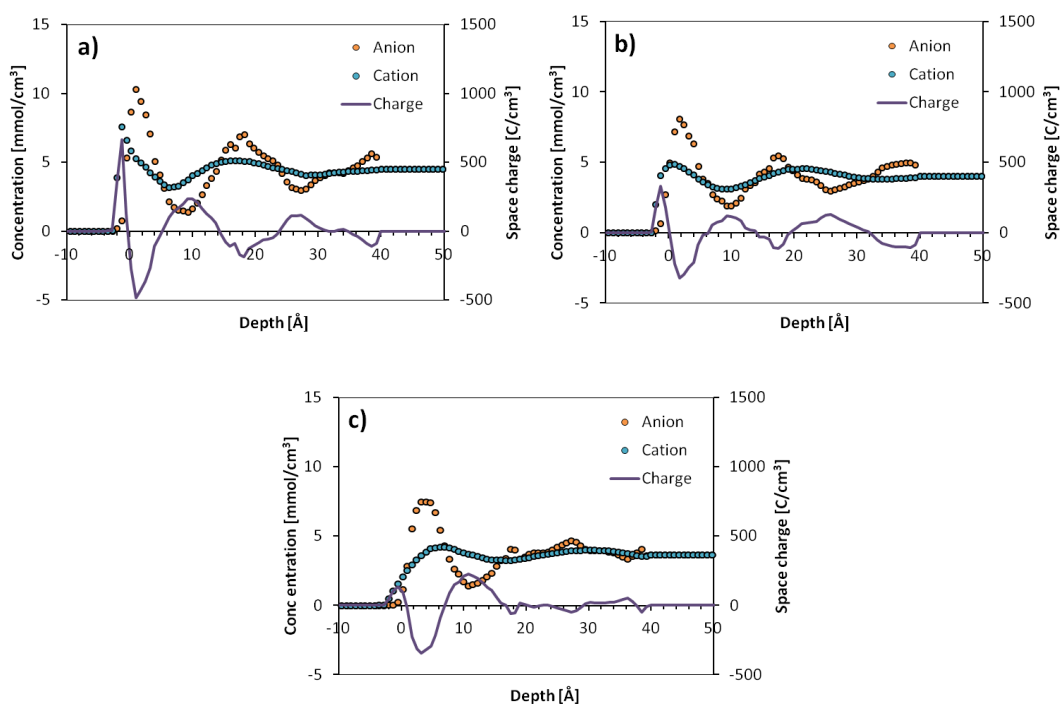
Figure 3-5. Comparing the deconvoluted anion (fluorine) and cation (nitrogen) concentration depth profiles and the space charge for (a) [C_6mim][BF_4], (b) [C_8mim][BF_4] and (c) [C_{10}mim][BF_4].

As there are two nitrogen atoms present on the imidazole ring, the concentration depth profile of the cation is given by dividing the nitrogen profile by two. Similarly, with four fluorine atoms present in tetrafluroborate, the anion profile is given by dividing the fluorine profile by four. Knowing the ion profiles directly, it is possible to obtain the space charge profile by[40]

$$\rho(z) = m_+Fc_+(z) + m_-Fc_-(z)$$

Eq. 3-1

where ρ is the space charge, z is depth, m is the valency of the ions, F is Faraday's Constant, c is the concentration and the subscript +/- denotes cation and anion, respectively. Figure 3-5 shows the concentration depth profiles of the cation and anion along with the space charge for each of the studied ILs. By comparing the profiles in Figure 3-5, the effect of increasing aliphatic chain length on the electrical EDL in the IL

[C_6mim][BF_4]

[C_8mim][BF_4]

[C_{10}mim][BF_4]
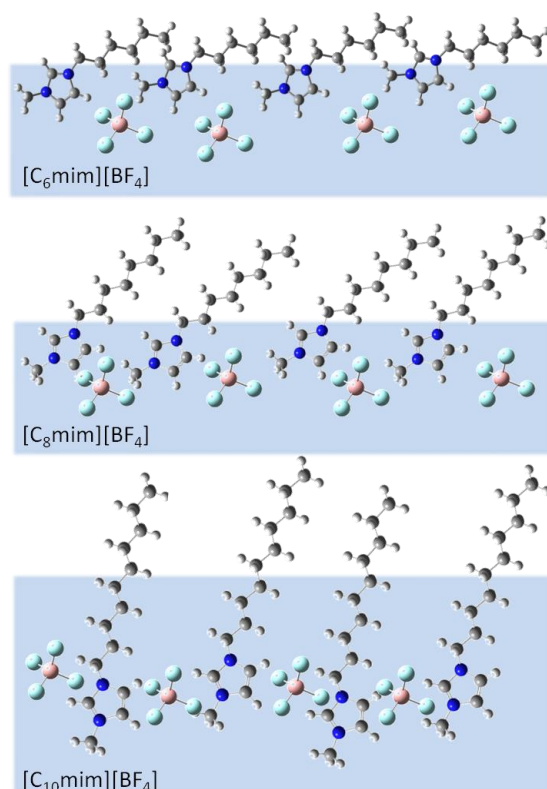
Figure. 3-6. Schematic illustrating the surface orientation and distribution of the cation and anion in the three ILs as interpreted from the concentration depth profiles.

series can be seen, with the positive surface charge decreasing with increasing aliphatic chain length. Lauw et al. have similarly observed a positive surface charge in 1-butyl-1-methylpyrrolidinium trifluoromethylsulfonylimide mixtures with water using x-ray reflectivity.[48] The profiles shown here indicate that neither the cation nor anion are exclusively adsorbed or depleted at the surface. What is clear from the present study is that the cation is shifted towards the bulk by a greater amount than the anion with increasing aliphatic chain length. This results in a decreasing positive charge at the IL/vapour interface with increasing aliphatic chain length. Additionally, the ions are layered such that a region of cation vs. anion depletion coincides with a region of anion vs. cation enrichment, forming an EDL structure. The exact depth at which the concentrations of cation and anion return to their bulk concentration is unclear due to uncertainty in the deconvolution procedure for the elements. Therefore the exact length over which charge separation occurs cannot be accurately determined with the given data.

The reason for the change in charge separation of the series of ILs investigated in the present study has most likely to be attributed to the competition between the propensity of the ions to adsorb at the surface and the increase in energy in the system due to charge separation. Covering the outermost layer with the alkyl chain rather than the imidazolium ring seems to be more favourable as the imidazolium ring moves away from the surface with increasing length of the alkyl chain from 6 to 10 carbon atoms. This can be easily explained as covering the surface with the non-polar aliphatic chain results in a lower surface energy than covering the surface with the polar imidazolium ring. In contrast, the shift of the tetrafluroborate ion is less than that of the imidazolium ion. The reason for this difference might be due to differences in the polarisability of the imidazolium ring and the tetrafluroborate as the latter is the larger and more polarisable species. Hence the tetrafluroborate should have a higher propensity to adsorb at a surface than the imidazolium ring. The change in the position of the tetrafluroborate ion might also be due to the tendency in avoiding separation of the charges. The electrostatic contribution to the surface organisation would be limited by the screening length of charges, which could be expected to be quite short in an IL (in the order of a few Å) due to the high concentration of charges. However, as Min et al. point out, hydrogen bonding decreases electrostatic interactions, resulting in an overestimation of the screening behaviour of ions as predicted

by Debye-Hückel theory. Using a surface forces apparatus (SFA) they evaluate that the screening length in [C$_4$mim][BF$_4$] is 3.8 nm, which is much greater than the predicted 0.7 nm.[5] This effect has also been observed in simulations.[49]

The present results can be compared with the studies of Hammer et al. who investigated the surface structure of [C$_n$mim] [Tf$_2$N] (n = 4, 6, 8) and conclude that at [C$_4$mim] both anion and cation ring occupy the surface, whereas in [C$_8$mim] the anion is covered spherically by the aliphatic chain of the cation and is thus pushed toward the bulk.[42] Qualitatively their conclusions about the shift in the anion position are similar to those in the present study. However, there are differences in the conclusion about the position of the positive charge (ring). The reason for the difference might be that they have not focussed on the profiles of the imidazolium ring and the distribution of charges but on the position of the anion and the cation aliphatic chain. Additionally, Hammer et al., have been studying a different anion.

Computer simulations in general find that the aliphatic chains of the [C$_n$mim] cation are oriented towards the surface [29,31] which is in agreement with experimental studies as well [6,37] and has been found also in the present study. Jiang et al. found by means of computer simulations a layered structure of [C$_n$mim] ILs with various anions.[29] The authors also found that the charge centres (anion and imidazolium ring) shift towards the bulk with increasing length of the cation aliphatic chain. However, in their study the shift of the anion is slightly larger than that of the centre of the positive charge which is different to our results. It must be noted that Jiang et al. did not specifically model the structure of the anions but considered differences in the number of electrons on the anion.

3.3   Conclusions

The effect of aliphatic chain length on the surface structure of the 1-alkyl-3-methylimidazolium tetrafluoroborate homologous series of ILs was studied by measuring concentration depth profiles of the elements in alkyl chain lengths of C$_6$, C$_8$ and C$_{10}$ ([C$_6$mim], [C$_8$mim] and [C$_{10}$mim] [BF$_4$] respectively). The concentration depth profiles of the cation and anion have been measured directly, which allows for the determination of the space charge at the surface. The results show that all three ILs have a positively charged surface, but that the magnitude of this charge decreases with increasing chain

length of the cation. While the exact value for the surface charge is somewhat unclear due to uncertainties in the evaluation procedure, the depth shift experienced by the cation and anion is unambiguous hence making this decrease in positive surface charge with increasing chain length of the cation a clear conclusion. From the shift of the maximum in the nitrogen profile it is concluded that the orientation of the alkyl chain changes from more parallel to the surface for [C_6mim] [BF_4] to more parallel to the surface normal for the [C_{10}mim] [BF_4].

3.4 References

1   Rogers, R. D. & Seddon, K. R. *Ionic Liquids IIIB: Fundamentals, Progress, Challenges, and Opportunities : Transformations and Processes*. (Oxford University Press, 2005).

2   Scovazzo, P. Determination of the upper limits, benchmarks, and critical properties for gas separations using stabilized room temperature ionic liquid membranes (SILMs) for the purpose of guiding future research. *Journal of Membrane Science* **343**, 199-211 (2009).

3   Ren, W. & Scurto, A. M. Global phase behavior of imidazolium ionic liquids and compressed 1,1,1,2-tetrafluoroethane (R-134a). *AIChE Journal* **55**, 486-493 (2009).

4   Yokozeki, A. & Shiflett, M. B. Separation of Carbon Dioxide and Sulfur Dioxide Gases Using Room-Temperature Ionic Liquid [hmim][Tf2N]. *Energy & Fuels* **23**, 4701-4708 (2009).

5   Min, Y. *et al.* Measurement of Forces across Room Temperature Ionic Liquids between Mica Surfaces. *The Journal of Physical Chemistry C* **113**, 16445-16449 (2009).

6   Santos, C. S. & Baldelli, S. Gas-liquid interface of room-temperature ionic liquids. *Chemical Society Reviews* **39**, 2136-2145 (2010).

7   Lockett, V., Sedev, R., Bassell, C. & Ralston, J. Angle-resolved X-ray photoelectron spectroscopy of the surface of imidazolium ionic liquids. *Physical Chemistry Chemical Physics* **10**, 1330-1335 (2008).

8   Kolbeck, C. *et al.* Influence of Different Anions on the Surface Composition of Ionic Liquids Studied Using ARXPS. *The Journal of Physical Chemistry B* **113**, 8682-8688 (2009).

9   Maier, F. *et al.* Insights into the surface composition and enrichment effects of ionic liquids and ionic liquid mixtures. *Physical Chemistry Chemical Physics* **12**, 1905-1915 (2010).

10   Caporali, S., Bardi, U. & Lavacchi, A. X-ray photoelectron spectroscopy and low energy ion scattering studies on 1-buthyl-3-methyl-imidazolium bis(trifluoromethane) sulfonimide. *Journal of Electron Spectroscopy and Related Phenomena* **151**, 4-8 (2006).

11   Iwahashi, T. *et al.* Surface Structural Study on Ionic Liquids Using Metastable Atom Electron Spectroscopy. *The Journal of Physical Chemistry C* **113**, 19237-19243 (2009).

12   Krischok, S. *et al.* Temperature-Dependent Electronic and Vibrational Structure of the 1-Ethyl-3-methylimidazolium Bis(trifluoromethylsulfonyl)amide Room-Temperature Ionic Liquid Surface: A Study with XPS, UPS, MIES, and HREELS†. *The Journal of Physical Chemistry B* **111**, 4801-4806 (2007).

13   Höfft, O. *et al.* Electronic Structure of the Surface of the Ionic Liquid [EMIM][Tf2N] Studied by Metastable Impact Electron Spectroscopy (MIES), UPS, and XPS. *Langmuir* **22**, 7120-7123 (2006).

14   Günster, J., Höfft, O., Krischok, S. & Souda, R. A time-of-flight secondary ion mass spectroscopy study of 1-ethyl-3-methylimidazolium bis(trifluoromethylsulfonyl)imide RT-ionic liquid. *Surface Science* **602**, 3403-3407 (2008).

15   Smith, E. F., Rutten, F. J. M., Villar-Garcia, I. J., Briggs, D. & Licence, P. Ionic Liquids in Vacuo: Analysis of Liquid Surfaces Using Ultra-High-Vacuum Techniques. *Langmuir* **22**, 9386-9392 (2006).

16   Nakajima, K., Ohno, A., Suzuki, M. & Kimura, K. Surface structure of an ionic liquid with high-resolution Rutherford backscattering spectroscopy. *Nuclear Instruments and Methods in Physics Research Section B: Beam Interactions with Materials and Atoms* **267**, 605-609 (2009).

17   Hashimoto, H. *et al.* Surface characterization of imidazolium ionic liquids by high-resolution Rutherford backscattering spectroscopy and X-ray photoelectron spectroscopy. *Surface Science* **604**, 464-469 (2010).

18   Sloutskin, E. *et al.* Surface Layering in Ionic Liquids: An X-ray Reflectivity Study. *Journal of the American Chemical Society* **127**, 7796-7804 (2005).

19   Sha, M., Wu, G., Dou, Q., Tang, Z. & Fang, H. Double-Layer Formation of [Bmim][PF6] Ionic Liquid Triggered by Surface Negative Charge. *Langmuir* **26**, 12667-12672 (2010).

20   Mezger, M. *et al.* Molecular Layering of Fluorinated Ionic Liquids at a Charged Sapphire (0001) Surface. *Science* **322**, 424-428 (2008).

21   Rivera-Rubero, S. & Baldelli, S. Influence of Water on the Surface of the Water-Miscible Ionic Liquid 1-Butyl-3-methylimidazolium Tetrafluoroborate: A Sum Frequency Generation Analysis. *The Journal of Physical Chemistry B* **110**, 15499-15505 (2006).

22   Santos, C. S. & Baldelli, S. Alkyl Chain Interaction at the Surface of Room Temperature Ionic Liquids: Systematic Variation of Alkyl Chain Length (R = C1−C4, C8) in both Cation and Anion of [RMIM][R−OSO3] by Sum Frequency Generation and Surface Tension. *The Journal of Physical Chemistry B* **113**, 923-933 (2009).

23   Iimori, T. *et al.* Local Structure at the Air/Liquid Interface of Room-Temperature Ionic Liquids Probed by Infrared−Visible Sum Frequency Generation Vibrational Spectroscopy: 1-Alkyl-3-methylimidazolium Tetrafluoroborates†. *The Journal of Physical Chemistry B* **111**, 4860-4866 (2007).

24   Law, G., Watson, P. R., Carmichael, A. J. & Seddon, K. R. Molecular composition and orientation at the surface of room-temperature ionic liquids: Effect of molecular structure. *Physical Chemistry Chemical Physics* **3**, 2879-2885 (2001).

25   Ikari, T. *et al.* Surface Electronic Structure of Imidazolium-Based Ionic Liquids Studied by Electron Spectroscopy. *e-Journal of Surface Science and Nanotechnology* **8**, 241-245 (2010).

26   Lockett, V. *et al.* Orientation and mutual location of ions at the surface of ionic liquids. *Physical Chemistry Chemical Physics* **12**, 13816-13827 (2010).

27   Rivera-Rubero, S. & Baldelli, S. Surface Characterization of 1-Butyl-3-methylimidazolium Br-, I-, PF6-, BF4-, (CF3SO2)2N-, SCN-, CH3SO3-, CH3SO4-, and (CN)2N- Ionic Liquids by Sum Frequency Generation. *The Journal of Physical Chemistry B* **110**, 4756-4765 (2006).

28   Endres, F. *et al.* Do solvation layers of ionic liquids influence electrochemical reactions? *Physical Chemistry Chemical Physics* **12**, 1724-1732 (2010).

29   Jiang, W., Wang, Y., Yan, T. & Voth, G. A. A Multiscale Coarse-Graining Study of the Liquid/Vacuum Interface of Room-Temperature Ionic Liquids with Alkyl Substituents of Different Lengths. *The Journal of Physical Chemistry C* **112**, 1132-1139 (2008).

30   Wick, C. D., Chang, T.-M. & Dang, L. X. Molecular Mechanism of CO2 and SO2 Molecules Binding to the Air/Liquid Interface of 1-Butyl-3-methylimidazolium Tetrafluoroborate Ionic Liquid: A Molecular Dynamics Study with Polarizable Potential Models. *The Journal of Physical Chemistry B* **114**, 14965-14971 (2010).

31   Lynden-Bell, R. M. & Del Popolo, M. Simulation of the surface structure of butylmethylimidazolium ionic liquids. *Physical Chemistry Chemical Physics* **8**, 949-954 (2006).

32   Bresme, F. & et al. Influence of ion size asymmetry on the properties of ionic liquid–vapour interfaces. *Journal of Physics: Condensed Matter* **17**, S3301 (2005).

33   Yan, T. *et al.* Structure of the Liquid−Vacuum Interface of Room-Temperature Ionic Liquids: A Molecular Dynamics Study. *The Journal of Physical Chemistry B* **110**, 1800-1806 (2006).

34   Bhargava, B. L. & Balasubramanian, S. Layering at an Ionic Liquid−Vapor Interface: A Molecular Dynamics Simulation Study of [bmim][PF6]. *Journal of the American Chemical Society* **128**, 10073-10078 (2006).

35   Sloutskin, E., Lynden-Bell, R. M., Balasubramanian, S. & Deutsch, M. The surface structure of ionic liquids: comparing simulations with x-ray measurements. *J. Chem. Phys.* **125**, 174715-174722 (2006).

36   Bowers, J., Vergara-Gutierrez, M. C. & Webster, J. R. P. Surface Ordering of Amphiphilic Ionic Liquids. *Langmuir* **20**, 309-312 (2003).

37   Jeon, Y. *et al.* Interfacial Restructuring of Ionic Liquids Determined by Sum-Frequency Generation Spectroscopy and X-Ray Reflectivity. *The Journal of Physical Chemistry C* **112**, 19649-19654 (2008).

38   Knapp, R. *et al.* Corrugated Ionic Liquid Surfaces with Embedded Polymer Stabilized Platinum Nanoparticles. *The Journal of Physical Chemistry C* **114**, 13722-13729 (2010).

39   Krebs, T., Andersson, G. & Morgner, H. Chemical Potential of a Nonionic Surfactant in Solution. *The Journal of Physical Chemistry B* **110**, 24015-24020 (2006).

40   Schulze, K. D. & Morgner, H. Investigation of the electric charge structure and the dielectric permittivity at surfaces of solutions containing ionic surfactants. *Journal of Physics: Condensed Matter*, 9823 (2006).

41   Andersson, G. & Morgner, H. Investigations on solutions of tetrabutylonium salts in formamide with NICISS and ICISS: concentration depth profiles and composition of the outermost layer. *Surface Science* **445**, 89-99 (2000).

42   Hammer, T., Reichelt, M. & Morgner, H. Influence of the aliphatic chain length of imidazolium based ionic liquids on the surface structure. *Physical Chemistry Chemical Physics* **12**, 11070-11080 (2010).

43   Andersson, G., Krebs, T. & Morgner, H. Angle resolved ion scattering spectroscopy reveals the local topography around atoms in a liquid surface. *Physical Chemistry Chemical Physics* **7**, 2948-2954 (2005).

44   Andersson, G. & Morgner, H. Impact collision ion scattering spectroscopy (ICISS) and neutral impact collision ion scattering spectroscopy (NICISS) at surfaces of organic liquids. *Surface Science* **405**, 138-151 (1998).

45   Tanford, C. Micelle shape and size. *The Journal of Physical Chemistry* **76**, 3020-3024 (1972).

46   Ohno, A., Hashimoto, H., Nakajima, K., Suzuki, M. & Kimura, K. Observation of surface structure of 1-butyl-3-methylimidazolium hexafluorophosphate using high-resolution Rutherford backscattering spectroscopy. *J. Chem. Phys.* **130** (2009).

47   Iimori, T. *et al.* Orientational ordering of alkyl chain at the air/liquid interface of ionic liquids studied by sum frequency vibrational spectroscopy. *Chemical Physics Letters* **389**, 321-326 (2004).

48   Lauw, Y. *et al.* X-Ray reflectometry studies on the effect of water on the surface structure of [C4mpyr][NTf2] ionic liquid. *Physical Chemistry Chemical Physics* **11**, 11507-11514 (2009).

49   Lehmann, S. B. C., Roatsch, M., Schoppke, M. & Kirchner, B. On the physical origin of the cation-anion intermediate bond in ionic liquids Part I. Placing a (weak) hydrogen bond between two charges. *Physical Chemistry Chemical Physics* **12**, 7473-7486 (2010).

Chapter 4

Effect of water on the charge distribution at the surface of [C$_6$mim][Cl]

4.1 Introduction

Ionic liquids (ILs) have a wide range of unique tuneable properties [1] that make them ideal for many applications such as solvents,[2] gas capture media,[3,4] electrolytes in solar cells,[5] and catalysis.[6] Impurities such as halides, silicon and water are known to affect both the bulk and surface physical properties of ILs.[7-10] An understanding of how these impurities influence the surface composition and the orientation of molecules at the surface is important both for fundamental studies of the surface properties of ILs such as surface tension [8] as well as for the various applications, particularly gas phase catalysis and gas capture media.[3,4,7]

Studying mixtures of water and ILs has attracted attention in the past decade amongst others due to the hygroscopic nature of ILs regardless of their hydrophobicity or hydrophilicity. Studies of water/IL mixtures have mainly focussed on either bulk properties of the mixtures [11-19] or bulk properties of water with small amounts of ILs.[20,21] These studies show that hydrogen bonds are formed between water and some of the ions used in ILs, especially between water and the anions.[19] Jeon et al. investigated the addition of 1-butyl-3-methylimidazolium tetrafluroborates ([C$_4$mim][BF$_4$]) to water and noted in infra-red and Raman spectra a significant intensity decrease of the peaks related to the hydrogen bonding even at low IL concentrations.[12] Wang et al. have performed quantum chemical calculations to investigate the interaction between water molecules and the 1-ethyl-3-methylimidazolium [C$_2$mim] cation using various anions.[17] The results indicate that water forms hydrogen bonds with the anions, in particular with chloride where 2H$_2$O-2Cl clusters are formed. The results also indicate that it is possible for the water molecules and ions to aggregate in a variety of different clusters, facilitated by hydrogen bonding.

This aggregation of ion-clusters mediated by hydrogen bonding is also noted by Moreno et al..[22] It has also been concluded that the presence of water weakens the ionic interactions in ILs due to competitive hydrogen bonding.[14,15]

While there are many results that show the interactions between water and ILs, investigations into water as a surface impurity are rare. Surface tension data show in some cases a decrease in the surface tension when small amounts of water are added. Examples are 1-butyl-3-methylpyrrolidinium trifluoromethylsulfonylimide [23] and imidazolium based ILs,[8] the class of ILs used in the present study. According to the Gibbs equation a decrease of the surface tension upon adding water means that there is a surface excess of water at low water concentrations and thus water could influence the surface structure at low water concentrations. This observation is in contrast to solutions with a high mole fraction of water where the surface tension increases when increasing the water concentration.[24,25] In case the surface tension increases with increasing water content, a depletion of water at the surface must be concluded based on the Gibbs equation.

Rivera-Rubero and Baldelli have investigated the influence of water on the surface structure of imidazolium-based ILs via sum-frequency generation spectroscopy (SFG).[26,27] Their results show that water has a preference to solvate ions in the bulk of water-miscible ILs as peaks due to water were not found in the SFG spectra of $[C_4mim][BF_4]$ exposed to water at saturation vapour pressure. In contrast, water has a preference to solvate ions at the surface in the case of the hydrophobic IL 1-butyl-3-methylimidazolium bis(perfluoralkyl)-imides as in this case a strong peak due to water was found in the SFG spectra when the IL was exposed to water at saturation vapour pressure.

Very little so far is known about the effect of water on the electrical double layer at the IL/vacuum interface. Lauw et al. have observed a positive surface charge at the 1-butyl-3-methylpyrrolidinium trifluoromethylsulfonylimide/vacuum interface using X-ray reflectometry.[23] They have demonstrated that at low water content, the addition of water does not change the surface thickness of this IL whereas when the water content increased, the surface swelled. As the electrical double layer and thus the surface potential is directly related to the preferential adsorption of either cations or anions to the surface, understanding whether the presence of water affects the electrical double layer is of great importance in understanding the surface structure of ILs for fundamental studies and in

applications. This problem is particularly of importance as the hygroscopic nature of all ILs ensures water will be present at some concentration if exposed to atmosphere.

The negligible vapour pressure of ILs makes them suitable for analysis using vacuum-based techniques such as Rutherford backscattering spectroscopy (RBS),[28,29] X-ray and ultraviolet photoelectron spectroscopies (XPS, UPS),[30-34] metastable induced electron spectroscopy (MIES),[35,36] and neutral impact collision ion scattering spectroscopy (NICISS).[37] NICISS is a low-energy ion scattering technique that can investigate the concentration depth profiles of the elements in soft-matter samples with a depth range of around 20 nm and a resolution of a few Å close to the surface.[38,39] It has already been shown how NICISS is capable of investigating the surface structure of liquids thus making it highly suited for investigating the effect of impurities on the surface structure of ILs.[37,38,40-44]

The aim of this study is to determine how the presence of water at low concentrations influences the surface structure of the 1-hexyl-3-methylimidazolium chloride IL, i.e. the composition of the surface and the orientation of molecules. This specific IL was chosen as it has been frequently investigated as well as for the known strength of the interaction between water molecules and the chloride anion. By determining the concentration depth profiles of the elements in [C$_6$mim][Cl]/water with known water concentrations it will be possible to determine the effect of water on the surface organisation and charge structure of the IL.

4.2 Experimental

4.2.1 Materials

The IL was purchased from Merck (synthesis grade) and purified by several steps: firstly, dissolution in ultra pure water (Millipore), adsorption with ultra high purity charcoal (Sigma-Aldrich), and filtration through 0.2 μm Teflon filters (Watman); secondly, extraction with acetyl acetate (Chemsupply, HPLC); and finally, water and volatile organic substances were removed by evaporation under moderate vacuum (10^{-2} mbar). The procedure and analysis of purified ILs is carefully described in [45]. XPS and nuclear magnetic resonance (NMR) [32,45] of purified [C$_6$mim][Cl] confirmed that there were no impurities and the elemental and structural compositions were equal to theoretical values.

4.2.2   Experimental setup

Table 4-1. Water content as obtained from KF titration at different exposure times to vacuum.

Time [hrs]	Water content [ppm]	Mole fraction	Water content [mol cm^{-3}]
0	40000 ± 4000	0.025 ± 0.0025	0.20 ± 0.02
1	10000 ± 1000	0.01 ± 0.001	0.051 ± 0.0051
2.5	6000 ± 600	0.006 ± 0.0006	0.031 ± 0.0031
20	2500 ± 250	0.0025 ± 0.00025	0.013 ± 0.0013

A small amount of water was added to the IL prior to measurement In order to determine the effect of water at different concentrations on the IL/vacuum interface. The exact concentration of water was determined via Karl Fischer (KF) titration. The liquid target was then placed inside a vacuum chamber of the NICISS apparatus. The vacuum chamber used for the measurements is kept at a pressure of 10^{-5} mbar while the TOF tube and microchannel plates are kept at low 10^{-7} mbar. One hour after the evacuation of the vacuum chamber had been started, a sample of the IL under vacuum was removed and the water content determined. A NICIS spectrum was then taken for 90 mins. Next, the water content of the IL under vacuum was again determined (the IL had been exposed then to vacuum for a total 2.5 hours), and a new NICIS spectrum was taken for 2 hours. The IL was left under vacuum overnight and after 20 hours total exposure to vacuum another NICIS spectrum was measured and subsequently the water content was measured again. This procedure was repeated several times with fresh samples and the individual spectra from each time interval were added together to achieve a NICIS spectrum with sufficient count rate at each of the time intervals. The surface structure of [C$_6$mim][Cl] could be determined as a function of water content from the NICIS spectra at the different time intervals along with the corresponding KF titration data. The water content after the various vacuum exposure times is listed in Table 4-1. The chosen IL is very hydroscopic due to the hydrogen bonds between the chloride and water.[16,17] As such even after 20 hours of exposure to 10^{-5} mbar the IL still has measurable water content and thus has to be considered as not fully dried.

4.3   Results and discussion

4.3.1   NICIS Spectra

Figure 4-1 shows the NICIS spectra as measured after the three vacuum exposure times, with vertical offsets added to some of the spectra for clarity. The TOF onset for each element in the sample is marked in the spectra and the peak of Cl of the gas phase spectrum is given as an indication of the zero-depth position as well as of its full-width-half-maximum (FWHM) due to the inelastic energy loss during the backscattering process. A step for oxygen due to the presence of water is not seen in the NICIS spectra as the concentration of water leads to a step height that would not be significant within the data scattering.

A full description of the data evaluation process for NICIS spectra is given in references [39,41] but the main steps are summarised here. Photons are generated as part of the ion beam interaction with matter, and these photons are able to be detected by the micro channel plates. Knowing the TOF length and the speed of the photons allows the zero mark of the TOF spectrum to be gauged. As the condition for backscattering (scattering angle > 90°) is
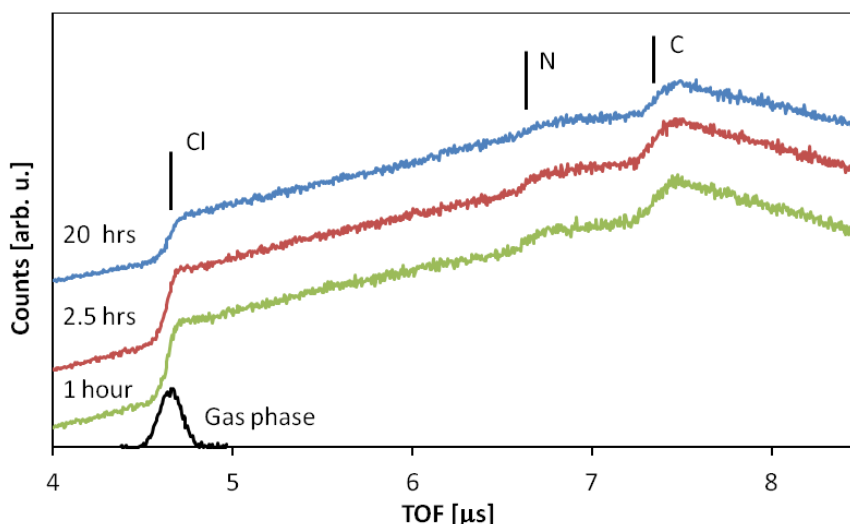
Figure 4-1. NICISS TOF spectra of [C6mim][Cl] measured at the three different vacuum exposure times. The lines mark the TOF onset for the respective elements. The spectra are vertically offset for clarity.

that the target mass must be greater than the projectile mass, the use of helium ions as the projectiles results in not finding backscattered projectiles from hydrogen. Instead, hydrogen is found as sputtered hydrogen with a broad background over a wide range of energies.[39] Apart from the signal due to the photons and the hydrogen background, the only other feature of a NICIS spectrum is the signal due to the backscattering of projectiles from the elements in the target. The profile due to an element can be separated from the total spectrum by fitting a low-order polynomial to account for the background. The depth scale for each element is then calculated from the final energy scale of each element, with the zero mark of depth being calibrated using the gas phase spectra, as described above. The accuracy of the gauging procedure depends in first instance on determining the TOF position for the gas phase peak maxima. The accuracy of the zero mark for both nitrogen and chlorine is about 2 Å. However, as the uncertainty affects all profiles in the same way, it does not affect the accuracy in comparing the profiles. Therefore while the absolute position of anion and cation has an uncertainty, the change in the position of the cation relative to that of the anion investigated is unambiguous when comparing the spectra with different water content.

Figure 4-2 shows the concentration depth profiles as measured for carbon, nitrogen and chlorine at the different vacuum exposure times. In the concentration depth profiles, zero depth marks the outermost layer of the target, with increasing depth indicating the direction towards the bulk. It is important to note that signal in the measured profiles can be seen at negative depths. However this is not due to finite concentration at negative depth, but rather due to the finite energy resolution of the method as indicated by the FWHM of the chloride gas phase peak. Additionally, as each data point in the measured element profiles for carbon and nitrogen corresponds to less than 0.5 Å on the depth scale, three data points have been summed up to a single value in order to decrease data scattering.

The carbon profile (Figure 4-2a) shows a clear surface excess after 20 hours exposure to vacuum compared to the shorter exposure times as is noted by the increased slope at the onset of the step as well as increased concentration seen up to the depth of 12 Å. The chloride profile (Figure 4-2b) shows an opposite trend with a reduced slope at the onset of the step after 20 hours of exposure of the sample to vacuum compared to the steeper slope at shorter exposure times. Additionally, the chloride step at 20 hours vacuum exposure is
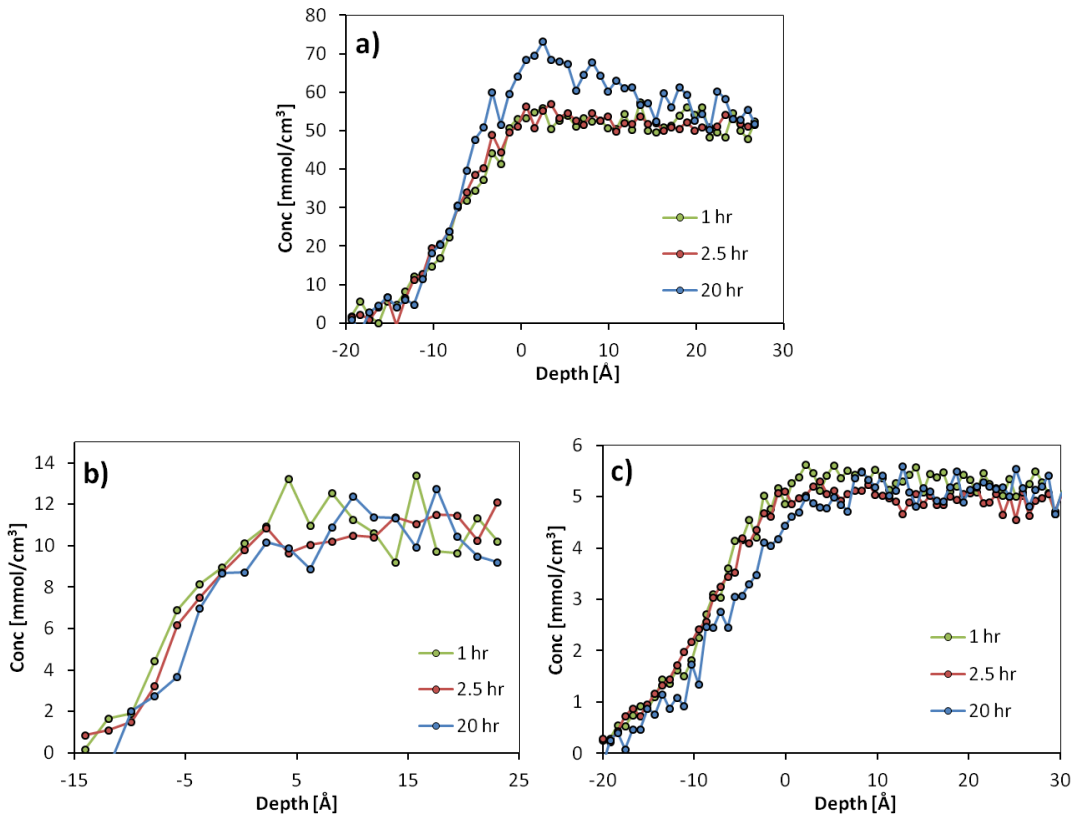
Figure 4-2. Concentration depth profiles as measured of (a) carbon, (b) nitrogen and (c) chloride at each of the three vacuum exposure times.

shifted towards the bulk by a few Å compared to the chloride steps at shorter exposure times. It will be shown below that these differences in the top few Å of the measured profiles result in distinct differences between the deconvoluted chloride profiles. This finding shows a depletion of chloride at the surface after 20 hours vacuum exposure. The nitrogen profiles (Figure 4-2c) at the different exposure times almost overlap within data scattering.

The profiles of all elements for 1 and 2.5 hour vacuum exposure times are almost identical, showing that the presence of water influences the structure of the surface in a similar way between 6000 and 10000 ppm water content. Additionally, the fact that the surface structure experiences negligible change between 1 hour and 2.5 hours vacuum exposure gives an indication that the observed concentration depth profiles represent an equilibrium and are not affected by the evaporation of water from the sample during the measurements. In case the evaporation of the water would affect the concentration depth

profiles, the spectra at 1 hour and 2.5 hours should differ as in the first case the water evaporation rate is higher due to the higher water content compared to the second case.

4.3.2 Deconvolution

The measured concentration depth profiles give a clear indication that at 2500 ppm water content chloride is shifted more towards the bulk compared to 6000 - 10000 ppm water content. In order to understand in more detail, how the presence of water influences the charge distribution at the anion at the IL/vacuum interface, the chloride profiles at 1 and 20 hours vacuum exposure time have been deconvoluted with the chlorine gas phase peak. Figure 4-3 shows the measured concentration depth profile for chloride along with the deconvoluted profiles and the fitted profiles (convolution of the deconvolted profiles) at a) 1 hour vacuum exposure and b) 20 hours vacuum exposure. The residuum demonstrates that the fitted profiles fit the measured profiles very well. The error bars of the deconvoluted profiles in Figure 4-3 are due to the uncertainty of the deconvolution procedure.

The deconvoluted profiles for chloride at 1 and 20 hour vacuum exposure are compared in Figure 4-4. The profiles show that chloride is shifted towards the bulk by a few Å at both vacuum exposure times, indicating that chloride is depleted in the outermost layer. However, at higher water content (1 hour) the chloride is closer to the surface than at the lower water content (20 hours). The difference in the position of the maxima is about 3 Å.
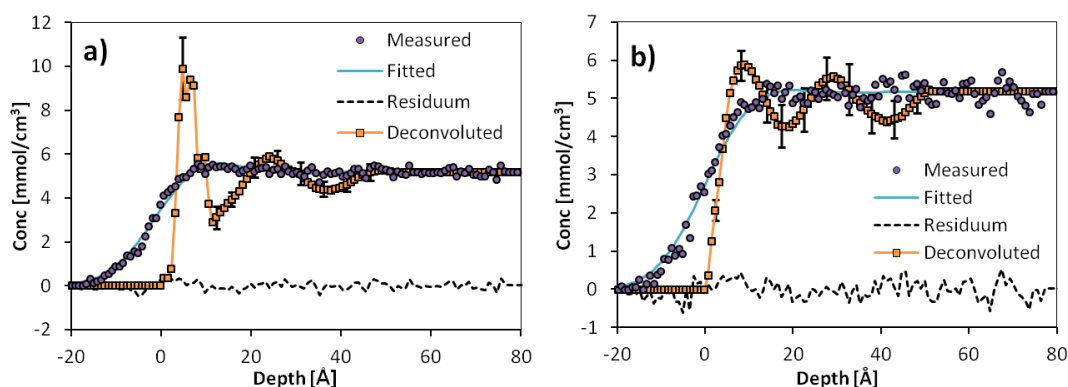
Figure 4-3. Measured, deconvoluted, fitted chloride concentration depth profiles and residua at (a) 1 hour and (b) 20 hours exposure to vacuum.
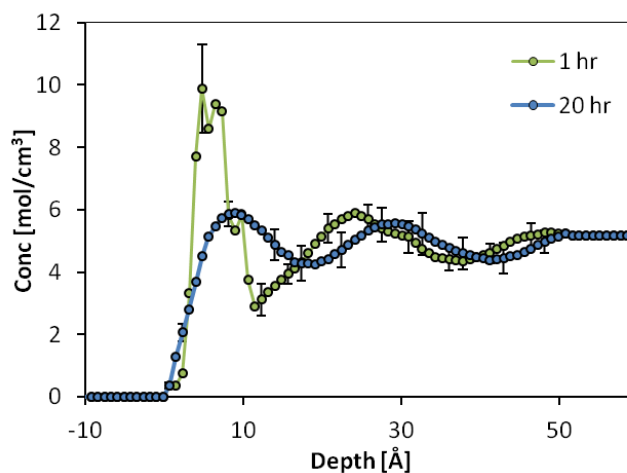
Figure 4-4. Comparing the deconvoluted chloride concentration depth profiles at vacuum exposure times of 1 and 20 hours. The error bars are due to the uncertainty of the deconvolution procedure.

Further, in case of the lower water content the chloride shows a high concentration in a thin layer just below the surface as the chloride profile shows a clear maximum at 6 Å followed by a minimum at about 15 Å. This maximum and minimum of concentration in the chloride profile at higher water content (1 hour) has to be considered as significant within the error bars while the oscillations at larger depth are not significant. The oscillations in the concentration depth profile at lower water content (20 hours) are not significant within the error bars. Due to the amount of data scattering present in the measured carbon and nitrogen profiles the deconvolution would not yield in more details for the discussion of these profiles. Hence, the carbon and nitrogen profiles have not been deconvoluted.

The accuracy of the zero mark for both nitrogen and chloride is about 2 Å. As the uncertainty affects all profiles in the same way, the uncertainty does not affect the accuracy in comparing the profiles of the different spectra. As a consequence, while the absolute positions of anion and cation have uncertainties, the relative change in the position is unambiguous and thus also the conclusion about the change of the surface potential as a result of the changing water content.

4.3.3 Effect of water

The results indicate that the effects of water as a surface impurity in [C_6mim][Cl] are largely the same between 10000 and 6000 ppm water. However after the water content is reduced to 2500 ppm a noticeable difference in the carbon and chloride concentration depth profiles can be seen. Compared to the spectra at 10000 and 6000 ppm water, the spectrum at 2500 ppm water content shows a shift of carbon towards the outermost layer of the IL/vacuum interface along with an increasing surface excess of carbon. At the same time the chloride concentration at the surface decreases and shifts towards the bulk as can be seen in the deconvoluted profiles. As carbon is only present in the cation, the increased excess of carbon at 20 hours exposure time directly indicates that the shift of chloride towards the bulk is followed by an excess of cation replacing it at the surface. As the only difference between the spectra is in their water content, it has to be concluded that the presence of water influences the composition and charge distribution at the surface of [C_6mim][Cl] as described.

Conclusions regarding the change in surface charge of the IL with changing water content can be made by comparing the chloride profiles with the nitrogen profiles, as these give the position of anion and cation, respectively. While the nitrogen profiles have not been deconvoluted, Figure 4-2 shows that the nitrogen profile does not considerably change with change in water content. The data scattering adds an uncertainty of $\pm$ 1 Å to the position of the onset of the nitrogen profiles. Hence the maximum difference between the onset of the 1 hour and 20 hours nitrogen profiles can only be 2 Å. Conversely, the deconvoluted chloride profiles in Figure 4-3 show a substantial increase in chloride concentration in the near-surface region and a shift of the maximum in the chloride concentration depth profile towards the surface. Given the lack of change in the cation profile with changing water content, it can be concluded that increasing water content results in an increase in the amount of negative charge at the IL surface.

This finding has to be related to two observations. Firstly, the surface tension of the solution of water in [C_4mim][PF_6] and [C_8mim][PF_6] decreases upon adding water at low water concentrations in the range of 0 to 0.05 molefraction which means according to the Gibbs equation that water is surface active in this concentration range.[8] Even though a different anion is used in the present study, a similar reduction of the surface tension can

be expected for [C$_6$mim][Cl]. Secondly, water has a propensity to form complexes with chloride via hydrogen bonding.[16,17,22] The increased water content at 1 and 2.5 hours vacuum exposure leads to hydrogen bonding between water and the anions that decreases the dominance of electrostatic interaction between the anion and cation in governing the surface structure.[14,15,22] Thus at low water content, the surface structure of [C$_6$mim][Cl] is dominated by the influence of the intermolecular forces between cation and anion alone. This results in an increased propensity of the cation to adsorb at the surface with the alkyl chains oriented towards the vacuum or gas phase, pushing the anion towards the bulk as has been observed in previous studies.[26, 36-38] Rivera-Rubero et al. reported a similar result for [C$_4$mim][BF$_4$].[26] The authors observed a small but observable change in cation alkyl chain orientation of less than 10° with addition of water to [C$_4$mim][BF$_4$]. The change in surface structure observed for [C$_4$mim][BF$_4$] seems to be small compared to the results found here as such a small change in the orientation of the alkyl chain hardly can explain the change in the carbon concentration depth profiles in Figure 4-2a. This might be due to factors such as a shorter cation alkyl chain length of the cation in the study of Rivera-Rubero et al., but also the higher water concentration used by the authors, or a decreased propensity of water to form hydrogen bonds with BF$_4^-$ compared to Cl$^-$. Another reason for this finding could be the increased radius of the BF$_4^-$ compared to that of Cl$^-$ which adds additional steric hindrance to adsorption at the IL/vacuum interface.[26]

The surface structure found for the [C$_6$mim][Cl] with low water content has similarities with the surface structure reported for various imidazolium based ILs. In a number of cases it is reported that the surface is covered with the alkyl chain of the cation where the coverage increases with increasing length of the alkyl chain.[10,12,26,27,31,32,37] X-ray reflectivity studies showed a layer with increased electron density close to the surface giving evidence that the surface structure differs from that of the bulk.[12,46] Sloutskin et al. propose a surface structure of [C$_4$mim][BF$_4$] and [C$_4$mim][PF$_6$] with an enhanced density at the surface but with the same composition as in the bulk.[46] Jeon et al. interpreted the reflectivity data with a layer of enhanced anion density below the cation layer at the surface (for [C$_4$mim][I]).[12] The presence of an electrical double layer at ILs/vacuum interface was also found for pure ILs by angle resolved and synchrotron XPS techniques.[32] However, the conclusions about the sign of the excess charge at the free surface vary and depend on the IL and on the amount of water or other contaminations in ILs.

Recently Martinez et al. showed by means of surface potential measurements of three thoroughly dried imidazolium based ILs ([C$_4$mim][trifluoromethane], [C$_4$mim][BF4] and [C$_4$mim][diciamide]) that the anions are located at slightly larger depth compared to the cations (imidazolium rings).[47] Qualitatively Martinez' results correspond to the observations in the present work where it is found that the anion withdraws from the surface when reducing the water content. However, it has to be taken into account that Martinez et al. investigated ILs with a different length of the cation alkyl chain, different anions and with a low, but not quantified, water content thus possibly with a water content different to that in the present study.

4.4   Conclusion

By exposing [C$_6$mim][Cl] with a known initial water concentration to vacuum for controlled periods of time, it was investigated how the presence of water influences the surface structure of [C$_6$mim][Cl]. Concentration depth profiles of the elements in the IL/water sample reveal that at low water concentrations the cation is preferentially adsorbed at the surface with the cation alkyl chains forming the outermost layer while the anion is located in a layer below the alkyl chains. With increasing water content the anion has a higher propensity for the IL/vacuum interface leading to an increase in negative surface charge and negative surface potential. While there has been little work done on the role of water as a surface impurity, this study highlights the importance in understanding the presence of water on the surface structure of ILs. This is especially prevalent when comparing surface studies of ILs which have absorbed water to those studies that used dried ILs as well as for applications of ILs where the surface structure and charge is of significant importance. Thus for any investigation of the surface structure of ILs their water content should be measured as well.

4.5 References

1 Welton, T. Room-Temperature Ionic Liquids. Solvents for Synthesis and Catalysis. *Chemical Reviews* **99**, 2071-2084 (1999).

2 Rogers, R. D. & Seddon, K. R. *Ionic Liquids IIIB: Fundamentals, Progress, Challenges, and Opportunities : Transformations and Processes*. (Oxford University Press, 2005).

3 Scovazzo, P. Determination of the upper limits, benchmarks, and critical properties for gas separations using stabilized room temperature ionic liquid membranes (SILMs) for the purpose of guiding future research. *Journal of Membrane Science* **343**, 199-211 (2009).

4 Ren, W. & Scurto, A. M. Global phase behavior of imidazolium ionic liquids and compressed 1,1,1,2-tetrafluoroethane (R-134a). *AIChE Journal* **55**, 486-493 (2009).

5 Pinilla, C., Del Pópolo, M. G., Lynden-Bell, R. M. & Kohanoff, J. Structure and Dynamics of a Confined Ionic Liquid. Topics of Relevance to Dye-Sensitized Solar Cells. *The Journal of Physical Chemistry B* **109**, 17922-17927 (2005).

6 Itoh, T., Akasaki, E., Kudo, K. & Shirakami, S. Lipase-Catalyzed Enantioselective Acylation in the Ionic Liquid Solvent System: Reaction of Enzyme Anchored to the Solvent. *Chemistry Letters* **30**, 262-263 (2001).

7 Seddon, K. R., Stark, A. & Torres, M. J. Influence of chloride, water, and organic solvents on the physical properties of ionic liquids. *Pure Appl. Chem.* **72**, 2275-2287 (2000).

8 Freire, M. G. *et al.* Surface tensions of imidazolium based ionic liquids: Anion, cation, temperature and water effect. *Journal of Colloid and Interface Science* **314**, 621-630 (2007).

9 Smith, E. F., Rutten, F. J. M., Villar-Garcia, I. J., Briggs, D. & Licence, P. Ionic Liquids in Vacuo: Analysis of Liquid Surfaces Using Ultra-High-Vacuum Techniques. *Langmuir* **22**, 9386-9392 (2006).

10 Baldelli, S. Influence of Water on the Orientation of Cations at the Surface of a Room-Temperature Ionic Liquid: A Sum Frequency Generation Vibrational Spectroscopic Study. *The Journal of Physical Chemistry B* **107**, 6148-6152 (2003).

11 Katayanagi, H. *et al.* Mixing Schemes in Ionic Liquid−H2O Systems: A Thermodynamic Study. *The Journal of Physical Chemistry B* **108**, 19451-19457 (2004).

12 Jeon, Y. *et al.* Structural Change of 1-Butyl-3-methylimidazolium Tetrafluoroborate + Water Mixtures Studied by Infrared Vibrational Spectroscopy. *The Journal of Physical Chemistry B* **112**, 923-928 (2008).

13 Bernardes, C. E. S., Minas da Piedade, M. E. & Canongia Lopes, J. N. The Structure of Aqueous Solutions of a Hydrophilic Ionic Liquid: The Full Concentration Range of 1-Ethyl-3-methylimidazolium Ethylsulfate and Water. *The Journal of Physical Chemistry B* **115**, 2067-2074 (2011).

14 Sarkar, S., Pramanik, R., Ghatak, C., Setua, P. & Sarkar, N. Probing the Interaction of 1-Ethyl-3-methylimidazolium Ethyl Sulfate ([Emim][EtSO4]) with Alcohols and Water by Solvent and Rotational Relaxation. *The Journal of Physical Chemistry B* **114**, 2779-2789 (2010).

15 Zhang, Q.-G., Wang, N.-N. & Yu, Z.-W. The Hydrogen Bonding Interactions between the Ionic Liquid 1-Ethyl-3-Methylimidazolium Ethyl Sulfate and Water. *The Journal of Physical Chemistry B* **114**, 4747-4754 (2010).

16 Hanke, C. G. & Lynden-Bell, R. M. A Simulation Study of Water−Dialkylimidazolium Ionic Liquid Mixtures. *The Journal of Physical Chemistry B* **107**, 10873-10878 (2003).

17   Wang, Y., Li, H. & Han, S. A Theoretical Investigation of the Interactions between Water Molecules and Ionic Liquids. *The Journal of Physical Chemistry B* **110**, 24646-24651 (2006).

18   Moreno, M., Castiglione, F., Mele, A., Pasqui, C. & Raos, G. Interaction of water with the model ionic liquid [bmim][BF$_4$]: Molecular dynamics simulations and comparison with NMR data. *Journal of Physical Chemistry B* **112**, 7826-7836 (2008).

19   Cammarata, L., Kazarian, S. G., Salter, P. A. & Welton, T. Molecular states of water in room temperature ionic liquids. *Physical Chemistry Chemical Physics* **3**, 5192-5200 (2001).

20   Miki, K., Westh, P., Nishikawa, K. & Koga, Y. Effect of an "Ionic Liquid" Cation, 1-Butyl-3-methylimidazolium, on the Molecular Organization of H2O. *The Journal of Physical Chemistry B* **109**, 9014-9019 (2005).

21   Singh, T. & Kumar, A. Cation-anion-water interactions in aqueous mixtures of imidazolium based ionic liquids. *Vibrational Spectroscopy* **55**, 119-125 (2011).

22   Moreno, M., Castiglione, F., Mele, A., Pasqui, C. & Raos, G. Interaction of Water with the Model Ionic Liquid [bmim][BF4]: Molecular Dynamics Simulations and Comparison with NMR Data. *The Journal of Physical Chemistry B* **112**, 7826-7836 (2008).

23   Lauw, Y. *et al.* X-Ray reflectometry studies on the effect of water on the surface structure of [C4mpyr][NTf2] ionic liquid. *Physical Chemistry Chemical Physics* **11**, 11507-11514 (2009).

24   Torrecilla, J. S., Rafione, T., García, J. & Rodríguez, F. Effect of Relative Humidity of Air on Density, Apparent Molar Volume, Viscosity, Surface Tension, and Water Content of 1-Ethyl-3-methylimidazolium Ethylsulfate Ionic Liquid. *Journal of Chemical & Engineering Data* **53**, 923-928 (2008).

25   Rilo, E., Pico, J., García-Garabal, S., Varela, L. M. & Cabeza, O. Density and surface tension in binary mixtures of CnMIM-BF4 ionic liquids with water and ethanol. *Fluid Phase Equilibria* **285**, 83-89 (2009).

26   Rivera-Rubero, S. & Baldelli, S. Influence of Water on the Surface of Hydrophilic and Hydrophobic Room-Temperature Ionic Liquids. *Journal of the American Chemical Society* **126**, 11788-11789 (2004).

27   Rivera-Rubero, S. & Baldelli, S. Influence of Water on the Surface of the Water-Miscible Ionic Liquid 1-Butyl-3-methylimidazolium Tetrafluoroborate: A Sum Frequency Generation Analysis. *The Journal of Physical Chemistry B* **110**, 15499-15505 (2006).

28   Nakajima, K., Ohno, A., Suzuki, M. & Kimura, K. Surface structure of an ionic liquid with high-resolution Rutherford backscattering spectroscopy. *Nuclear Instruments and Methods in Physics Research Section B: Beam Interactions with Materials and Atoms* **267**, 605-609 (2009).

29   Ohno, A., Hashimoto, H., Nakajima, K., Suzuki, M. & Kimura, K. Observation of surface structure of 1-butyl-3-methylimidazolium hexafluorophosphate using high-resolution Rutherford backscattering spectroscopy. *J. Chem. Phys.* **130** (2009).

30   Caporali, S., Bardi, U. & Lavacchi, A. X-ray photoelectron spectroscopy and low energy ion scattering studies on 1-buthyl-3-methyl-imidazolium bis(trifluoromethane) sulfonimide. *Journal of Electron Spectroscopy and Related Phenomena* **151**, 4-8 (2006).

31   Lockett, V., Sedev, R., Bassell, C. & Ralston, J. Angle-resolved X-ray photoelectron spectroscopy of the surface of imidazolium ionic liquids. *Physical Chemistry Chemical Physics* **10**, 1330-1335 (2008).

32   Lockett, V. *et al.* Orientation and mutual location of ions at the surface of ionic liquids. *Physical Chemistry Chemical Physics* **12**, 13816-13827 (2010).

33   Ikari, T. *et al.* Surface Electronic Structure of Imidazolium-Based Ionic Liquids Studied by Electron Spectroscopy. *e-Journal of Surface Science and Nanotechnology* **8**, 241-245 (2010).

34   Lovelock, K. R. J., Villar-Garcia, I. J., Maier, F., Steinrück, H.-P. & Licence, P. Photoelectron Spectroscopy of Ionic Liquid-Based Interfaces. *Chemical Reviews* **110**, 5158-5190 (2010).

35   Höfft, O. *et al.* Electronic Structure of the Surface of the Ionic Liquid [EMIM][Tf2N] Studied by Metastable Impact Electron Spectroscopy (MIES), UPS, and XPS. *Langmuir* **22**, 7120-7123 (2006).

36   Iwahashi, T. *et al.* Surface Structural Study on Ionic Liquids Using Metastable Atom Electron Spectroscopy. *The Journal of Physical Chemistry C* **113**, 19237-19243 (2009).

37   Hammer, T., Reichelt, M. & Morgner, H. Influence of the aliphatic chain length of imidazolium based ionic liquids on the surface structure. *Physical Chemistry Chemical Physics* **12**, 11070-11080 (2010).

38   Ridings, C., Lockett, V. & Andersson, G. Effect of the aliphatic chain length on electrical double layer formation at the liquid/vacuum interface in the [Cnmim][BF4] ionic liquid series. *Physical Chemistry Chemical Physics* **13**, 17177-17184 (2011).

39   Andersson, G. & Morgner, H. Impact collision ion scattering spectroscopy (ICISS) and neutral impact collision ion scattering spectroscopy (NICISS) at surfaces of organic liquids. *Surface Science* **405**, 138-151 (1998).

40   Andersson, G., Krebs, T. & Morgner, H. Activity of surface active substances determined from their surface excess. *Physical Chemistry Chemical Physics* **7**, 136-142 (2005).

41   Andersson, G., Krebs, T. & Morgner, H. Angle resolved ion scattering spectroscopy reveals the local topography around atoms in a liquid surface. *Physical Chemistry Chemical Physics* **7**, 2948-2954 (2005).

42   Andersson, G. & Morgner, H. Investigations on solutions of tetrabutylonium salts in formamide with NICISS and ICISS: concentration depth profiles and composition of the outermost layer. *Surface Science* **445**, 89-99 (2000).

43   Krebs, T., Andersson, G. & Morgner, H. Chemical Potential of a Nonionic Surfactant in Solution. *The Journal of Physical Chemistry B* **110**, 24015-24020 (2006).

44   Ridings, C. & Andersson, G. Determining concentration depth profiles of thin foam films with neutral impact collision ion scattering spectroscopy. *Review of Scientific Instruments* **81**, 113907-113915 (2010).

45   Lockett, V., Sedev, R., Ralston, J., Horne, M. & Rodopoulos, T. Differential Capacitance of the Electrical Double Layer in Imidazolium-Based Ionic Liquids: Influence of Potential, Cation Size, and Temperature. *The Journal of Physical Chemistry C* **112**, 7486-7495 (2008).

46   Sloutskin, E. *et al.* Surface Layering in Ionic Liquids: An X-ray Reflectivity Study. *Journal of the American Chemical Society* **127**, 7796-7804 (2005).

47   Martinez, I. S. & Baldelli, S. On the Arrangement of Ions in Imidazolium-Based Room Temperature Ionic Liquids at the Gas−Liquid Interface, Using Sum Frequency Generation, Surface Potential, and Surface Tension Measurements. *The Journal of Physical Chemistry C* **114**, 11564-11575 (2010).

Chapter 5

Comparing the charge distribution along the surface normal in the [C$_6$mim]$^+$ ionic liquid with different anions

5.1 Introduction

Ionic liquids (ILs) are organic salts that are a liquid below 100$^\text{o}$C. Their wide range of tuneable properties have seen them involved in many different applications such as solvents in organic synthesis and extraction technologies,[1] electrolytes for energy storage devices and electrodeposition,[1] heterogeneous catalysis,[2] and gas capture media.[3,4] For these last two applications it is desirable to understand and control the surface properties of ILs. Unlike typical solvent/salt solutions, ILs provide a system consisting exclusively of charged species. It is therefore of interest to investigate properties such as surface charge, surface potential and the role of electrostatic forces in ILs compared to systems of more dilute concentration of ions. Investigations into the surface charge at the IL/solid interface show that a layered structure of ions exists.[5-7] This effect is also observed by molecular dynamics simulations at the IL/vapour interface and that the structure itself is influenced by asymmetry in the size of the cation and anion.[8-11] A number of experimental techniques have been used to show the non-uniform distribution of ions at the surface such as x-ray and neutron reflectivity,[12-15] angle-resolved and energy-resolved x-ray photoelectron spectroscopy (XPS),[16,17] metastable induced electron spectroscopy (MIES),[18] and neutral impact collision ion scattering spectroscopy (NICISS).[19-21] NICISS has been used to investigate the effect of the cation aliphatic chain length on the charge distribution in the 1-alkyl-3-methylimidazolium tetrafluroborate [C$_n$mim][BF$_4$] (n = 6, 8, 10)[20] as well as the effect of small amount of water on the surface charge of 1-hexyl-3-methylimidazolium chloride [C$_6$mim][Cl].[21] It was found in the former case that an increase in aliphatic chain

length led to the cation ring experiencing a greater shift away from the surface compared to the anion, resulting in an increase in negative surface charge or surface potential. The latter study demonstrated that increasing the water content from 0.25% to 1% results in a large increase in the amount of anion present at the surface. Freire et al. have shown that the surface tension of imidazolium-based ILs depends on the cation-anion combination, rather than the interactions of ion pairs.[22] $[C_4mim]^+$ ILs show little differences in surface tension between $[BF_4]^-$, $[PF_6]^-$ while for the larger anions $[Tf_2N]^-$ and $[CF_3SO_3]^-$ the surface tension decreases more drastically. Similar results have been seen in other experiments[17,23,24] and simulations[10,11], however the ion distribution profiles along the surface normal have not been explicitly determined. This paper aims at comparing the ion distribution along the surface normal of $[C_6mim][BF_4]$ and $[C_6mim][Cl]$ with insignificant but comparable water content, therefore giving the difference in surface propensity of different anions and how this may affect the charge distribution at the surface of imidazolium-based ILs.

5.2   **Results and discussion**

5.2.1   NICIS Spectra

A detailed description of the data evaluation procedure has already been described in detail in ref. [25] however a brief description is given here. Photons (which are detectable by the micro channel plates) are generated by the interaction of the ion beam with matter. By knowing the TOF length and the speed of the photons, the zero mark of TOF can be determined. The condition for backscattering with an angle of $> 90^o$ is that the mass of the projectile must be greater than the mass of the target. Therefore the use of He^+ as the choice of projectile does not yield projectiles being backscattered from hydrogen. Instead, sputtered hydrogen appears as a background in a NICIS spectrum. Apart from the photon signal and the sputtered hydrogen signal, the only other signal is due to the elements in the target. The profiles owing to an element can be separated from the total spectrum by fitting a low-order polynomial to both sides of the element's profile. The depth scale of each element is then calculated from the final energy scale of each element, with the zero mark of depth being calibrated experimentally via gas phase as described in section 2.1.2. The accuracy in determining the zero mark of depth depends primarily on determining the

TOF position for the gas phase maxima, which is approximately 2 Å for the elements investigated in this study. This uncertainty affects all profiles in the same way, therefore, while there is some inaccuracy in determining the absolute zero mark of depth for an element, this affects the profiles of an element in any sample in the same manner. Thus the relative position of two elements with respect to the depth scale can be determined with a higher accuracy.

The TOF spectra for the two ILs investigated are shown in Figure 5-1. Steps due to each individual element in the spectrum are indicated, where elements of higher mass result in backscattered projectiles having a higher kinetic energy and are thus detected at shorter TOFs. A calibration factor that is determined from the composition of the sample is then used to convert counts to concentration.

In this study the focus is on comparing the profiles of several elements. Thus the concentration of each species is normalised to their bulk concentration which is set to unity. The concentration depth profiles of carbon and nitrogen for both ILs are shown in
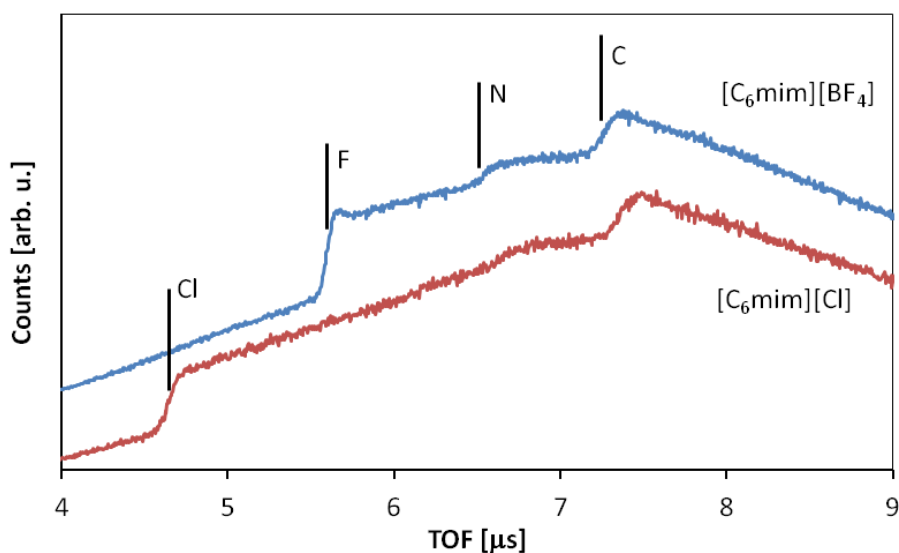
Figure 5-1. NICISS TOF spectra of [C6mim][Cl] and [C6mim][BF4]. The spectra are vertically offset for clarity. [C$_6$mim][Cl] data as seen in Chapter 4 and [C$_6$mim][BF4] data as seen in Chapter 3.
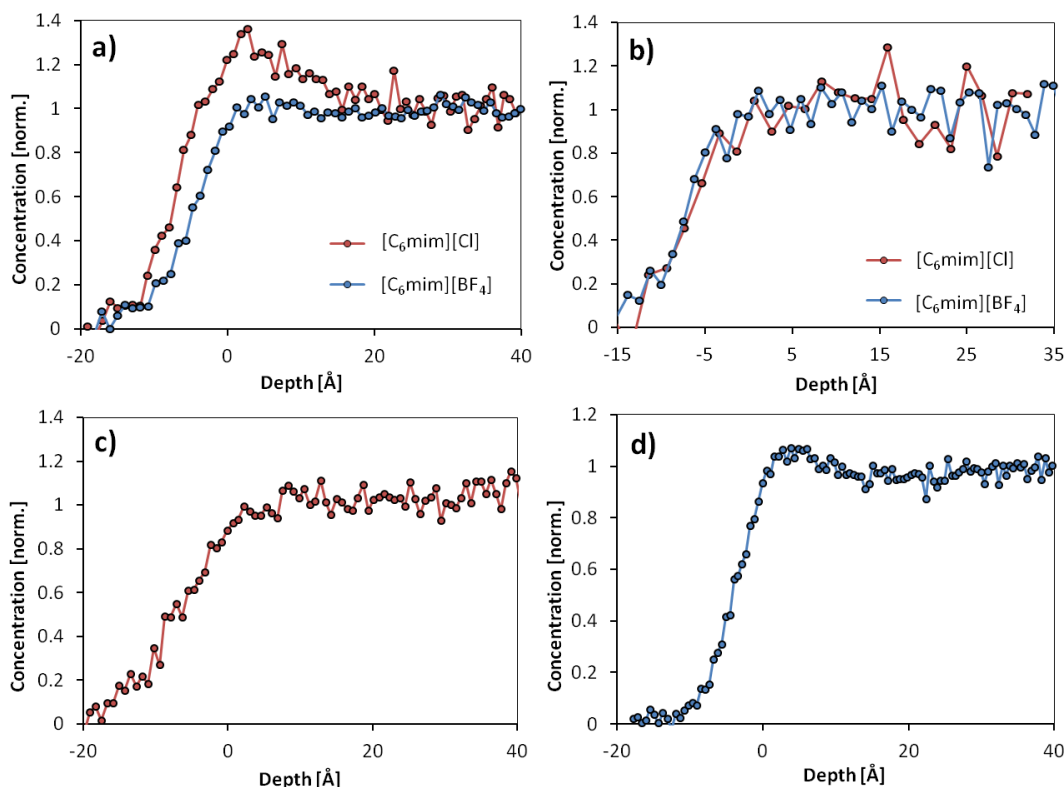
Figure 5-2. Concentration depth profiles as measured of (a) carbon and (b) nitrogen for both of the ionic liquids studied, and (c) chloride for [C$_6$mim][Cl] and (d) fluorine for [C$_6$mim][BF$_4$]. Concentrations have been normalised to the bulk values of concentration for each individual element. [C$_6$mim][Cl] data as seen in Chapter 4and [C$_6$mim][BF$_4$] data as seen in Chapter 3.

Figure 5-2a and b (respectively), the concentration depth profile for chloride is in Figure 5-2c and the concentration depth profile for fluorine is shown in Figure 5-2d. Zero depth marks the outermost layer in the target with positive values indicating the direction towards the bulk. It must be noted that although these profiles as measured show concentration at negative depth, this does not represent a physical presence of the element above the outermost layer but is instead owing to the finite energy resolution of the method. As carbon and nitrogen are only found on the cation, their profiles can be used to determine the position of the cation relative to the IL/vacuum interface. Immediately it can be seen that nitrogen (owing directly to the cation ring) has the same depth profile in both of the ILs, while the carbon profile is much more pronounced at zero depth in the case of [C$_6$mim][Cl]. This indicates that while the cation ring itself shares a common profile

between the two ILs, the cation aliphatic chains in [C$_6$mim][Cl] are present in an increased amount near the outermost layer, indicating a possible increase in the amount of cation chains oriented towards the gas phase. This can be further understood by taking into account the corresponding anion profiles. Fluorine can be seen to have a steeper onset compared to chloride as well a region with higher than bulk concentration up to 10 Å, compared to the depletion of chloride noted in the top several Å. Therefore the depletion of chloride at the surface of [C$_6$mim][Cl] is related to the increased presence of carbon owing to the cation aliphatic chains. This agrees with the results of Jeon et al. who studied the surface of [C$_4$mim]X with sum frequency generation spectroscopy and X-ray reflectivity and concluded that the larger, fluorinated anions ([BF$_4$]$^-$ and [PF$_6$]$^-$) were located closer to the outermost layer, intermingling with the cation aliphatic chains compared to the smaller, halide anion, [I]$^-$, which is seen directly below the cation rings.[15]

5.2.2 Comparing ion depth profiles

In order to reveal more details of the concentration depth profiles, the measured concentration depth profiles of the elements can be deconvoluted as discussed in section 2.1.2. The details for the deconvolution of chloride is given in ref.[21] while the details for fluorine is given in ref.[20]. Figure 5-3 compares the deconvoluted profiles for chloride and fluorine ([Cl]$^-$ and [BF$_4$]$^-$ respectively). The deconvoluted profiles show fluorine to have a large region of excess in the top few Å, followed by a region of depletion, which then reverts to bulk concentration levels. Conversely the chloride profile shows a depletion of the anion in the top few Å along with an oscillation in concentration that is only just significant outside of the error bars. The NICIS spectra show that there are no detectable impurities (and XPS and NMR confirmed [17]) in either of the ILs, therefore the only difference between the two ILs (besides choice of anion) is the water content (600 ppm for [C$_6$mim][BF$_4$] and 2500 ppm for [C$_6$mim][Cl]). However as it has been seen that increasing the amount of water in [C$_6$mim][Cl] has the effect of increasing the amount of anion at the surface,[21] it can be safely assumed that in the complete absence of water the difference in surface concentration of both anions would only be stronger. Furthermore, it is also safe to assume that any difference in the anion profiles seen here is due solely to the specificity of the respective anions. It is known that fluorinated compounds have relatively low surface energies,[26] and thus can explain the increased surface concentration
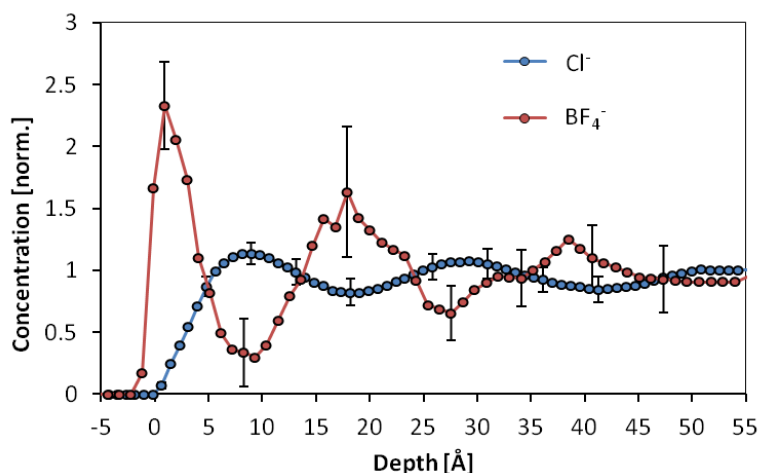
Figure 5-3. Deconvoluted concentration depth profiles of the anions in the two ionic liquids. Concentrations have been normalised to the bulk values of concentration for the individual elements (Cl and F). [C_6mim][Cl] data as seen in Chapter 4 and [C_6mim][BF_4] data as seen in Chapter 3.

of the [BF_4]$^-$ compared to [Cl]$^-$. This is in agreement with the results of Bagno et al. who measured the surface tension of 1,3-dialkylammonium salts with various anions, finding that fluorinated anions lead to lower surface tensions compared to halide anions.[27] Given that both ILs share very similar cation profiles, the increased surface concentration of the [BF_4]$^-$ anion compared to the [Cl]$^-$ anion directly indicates a more negative surface charge in [C_6mim][BF_4] compared to [C_6mim][Cl]. This difference in anion profile between the two ILs can be understood as competition between separation of charges at the IL/vacuum interface and the minimisation of surface energy. Surface energy minimisation can occur by the orientation of the cation aliphatic chains covering the surface as is shown by several techniques.[28,29] Covering the surface with a fluorinated species like the [BF_4]$^-$ anion should also assist in reducing the surface energy. Additionally, the [Cl]$^-$ anion, as a less polarisable ion than the [BF_4]$^-$ anion, does not act to minimise surface energy and instead interrupts the preferential orientation of the cation aliphatic chains thus hindering the surface energy optimisation. This increased surface propensity of more polarisable anions is also in agreement with experiments and simulations of aqueous salt solutions.[30-32] It is recognised that electrostatic forces account for majority of the interaction forces in ILs [33] therefore it is not unreasonable to assume that polarisation effects have an influence on the

surface structure given their importance in electrostatic interactions.[34,35] This could lead to structures dominated by the choice of hard/soft ions as seen in concentrated aqueous salt solutions.[36,37] However, for more general conclusions a larger variety of ions needs to be investigated.

5.3   **Conclusion**

The surface structure of $[C_6mim]X$ ILs were studied with two anions: $[Cl]^-$, a halide anion, and $[BF_4]^-$ a larger, fluorinated anion. The concentration depth profiles of the elements obtained by NICISS give detail on the structure of the cations, anions and aliphatic chains owing to the cations, and show that the $[BF_4]^-$ anion has a higher propensity than the $[Cl]^-$ anion for adsorbing at the IL/vacuum interface. The depletion of $[Cl]^-$ from the surface is accompanied by an excess of the cation aliphatic chains at the surface which indicates that optimisation of the surface energy of ILs is a significant force competing with the separation of charge at the surface of ILs.

5.4   **References**

1   Rogers, R. D. & Seddon, K. R. *Ionic Liquids IIIB: Fundamentals, Progress, Challenges, and Opportunities : Transformations and Processes*. (Oxford University Press, 2005).

2   Itoh, T., Akasaki, E., Kudo, K. & Shirakami, S. Lipase-Catalyzed Enantioselective Acylation in the Ionic Liquid Solvent System: Reaction of Enzyme Anchored to the Solvent. *Chemistry Letters* **30**, 262-263 (2001).

3   Scovazzo, P. Determination of the upper limits, benchmarks, and critical properties for gas separations using stabilized room temperature ionic liquid membranes (SILMs) for the purpose of guiding future research. *Journal of Membrane Science* **343**, 199-211 (2009).

4   Ren, W. & Scurto, A. M. Global phase behavior of imidazolium ionic liquids and compressed 1,1,1,2-tetrafluoroethane (R-134a). *AIChE Journal* **55**, 486-493 (2009).

5   Min, Y. *et al.* Measurement of Forces across Room Temperature Ionic Liquids between Mica Surfaces. *The Journal of Physical Chemistry C* **113**, 16445-16449 (2009).

6   Endres, F. *et al.* Do solvation layers of ionic liquids influence electrochemical reactions? *Physical Chemistry Chemical Physics* **12**, 1724-1732 (2010).

7   Mezger, M. *et al.* Molecular Layering of Fluorinated Ionic Liquids at a Charged Sapphire (0001) Surface. *Science* **322**, 424-428 (2008).

8   Jiang, W., Wang, Y. & Voth, G. A. Molecular dynamics simulation of nanostructural organization in ionic liquid/water mixtures. *Journal of Physical Chemistry B* **111**, 4812-4818 (2007).

9   Wick, C. D., Chang, T.-M. & Dang, L. X. Molecular Mechanism of CO2 and SO2 Molecules Binding to the Air/Liquid Interface of 1-Butyl-3-methylimidazolium Tetrafluoroborate Ionic Liquid: A Molecular Dynamics Study with Polarizable Potential Models. *The Journal of Physical Chemistry B* **114**, 14965-14971 (2010).

10   Lynden-Bell, R. M. & Del Popolo, M. Simulation of the surface structure of butylmethylimidazolium ionic liquids. *Physical Chemistry Chemical Physics* **8**, 949-954 (2006).

11   Bresme, F. & et al. Influence of ion size asymmetry on the properties of ionic liquid–vapour interfaces. *Journal of Physics: Condensed Matter* **17**, S3301 (2005).

12   Sloutskin, E., Lynden-Bell, R. M., Balasubramanian, S. & Deutsch, M. The surface structure of ionic liquids: comparing simulations with x-ray measurements. *J. Chem. Phys.* **125**, 174715-174722 (2006).

13   Bowers, J., Vergara-Gutierrez, M. C. & Webster, J. R. P. Surface Ordering of Amphiphilic Ionic Liquids. *Langmuir* **20**, 309-312 (2003).

14   Sloutskin, E. *et al.* Surface Layering in Ionic Liquids: An X-ray Reflectivity Study. *Journal of the American Chemical Society* **127**, 7796-7804 (2005).

15   Jeon, Y. *et al.* Interfacial Restructuring of Ionic Liquids Determined by Sum-Frequency Generation Spectroscopy and X-Ray Reflectivity. *The Journal of Physical Chemistry C* **112**, 19649-19654 (2008).

16   Kolbeck, C. *et al.* Influence of Different Anions on the Surface Composition of Ionic Liquids Studied Using ARXPS. *The Journal of Physical Chemistry B* **113**, 8682-8688 (2009).

17   Lockett, V. *et al.* Orientation and mutual location of ions at the surface of ionic liquids. *Physical Chemistry Chemical Physics* **12**, 13816-13827 (2010).

18   Iwahashi, T. *et al.* Surface Structural Study on Ionic Liquids Using Metastable Atom Electron Spectroscopy. *The Journal of Physical Chemistry C* **113**, 19237-19243 (2009).

19   Hammer, T., Reichelt, M. & Morgner, H. Influence of the aliphatic chain length of imidazolium based ionic liquids on the surface structure. *Physical Chemistry Chemical Physics* **12**, 11070-11080 (2010).

20   Ridings, C., Lockett, V. & Andersson, G. Effect of the aliphatic chain length on electrical double layer formation at the liquid/vacuum interface in the [Cnmim][BF4] ionic liquid series. *Physical Chemistry Chemical Physics* **13**, 17177-17184 (2011).

21   Ridings, C., Lockett, V. & Andersson, G. Significant changes of the charge distribution at the surface of an ionic liquid due to the presence of small amounts of water. *Physical Chemistry Chemical Physics* (2011).

22   Freire, M. G. *et al.* Surface tensions of imidazolium based ionic liquids: Anion, cation, temperature and water effect. *Journal of Colloid and Interface Science* **314**, 621-630 (2007).

23   Martinez, I. S. & Baldelli, S. On the Arrangement of Ions in Imidazolium-Based Room Temperature Ionic Liquids at the Gas−Liquid Interface, Using Sum Frequency Generation, Surface Potential, and Surface Tension Measurements. *The Journal of Physical Chemistry C* **114**, 11564-11575 (2010).

24   Jeon, Y. *et al.* Structures of Ionic Liquids with Different Anions Studied by Infrared Vibration Spectroscopy. *The Journal of Physical Chemistry B* **112**, 4735-4740 (2008).

25   Andersson, G., Krebs, T. & Morgner, H. Angle resolved ion scattering spectroscopy reveals the local topography around atoms in a liquid surface. *Physical Chemistry Chemical Physics* **7**, 2948-2954 (2005).

26   Lemal, D. M. Perspective on Fluorocarbon Chemistry. *The Journal of Organic Chemistry* **69**, 1-11 (2004).

27   Bagno, A. *et al.* The effect of the anion on the physical properties of trihalide-based N,N-dialkylimidazolium ionic liquids. *Organic & Biomolecular Chemistry* **3**, 1624-1630 (2005).

28   Santos, C. S. & Baldelli, S. Surface Orientation of 1-Methyl-, 1-Ethyl-, and 1-Butyl-3-methylimidazolium Methyl Sulfate as Probed by Sum-Frequency Generation Vibrational Spectroscopy†. *The Journal of Physical Chemistry B* **111**, 4715-4723 (2007).

29   Santos, C. S. & Baldelli, S. Alkyl Chain Interaction at the Surface of Room Temperature Ionic Liquids: Systematic Variation of Alkyl Chain Length (R = C1−C4, C8) in both Cation and Anion of [RMIM][R−OSO3] by Sum Frequency Generation and Surface Tension. *The Journal of Physical Chemistry B* **113**, 923-933 (2009).

30   Andersson, G., Morgner, H., Cwiklik, L. & Jungwirth, P. Anions of Alkali Halide Salts at Surfaces of Formamide Solutions: Concentration Depth Profiles and Surface Topography. *The Journal of Physical Chemistry C* **111**, 4379-4387 (2007).

31   Cwiklik, L., Andersson, G., Dang, L. X. & Jungwirth, P. Segregation of inorganic ions at surfaces of polar nonaqeuous liquids. *ChemPhysChem* **8**, 1457-1463 (2007).

32   Jungwirth, P. & Tobias, D. J. Molecular Structure of Salt Solutions: A New View of the Interface with Implications for Heterogeneous Atmospheric Chemistry. *The Journal of Physical Chemistry B* **105**, 10468-10472 (2001).

33   Dong, K. *et al.* Understanding Structures and Hydrogen Bonds of Ionic Liquids at the Electronic Level. *The Journal of Physical Chemistry B* (2011).

34   Kunz, W., Lo Nostro, P. & Ninham, B. W. The present state of affairs with Hofmeister effects. *Current Opinion in Colloid & Interface Science* **9**, 1-18 (2004).

35   Netz, R. R. Water and ions at interfaces. *Current Opinion in Colloid & Interface Science* **9**, 192-197 (2004).

36   Mucha, M. *et al.* Unified Molecular Picture of the Surfaces of Aqueous Acid, Base, and Salt Solutions. *The Journal of Physical Chemistry B* **109**, 7617-7623 (2005).

37   Knipping, E. M. *et al.* Experiments and simulations of ion-enhanced interfacial chemistry on aqueous NaCl aerosols. *Science* **288**, 301-306 (2000).

Chapter 6

Composition of the Outermost Layer and Concentration Depth Profiles of Ammonium Nitrate Ionic Liquid Surfaces

6.1   Introduction

Ionic liquids (ILs) have been a subject of interest in many applications[1] such as solar cells,[2,3] solvents,[4] catalysis, [5] and gas capture media.[6,7] Much of this attention is due to the vast range of possible cation/anion combinations which results in a large degree of freedom in tailoring the physical properties of the liquid.[4] Investigations into the surface structure of ILs play a key role in understanding surface physical properties such as surface potential and surface tension while also contributing to the fundamental understanding of processes occurring at the liquid/vapour interface. The IL/vapour interface has been studied using a wide variety of techniques such as the non-linear optical (NLO) methods,[8-10] x-ray reflectivity,[11-13] direct recoil spectroscopy (DRS),[14] x-ray photoelectron spectroscopy (XPS),[15-17] neutral impact collision ion scattering spectroscopy (NICISS),[18-20] and metastable induced electron spectroscopy/ultra-violet photoelectron spectroscopy (MIES/UPS).[21-23] These studies have all provided significant progress in understanding surface structure of ILs, but the vast majority focus solely on aprotic ILs. Protic ionic liquids are made by the process of transferring a proton from a Brønsted acid to a Brønsted base[13] thus resulting in a high-degree of hydrogen bonding between the cation and anion. Wakeham et al. have investigated the surface of ethylammonium nitrate (EAN), propylammonium nitrate (PAN) and ethylammonium formate (EAF) using x-ray reflectivity.[13] Their results indicate that there is structure existing at the surface that extends to the bulk sponge-like morphology for 38 Å and 44 Å for EAN and PAN, respectively and that this surface ordering is more pronounced in the case of PAN. This

ordering is suggested to be due to the layering of polar and non-polar domains where the increased solvolphobicity[24] (owing to the greater cation alkyl chain length) in PAN contributes to the increased definition of these layers, which can be seen in other results.[25-26] Furthermore the results by Wakeham et al. show a region of low density in the top several Å which is attributed to the formation of $C_8A_7^+$ (where C is cation and A is anion) aggregates at the surface. These clusters were originally observed by Kennedy and Drummond for a range of protic ILs and found to be independent of cation alkyl chain length.[25] Ludwig performed static quantum chemical calculations and determined that the $C_8A_7^+$ cluster is the most stable of the $C_nA_{n-1}^+$ series from n = 1 to 12. These clusters form two cubes sharing a common corner, where each corner is occupied by either a cation or an anion. [26] Wakeham et al. suggest that these clusters exist at the IL/air interface with a thin layer of air surrounding them with the forces between ions preventing these clusters from evaporating. This situation for protic ILs is vastly different from the accepted surface structure of aprotic ILs where smaller clusters have been known to form in only a few ILs [27] but are not seen at the IL/vapour interface. However, the explanation on the geometry of the clusters as given by Ludwig does not indicate the degree of freedom that the cation molecules have in their orientation,[26] therefore, the exact structure of the surface of protic ILs is still relatively unknown. Wakeham et al. have shown that x-ray reflectivity measurements indicate that the surface of EtAN is covered with clusters similar to EAN and PAN, however, there are no results to show what size or geometry these clusters would take. In fact, the lack of these clusters observed in other studies for diethanolammonium nitrate may be an indication that the extra hydroxyl functional group disrupts the hydrogen bonding network that stabilises these clusters. Therefore, there is still a large degree of uncertainty in our understanding of the surface structure of these protic ILs owing to the unknown orientation of the cations in these cluster, and to the unknown orientation of the clusters themselves.

Metastable induced electron spectroscopy (MIES) is a technique ideally suited for investigating the free surface of ILs. In electron spectroscopy methods that use photons as probes (XPS, UPS), the photon penetrates well into the bulk of a sample. Hence the surface sensitivity of these methods is determined by the inelastic mean free path of the electron which is in the order of a few nanometres. MIES instead uses metastable helium

atoms as the probes, which have a large cross section for de-excitation when colliding with an atom or a molecule.[28] The excitation and electron emission process is thus sensitive to only the composition of the outermost layer of a sample. The excitation energy of MIES using metastable atoms is 19.8 eV while that of UPS is 21.2 eV when using the He I line. In case of ionic liquids, the probing depth is usually at least as large as the distance between charge layers. Thus UPS can be used as a reference for identifying the molecular orbitals (MOs). A quantitative approach to the evaluation of MIES/UPS results can be achieved by calculating the MOs of the molecules constituting the target, which allows for accurate assignment of the individual MOs to their moiety of origin as described by Reinmöller et al..[29] Iwahashi et al. took this approach in their comprehensive investigation into the surface structure of the (aprotic) imidazolium-based IL series.[23] Although they did not take a quantitative approach to their evaluation, the calculation of MOs allows for a more precise approach to the data evaluation than would otherwise be possible.

MIES is complemented by neutral impact collision ion scattering spectroscopy (NICISS), which can be used to determine the concentration depth profiles of the elements up to a depth of around 20 nm and a resolution of a few Å close to the surface.[30] The three methods have not been combined before for analysing ILs and provide the opportunity for a quantitative and highly detailed investigation of the structure of protic IL surfaces. The aim of this study is to use MIES, UPS, and NICISS in combination to determine the composition of the surface and the concentration depth profiles of the anion and cation.

6.2   Experimental

The ILs were prepared by the dropwise addition of nitric acid (Sigma Aldrich) to the amine base (ethylamine, propylamine, ethanolamine, Fluka) in equimolar amounts. The solution was stirred over the course of the addition and kept below 15°C. Water was removed from the product by rotary evaporation at 50°C, then by purging with nitrogen while being heated to 110°C overnight. Water content was then measured using Karl Fischer titration and found to be less than 0.1% wt for all ILs after preparation. The structures of the ILs examined are shown in Figure 6-1.
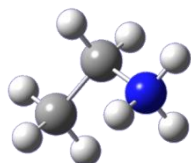
Ethylammonium⁺   **Propylammonium⁺**   **Ethanolammonium⁺**   **Nitrate⁻**
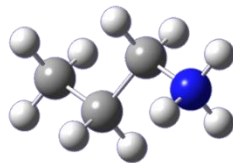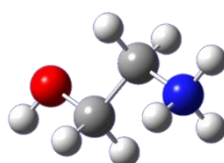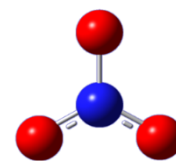
Figure 6-1. Structure of the ions constituting the three ionic liquids, where grey is carbon, blue is nitrogen and red is oxygen.

MO calculations were performed on an ion pair for each of the three ILs in this study with the aug-cc-pVTZ basis set (HF theory) using the Gaussian 09 package, with geometry optimisation performed. Original calculations were performed with the 6-31G** basis set with B3-LYP functional, however this resulted in the transfer of a proton from the cation $(R-NH_3^+)$ to the anion (NO_3^-) resulting in two neutral molecules, an effect also seen by Lehmann et al.,[31] while the use of aug-cc-pVTZ basis set avoided this. Molecules were created and MOs were visualised using the GaussView 5.0 package.

The measured spectra are first fitted to the least amount of Gaussian functions (hereafter referred to simply as 'functions') required, such that their sum fits the measured spectra closely and accounts for all calculated MO energies. Each function is intended to represent an individual MO with a specific binding energy, but in some cases a single function represents a number of MOs with similar binding energies. The initial positions of the functions were based on the MO energies as calculated. After the fitting had been performed the resulting functions were then assigned to the cation or anion based on which calculated MOs the functions best represented.

6.3   Results and Discussion

6.3.1   Outermost surface layer composition

Figure 6-2 shows the UPS and MIES spectra of the three ILs investigated, together with the calculated energies of the occupied MOs. As discussed by Yoshimura et al., all calculated energies shown have been shifted in this experiment by -7 eV.[32] Figure 6-2 also shows images of typical MOs, which facilitates their assignment to either cation or anion.

Figure 6-2. MIE and UP spectra of the three ILs studied on binding energy scale along with MO eigenvalues. MOs were assigned to either the cation (+), anion (-) or undefined (+/-) with the aid of MO visualisation. Samples of MO images are provided for the different assignments.

Figure 6-3. MIE spectra of the three ILs along with the calculated MO eigenvalues and the Gaussian functions used to account for the MOs in the spectra.

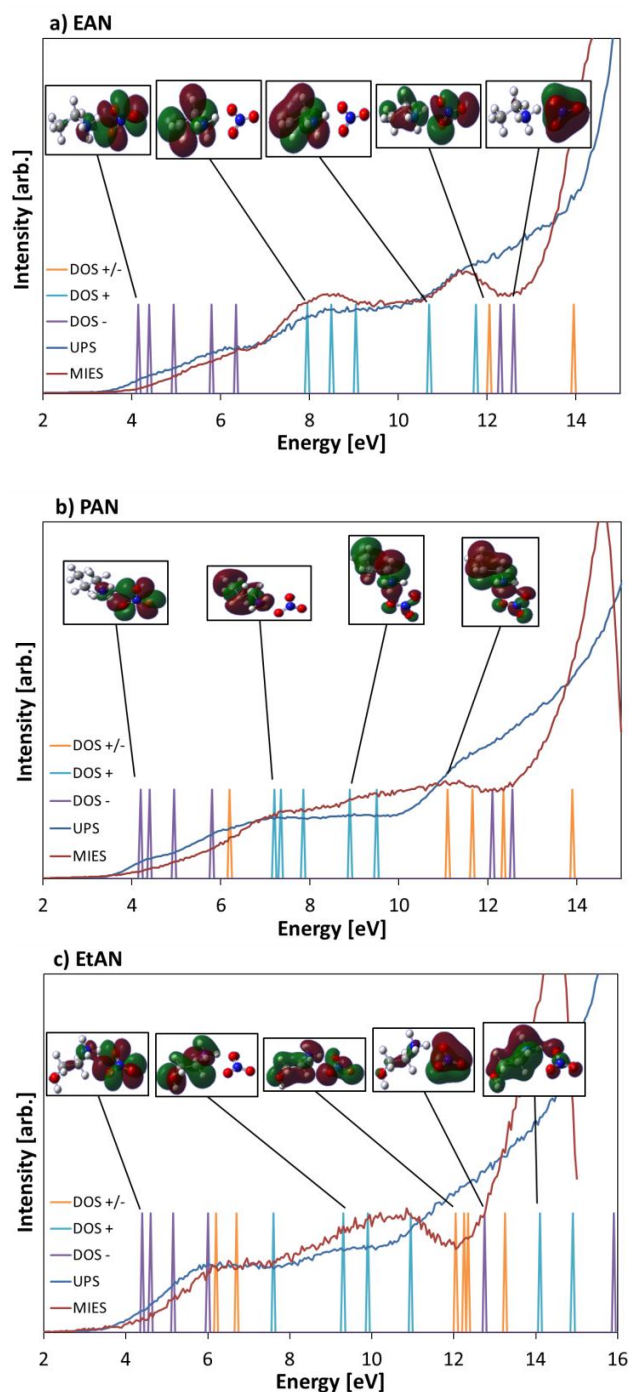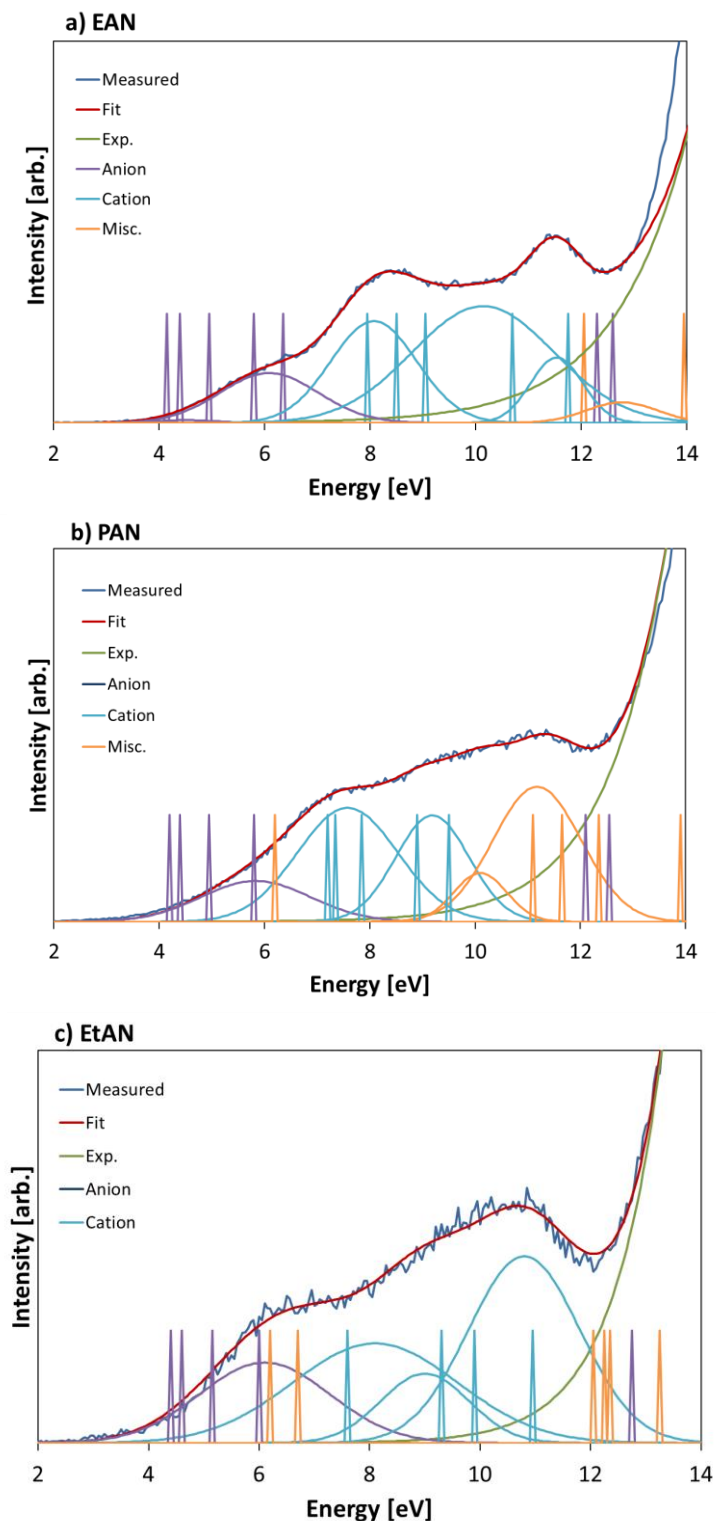The highest occupied molecular orbital (HOMO) of the anion is at a considerably lower binding energy than the cation. In fact the majority of MOs for both cation and anion are well separated from each other at the high and low binding energy sides of the energy spectrum which allows for easier assignment of the experimental peaks to individual species. The spectra of calculated MOs also consist of a few orbitals with electron densities dispersed rather equally over both the cation and anion that have been labelled as 'undefined'. These MOs sit at energies between the distinct anion and cation orbitals, therefore do not greatly hinder the assignment of MOs to the separate ions.

Figure 6-3 shows the functions and the fit to the measured MIE spectra for the three ILs. The only variable in the fitting between the two spectra was the intensity. Thus the change in intensity of the signals between MIES and UPS reflects differences in composition between the bulk and at interface. As Iwahashi et al. point out in their MIES investigation of aprotic ILs, truly quantitative evaluation of MIES results are difficult to obtain due to unknown ionisation cross sections and the difficulty in removing the secondary electron background.[23] However, below a procedure is presented which allows for a quantitative evaluation in the present work. The second step in peak assignment is to correlate the calculated MOs to the position of the fitted peaks. As can be seen in Figure 6-2, the MOs owing to the anion are primarily observed at 4 to 6 eV, and those of the cation at 7.5 to 12 eV (see Table 6-1). This distinction in energy ranges for the anion and cation allows for easier interpretation of the measured spectra.

Determining the surface composition with anion and cation for the ILs investigated can be achieved by comparing the ratios of cation to anion intensity found in the MIE spectra. However, because the cations are different for the three ILs investigated and because the cross sections of the interaction of the He* with the MOs are not known quantitatively, the intensity in the MIE spectra has to be normalised. Firstly the intensities for the cation and anion in the MIE and UP spectra are summed up for each IL. As the MOs for the anion between 4 and 6 eV have exactly the same character and the MOs of the cation between 6.5 and 11 eV have very similar character (both pi and sigma character), the cross section for the interaction between the He* and the UV photons with the MOs of cation and anion should be very similar for the ILs investigated. A direct comparison of the MIES and UPS intensities, however, is not possible as the number of MOs in the cation is different for the

investigated ILs. Comparison of the MIES intensities can be achieved by normalising the MIES intensities to the cation and anion UPS intensities, as the probing depth of UPS is at least 15 to 20 Å and a good approximation to the bulk 1:1 composition. (This will be confirmed below with the concentration depth profiles determined by NICISS.) The MO intensities can thus be normalised by calculating

$$R_S = \left(\frac{\sum_n I_{cation,n}}{\sum_n I_{anion,n}} \right)_S \qquad \textbf{Eq. 6-1}$$

where R is the cation to anion ratio, S indicates either MIES or UPS, I_{cation} and I_{anion} is the intensity of an individual function owing to the cation or anion, repectively, and n denotes the identity of the function being summed. The surface composition ratio or normalised intensity, I_{norm}, is then given by

$$I_{norm} = \frac{R_{MIES}}{R_{UPS}} \qquad \textbf{Eq. 6-2}$$

The larger I_{norm} is, the stronger is the presence of the specific cation at the surface. Table 6-1 shows the surface composition ratio for the three ILs examined, as well as which of the individual functions have been used. The results indicate that the cation is present in substantial excess over the anion at the outermost surface of all three ILs. While it is not surprising that PAN with its longer alkyl chain is present in greater excess than EAN, the

Table 6-1. Surface composition ratios, I_{norm}, derived from MIES and UPS, together with spectral data used in the determination.

	Anion peaks used (eV)	Cation peaks used (eV)	R_{MIES}	R_{UPS}	I_{norm}
EAN	4.5, 6.0	8, 10.1, 11.53	5.66	3.61	1.57
PAN	4.3, 5.8	7.5, 9.2	4.31	1.79	2.40
EtAN	4.6, 6.1	8.2, 9.0, 10.8	4.14	1.76	2.35

large excess of EtAN and its similarity with PAN is unexpected.

6.3.2   Concentration depth profiles
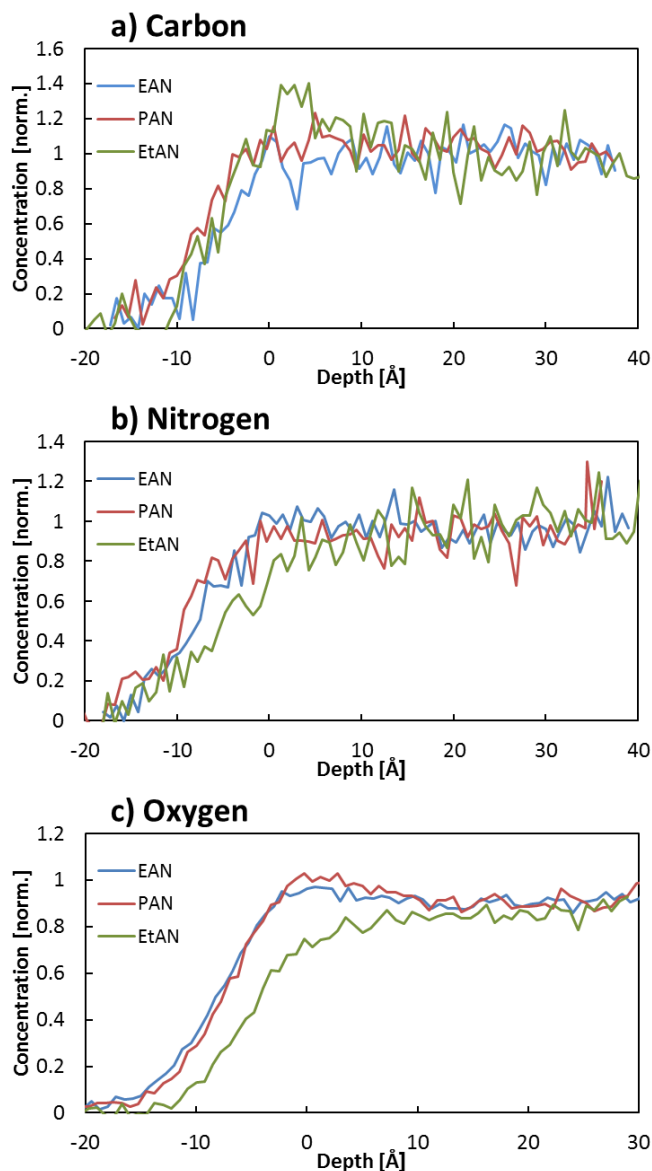
Figure 6-4. Normalised elemental depth profiles of the three ILs investigated. The carbon profiles show a clear excess at the surface in EtAN that is not seen in EAN or PAN. Additionally, both nitrogen and oxygen are seen to be depleted at the surface of EtAN compared to EAN and PAN.

Figure 6-4 compares the elemental concentration depth profiles of the ILs (carbon, nitrogen and oxygen) normalised to their bulk values. In all cases the concentrations have

reached their constant, bulk value by a depth of 10 Å, validating the use of UPS to normalise MIES results above.
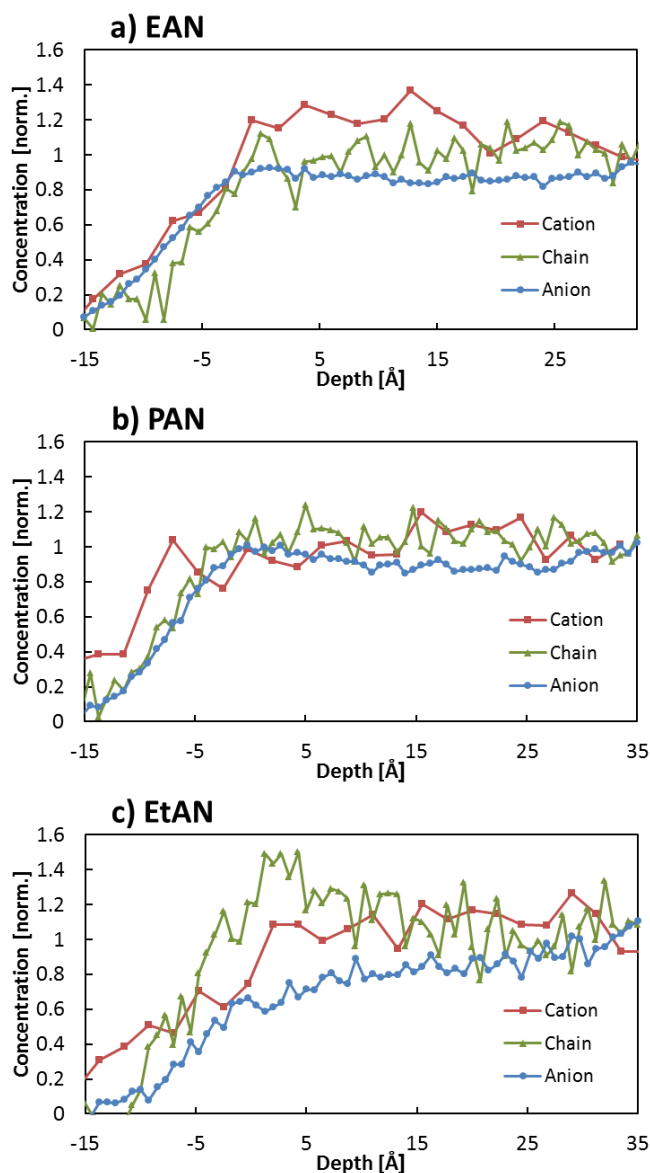
Figure 6-5. Concentration depth profiles of the cationic ammonium, anion and cation alkyl chain in each of the three ILs investigated. The profiles indicate that while the surface of EAN is an homogenous distribution of the cation and anion, PAN shows an increased orientation of cation alkyl chains protruding from the surface, while EtAN shows a clear excess of the cation chain.

Figure 6-4a shows that the carbon depth profile of PAN is shifted closer to the surface than the other ILs, indicating that cation chains are present at the outermost layer of the surface. The carbon profiles also show enrichment at the surface of EtAN that is not seen in the other two ILs, in the form of a 'spike' in concentration at zero depth for EtAN. This indicates that EtAN has a qualitatively different surface structure from PAN and EAN, with an excess of the cation alkyl chain at the surface. In contrast, the nitrogen and oxygen profiles show that they are both further away from the surface in EtAN than in EAN and PAN (as seen in Figure 6-4b and c), while the nitrogen and oxygen profiles show little difference between EAN and PAN. As the nitrogen is present on both the cation and the anion (as is oxygen in EtAN), the increased nitrogen presence at the surface of EAN and PAN compared to EtAN could indicate either increased anion presence at the surface, or a decrease in the amount of cation with specific orientation of chains directed away from the bulk, the latter having the effect of moving the $-NH_3^+$ group closer to the outermost layer instead of sitting at the 'bottom' of the alkyl chains. Due to the MOs being delocalised over most of the molecule (anion or cation), it is not possible for MIES to accurately distinguish between the surface presence of the cation headgroup, $-NH_3^+$, the cation alkyl chain, or the hydroxyl group in the case of EtAN, hence this result is only seen directly by NICISS.

Further evaluation of these profiles is needed to understand the composition in the surface near region. Concentration depth profiles of different constituent moieties of the ILs (cation $-NH_3^+$, alkyl chain, and anion) can be calculated from linear combinations of the elemental depth profiles. E.g. carbon is present only in the cation, oxygen is only present on the anion for EAN and PAN and nitrogen is present on both the cation and anion in fixed stoichiometries. The depth profiles of these moieties are shown in Figure 6-5 for each IL investigated. The results show:

- The anion in EAN is closer to the surface compared to the other moieties (Figure 6-5a) than in either PAN (b) or EtAN (c).
- Both EAN and PAN show rather homogenous distributions of all three moieties. Both cation and anion are present at the surface.
- EtAN is indeed qualitatively different, and shows a pronounced surface excess of the cation ethylene chain, accompanied by a shift of the cation head group and the

anion below the surface. The shift away from the surface of oxygen also indicates that the hydroxyl groups are oriented beneath the ethylene chains, as has been seen previously.[33]

6.3.3 Surface structure of the ILs

These results reveal some unexpected similarities and differences between the surface structures of the three ILs studied. Overall, EtAN is the most straightforward to interpret. Although both cations and anions are present at the surface, the methylene carbons of the cations form an enriched and oriented layer, below which the ammonium cation, hydroxyl group and nitrate anion are buried and hence depleted from the outermost surface layer. This can be seen clearly in the NICISS results and is consistent with previous vibrational sum frequency spectroscopy results.[33] This cannot be concluded from the MIES/UPS results as the MOs of the cation are spread over the cation and in the present case do not allow to clearly distinguish between the alkyl chain and the nitrate group.

Both MIES/UPS and NICISS show that both cation and anion are present at the surface of EAN and PAN. MIES/UPS shows that propylammonium is more enriched over nitrate than ethylammonium in the surface layer. NICISS also shows discrimination between cation and anion throughout the interfacial region. For EAN the cation and anion profiles fall on top of each other while in PAN the cation and anion profiles are separated with the anion profile shifted away from the surface. The outermost surface layer is expected to contain alkyl chains oriented away from the bulk liquid, and this has been confirmed for EAN by vibrational sum frequency spectroscopy.[34] However, coverage of the outermost layer with the cation is stronger in case of PAN than in EAN as shown by MIES/UPS. It is reasonable that the propyl group of PAN occupies a greater fraction of that surface than that of the ethyl on the grounds of both molecular volume and solvophobicity. Bulk neutron scattering studies have shown the existence of much more pronounced amphiphilic nanostructure in PAN than EAN.[35-37] X-ray reflectivity measurements also revealed layering of cations and anions (or polar and non-polar regions) in PAN and EAN, decaying over up to 30 Å into the bulk liquid. Quantitative analysis of scattering length density profiles showed that these correspond to only small compositional differences, and are thus not observed by NICISS.

6.4   Conclusions

The surface sensitive techniques NICISS and MIES/UPS were used to investigate the surface of the three protic ILs: EAN, PAN and EtAN. MO calculations were performed on ion pairs of the three ILs studied in order to perform a semi-quantitative evaluation of the electron spectroscopy data. MIES/UPS results show that the cation is enriched over the anion in the outermost surface layer of all three ILs examined, but that both ions are present. The degree of cation enrichment is smaller for EAN than EtAN and PAN, which had similar surface compositions. NICISS depth profiles reveal further information on the surface structure. EtAN shows an excess of carbon (owing to the cation alkyl chain) in the top several Å which is not seen in PAN or EAN. This is followed by a shifting away from the surface of nitrogen and oxygen as found in the concentration depth profiles, indicating that the carbon atoms in the cation chain are sitting above the centre of the cation and hydroxyl group in the surface. Conversely, the carbon profile being shifted toward the surface in the case of PAN indicates an orientation of the cation with the chains protruding straight out of the surface, pointing towards the vapour phase. The results are consistent with either clusters at the surface or a simple liquid interface with a sharp density profile at the interface. In both cases the description of the ion positions and orientations is the same for the outermost layer. Additionally, while the amount of cation seen at the outermost layer is different between the ILs it is important to note that the anion is always present, i.e. there is no exclusive selection of ions at the surface. In either regard, the results provide further evidence for the high extent of property tailoring in protic ILs.

6.5   References

1   Chowdhury, S., Mohan, R. S. & Scott, J. L. Reactivity of ionic liquids. *Tetrahedron* **63**, 2363-2389 (2007).

2   Pinilla, C., Del Pópolo, M. G., Lynden-Bell, R. M. & Kohanoff, J. Structure and Dynamics of a Confined Ionic Liquid. Topics of Relevance to Dye-Sensitized Solar Cells. *The Journal of Physical Chemistry B* **109**, 17922-17927 (2005).

3   Wei, D. Dye Sensitized Solar Cells. *International Journal of Molecular Sciences* **11**, 1103-1113 (2010).

4   Rogers, R. D. & Seddon, K. R. *Ionic Liquids IIIB: Fundamentals, Progress, Challenges, and Opportunities : Transformations and Processes*. (Oxford University Press, 2005).

5   Itoh, T., Akasaki, E., Kudo, K. & Shirakami, S. Lipase-Catalyzed Enantioselective Acylation in the Ionic Liquid Solvent System: Reaction of Enzyme Anchored to the Solvent. *Chemistry Letters* **30**, 262-263 (2001).

6   Scovazzo, P. Determination of the upper limits, benchmarks, and critical properties for gas separations using stabilized room temperature ionic liquid membranes (SILMs) for the purpose of guiding future research. *Journal of Membrane Science* **343**, 199-211 (2009).

7   Ren, W. & Scurto, A. M. Global phase behavior of imidazolium ionic liquids and compressed 1,1,1,2-tetrafluoroethane (R-134a). *AIChE Journal* **55**, 486-493 (2009).

8   Rivera-Rubero, S. & Baldelli, S. Influence of Water on the Surface of the Water-Miscible Ionic Liquid 1-Butyl-3-methylimidazolium Tetrafluoroborate: A Sum Frequency Generation Analysis. *The Journal of Physical Chemistry B* **110**, 15499-15505 (2006).

9   Santos, C. S. & Baldelli, S. Surface Orientation of 1-Methyl-, 1-Ethyl-, and 1-Butyl-3-methylimidazolium Methyl Sulfate as Probed by Sum-Frequency Generation Vibrational Spectroscopy†. *The Journal of Physical Chemistry B* **111**, 4715-4723 (2007).

10   Jeon, Y. *et al.* Interfacial Restructuring of Ionic Liquids Determined by Sum-Frequency Generation Spectroscopy and X-Ray Reflectivity. *The Journal of Physical Chemistry C* **112**, 19649-19654 (2008).

11   Sloutskin, E. *et al.* Surface Layering in Ionic Liquids: An X-ray Reflectivity Study. *Journal of the American Chemical Society* **127**, 7796-7804 (2005).

12   Lauw, Y. *et al.* X-Ray reflectometry studies on the effect of water on the surface structure of [C4mpyr][NTf2] ionic liquid. *Physical Chemistry Chemical Physics* **11**, 11507-11514 (2009).

13   Wakeham, D., Nelson, A., Warr, G. G. & Atkin, R. Probing the protic ionic liquid surface using X-ray reflectivity. *Physical Chemistry Chemical Physics* **13**, 20828-20835 (2011).

14   Law, G., Watson, P. R., Carmichael, A. J. & Seddon, K. R. Molecular composition and orientation at the surface of room-temperature ionic liquids: Effect of molecular structure. *Physical Chemistry Chemical Physics* **3**, 2879-2885 (2001).

15   Lockett, V. *et al.* Orientation and mutual location of ions at the surface of ionic liquids. *Physical Chemistry Chemical Physics* **12**, 13816-13827 (2010).

16   Lockett, V., Sedev, R., Bassell, C. & Ralston, J. Angle-resolved X-ray photoelectron spectroscopy of the surface of imidazolium ionic liquids. *Physical Chemistry Chemical Physics* **10**, 1330-1335 (2008).

17   Kolbeck, C. *et al.* Influence of Different Anions on the Surface Composition of Ionic Liquids Studied Using ARXPS. *The Journal of Physical Chemistry B* **113**, 8682-8688 (2009).

18   Ridings, C., Lockett, V. & Andersson, G. Significant changes of the charge distribution at the surface of an ionic liquid due to the presence of small amounts of water. *Physical Chemistry Chemical Physics* **13**, 21301-21307 (2011).

19   Ridings, C., Lockett, V. & Andersson, G. Effect of the aliphatic chain length on electrical double layer formation at the liquid/vacuum interface in the [Cnmim][BF4] ionic liquid series. *Physical Chemistry Chemical Physics* **13**, 17177-17184 (2011).

20   Hammer, T., Reichelt, M. & Morgner, H. Influence of the aliphatic chain length of imidazolium based ionic liquids on the surface structure. *Physical Chemistry Chemical Physics* **12**, 11070-11080 (2010).

21   Höfft, O. *et al.* Electronic Structure of the Surface of the Ionic Liquid [EMIM][Tf2N] Studied by Metastable Impact Electron Spectroscopy (MIES), UPS, and XPS. *Langmuir* **22**, 7120-7123 (2006).

22   Krischok, S. *et al.* Temperature-Dependent Electronic and Vibrational Structure of the 1-Ethyl-3-methylimidazolium Bis(trifluoromethylsulfonyl)amide Room-Temperature Ionic Liquid Surface: A Study with XPS, UPS, MIES, and HREELS†. *The Journal of Physical Chemistry B* **111**, 4801-4806 (2007).

23   Iwahashi, T. *et al.* Surface Structural Study on Ionic Liquids Using Metastable Atom Electron Spectroscopy. *The Journal of Physical Chemistry C* **113**, 19237-19243 (2009).

24   Ray, A. Solvophobic Interactions and Micelle Formation in Structure Forming Nonaqueous Solvents. *Nature* **231**, 313-315 (1971).

25   Kennedy, D. F. & Drummond, C. J. Large Aggregated Ions Found in Some Protic Ionic Liquids. *The Journal of Physical Chemistry B* **113**, 5690-5693 (2009).

26   Ludwig, R. A Simple Geometrical Explanation for the Occurrence of Specific Large Aggregated Ions in Some Protic Ionic Liquids. *The Journal of Physical Chemistry B* **113**, 15419-15422 (2009).

27   Bini, R., Bortolini, O., Chiappe, C., Pieraccini, D. & Siciliano, T. Development of Cation/Anion "Interaction" Scales for Ionic Liquids through ESI-MS Measurements. *The Journal of Physical Chemistry B* **111**, 598-604 (2006).

28   Morgner, H. in *Advances In Atomic, Molecular, and Optical Physics* Vol. Volume 42 (eds Bederson Benjamin & Walther Herbert) 387-488 (Academic Press, 2000).

29   Reinmoller, M. *et al.* Theoretical reconstruction and elementwise analysis of photoelectron spectra for imidazolium-based ionic liquids. *Physical Chemistry Chemical Physics* (2011).

30   Andersson, G. & Morgner, H. Impact collision ion scattering spectroscopy (ICISS) and neutral impact collision ion scattering spectroscopy (NICISS) at surfaces of organic liquids. *Surface Science* **405**, 138-151 (1998).

31   Lehmann, S. B. C., Roatsch, M., Schoppke, M. & Kirchner, B. On the physical origin of the cation-anion intermediate bond in ionic liquids Part I. Placing a (weak) hydrogen bond between two charges. *Physical Chemistry Chemical Physics* **12**, 7473-7486 (2010).

32   Yoshimura, D. *et al.* Electronic structure of ionic liquids at the surface studied by UV photoemission. *Journal of Electron Spectroscopy and Related Phenomena* **144-147**, 319-322 (2005).

33   Wakeham, D. *et al.* Surface structure of a "non-amphiphilic" protic ionic liquid. *Physical Chemistry Chemical Physics* **14**, 5106-5114 (2012).

34   Niga, P. *et al.* Structure of the Ethylammonium Nitrate Surface: An X-ray Reflectivity and Vibrational Sum Frequency Spectroscopy Study. *Langmuir* **26**, 8282-8288 (2010).

35   Hayes, R., Imberti, S., Warr, G. G. & Atkin, R. Pronounced sponge-like nanostructure in propylammonium nitrate. *Physical Chemistry Chemical Physics* **13**, 13544-13551 (2011).

36   Hayes, R., Warr, G. G. & Atkin, R. At the interface: solvation and designing ionic liquids. *Physical Chemistry Chemical Physics* **12**, 1709-1723 (2010).

37   Atkin, R. & Warr, G. G. The Smallest Amphiphiles: Nanostructure in Protic Room-Temperature Ionic Liquids with Short Alkyl Groups. *The Journal of Physical Chemistry B* **112**, 4164-4166 (2008).

Chapter 7

Deconvolution of NICISS profiles involving elements of similar masses

7.1   Introduction

Foam films are thin liquid films with two opposing liquid/vapour interfaces, where the interfaces are covered (to varying extents) with surfactant molecules that initially act to stabilise the film by lowering the interfacial tension.[1] These films are maintained in a metastable state by the interaction of surface forces, which can be described using the well-known approach in colloid science of DLVO theory.[2] Part of this theory involves the adsorption of a surface charge on each interface which can arise due to the presence of ionic species or the dissociation of the liquid into charged species, e.g. the autoionisation of water.[3] This surface charge is balanced by a diffuse region of counterions, whose excess decays away to bulk levels with increasing distance away from the surface. The close approach of the two liquid/vapour interfaces is hindered by electrostatic repulsion due to these electrical double layers.[1,2] DLVO theory allows for the calculation as to the repulsive pressure due to these double layers, but direct observation of these double layers is still limited.[4-6] Additionally, DLVO theory treats ions as point charges, thereby neglecting the chemical nature of ions and thus not accounting for specific ion effects which possibly could be present. At liquid surfaces it has been seen that larger, more polarisable halides, such as iodide, show preference for adsorption over the smaller, less polarisable halides, such as fluoride.[7-11] These specific ion effects have been seen to affect foam film thickness and stability,[12-14] however, the surface structure of ions in foam films has not been experimentally observed. Neutral impact collision ion scattering spectroscopy (NICISS) is an ion scattering method that is capable of determining the concentration depth profiles of the elements in soft matter surfaces, with a depth range of approximately 20 nm and a resolution of 1 – 3 Å close to the surface.[15] NICISS has been used in several investigations of liquid surfaces,[11,16-19] and recently a setup has been developed that is capable of generating and stabilising a foam film under vacuum for the

purposes of NICISS measurements.[20] This technique therefore provides an ideal platform for investigating specific ion effects in foam films. Two different types of surfactant can be used for these investigations, ionic and non-ionic surfactants, where the surface charge of ionic surfactants is regulated by the charge of the surfactant molecule, while the surface charge in non-ionic surfactant systems can be regulated by the addition of salt. A recent set of experiments investigated solutions of the non-ionic surfactant $C_{12}DMPO$ in glycerol with added sodium chloride, where the concentration depth profiles of the phosphorus headgroup and chloride anion were of direct interest. Due to their similar masses, the zero depth mark for these elements appear close on the TOF scale, and the measured spectrum which is a convolution of the real concentration depth profiles with inelastic energy loss distributions appear overlapped for both elements. A procedure is provided for the deconvolution of NICIS spectra where the concentration depth profiles of two elements overlap.

7.2 Experimental

Glycerol (>99.5%, spectrophotometric grade) and NaCl (>99.5%, SigmaUltra) were purchased from Sigma-Aldrich (Australia). These materials were used as received. $C_{12}DMPO$ was purchased from ABCR Chemicals (Germany) and re-crystallised twice from n-hexane prior to usage. All solutions investigated were prepared at 0.5 cmc of $C_{12}DMPO$ in glycerol (3.36 mmol/kg) as determined by surface tension measurements.

Glycerol is used as the solvent as it is a polar solvent with low vapour pressure, which makes it suitable for use under vacuum conditions. Foam films of 4 different salt concentrations were investigated: no salt, 0.1 mmol/kg, 1 mmol/kg, and 10 mmol/kg. Solutions are placed in a beaker and exposed to vacuum (10^{-4} torr) for at least 30 minutes prior to setup and measurement for degassing.

7.3   Results and Discussion

7.3.1   NICISS profiles

The aim of the investigation is to determine the effect of salt (NaCl) on the surface structure of a non-ionic surfactant (C_{12}DMPO) in glycerol. The concentration depth profiles of P and Cl are of direct interest as they indicate the position of the headgroup of the surfactant, and the anion in the film, respectively. Figure 7-1 shows the measured NICIS spectra for these systems on the TOF scale. Figure 7-1 shows the profiles of carbon and oxygen to appear as steps, as opposed to the Cl/P profile which appears as a peak. This is due to the bulk concentration of C and O being above the detection limit, hence the bulk concentration contributes towards the NICISS spectra. However the Cl/P bulk concentration is below the detection limit of the technique, only reaching above this limit in the case of an excess at the surface. Hence this signal appears only as a peak, with no bulk level seen. The TOF spectra indicate a steep onset for the C profile, as opposed to a broad and shallow onset for O, indicating a surface excess of the former, and depletion of the latter. This can be understood in terms of the adsorption of surfactant causing an excess of carbon due to the surfactant's carbon chain, with a corresponding depletion of glycerol and thus oxygen. The onset positions for P and Cl in NICISS spectra are closely positioned due to the relatively small ratio of masses, and the onset for the Cl profile is
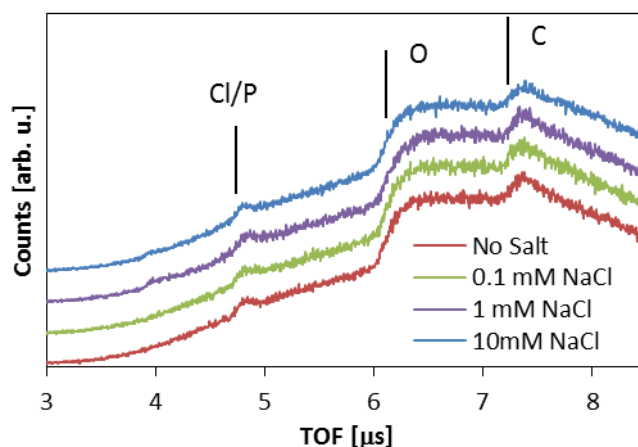

Figure 7-1. NICIS spectra on the TOF scale for the 4 solutions investigated. The onset for the step of each element is indicated by a vertical line. The spectra are vertically offset for clarity.

difficult to observe due to its low surface concentration. The appearance of P as a peak rather than a step indicates that it is present as a surface excess rather than a constant profile.

The concentration depth profile of P is shown in Figure 7-2. The fact that an apparent concentration appears at negative depths (i.e. above the surface) is due to two reasons: the convolution of the real concentrations depth profiles with the inelastic contribution to the backscattering process, and the presence of Cl whose onset would appear around the -15 Å mark on the P depth scale. Deconvoluting these depth profiles will therefore give evidence to the existence of chlorine at the surface that would otherwise be 'hidden' by the convoluted phosphorus signal. However, as will be noted in the following section, due to the limitations in performing this deconvolution only a qualitative assessment about the presence of chlorine can be drawn from this data.
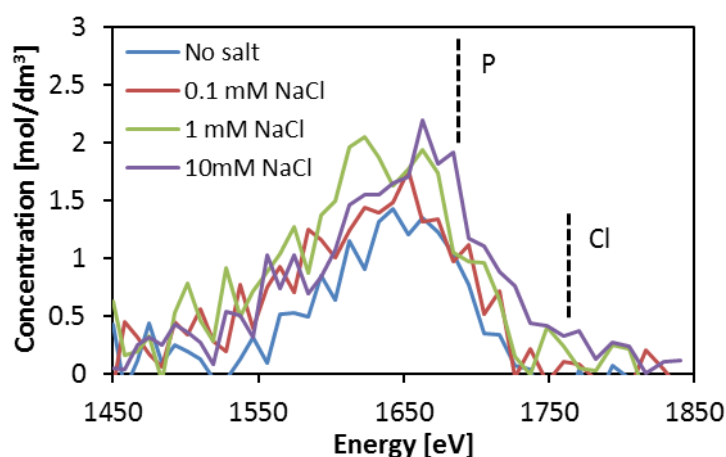
Figure 7-2. Concentration depth profile of phosphorus for the 4 systems investigated on the energy scale. The vertical dashed lines indicate the energy for zero depth of the respective element, with decreasing energy indicating increasing depth towards the bulk. The increased concentration of the 10 mM NaCl profile between the Cl and P onset compared to the other systems is a possible indication of the detection of Cl.

7.3.2 Deconvolution

The specific procedure for the deconvolution is described elsewhere, but generally involves using the genetic algorithm to reconstruct the measured profiles by convoluting a simulated spectrum.[21] The deconvolution is performed on the energy scale (i.e. converting

TOF to energy loss of the projectiles) and is performed on a set range of data points either side of the energy value corresponding to zero depth for that element. However the close appearance of Cl to the onset of P causes difficulties in fitting the P signal. This is because in the deconvolution procedure it is not possible to differentiate between the contribution of the Cl signal and the P signal while it is possible to differentiate between both signals to some extent in the as measured data. For this reason the deconvolution needs to be performed on the energy loss scale for Cl rather than P. The issue with this approach is that the energy loss straggling starts at zero depth for Cl and therefore skews the P profile, which appears at a significant depth on the Cl depth scale. For this reason the deconvolution was performed on the Cl depth scale without the energy loss straggling being accounted for.

Figure 7-3 gives the deconvolution of the P/Cl signal for the 0.1 mmol/kg NaCl solution. The 'convoluted' profile fits well to the measured profile, and yields a deconvoluted profile that shows signal only for P, as Cl would appear at larger energies. Additionally, the P is present as a surface excess as would be expected for the surfactant.

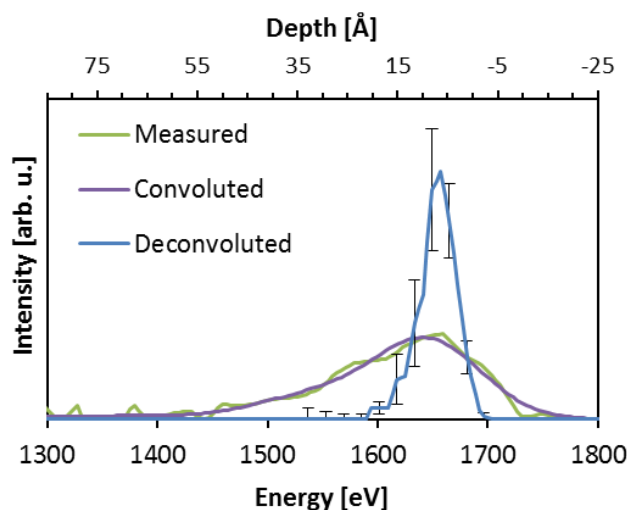

Figure 7-3. Deconvoluted P/Cl profile of the 0.1 mmol/kg NaCl solution with both the energy scale and the depth scale for P indicated. A deconvoluted profile is determined using a genetic algorithm, and then convoluted to produce the fit to the measured profile. The standard deviation of all data sets to the final averaged profile (deconvoluted) gives the error bars for the deconvolution.
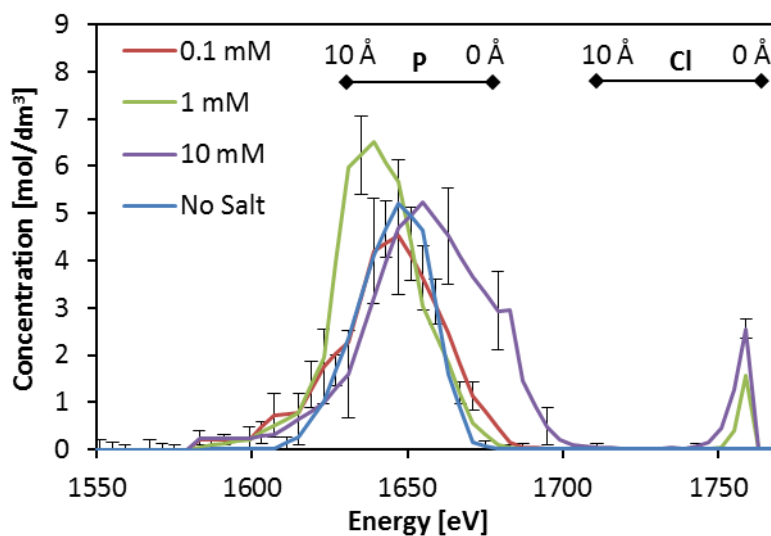
Figure 7-4. Deconvoluted profiles of the four systems studied. The energy corresponding to zero depth for Cl is 1759 eV, as indicated by the dashed line. The profiles at lower energies correspond to P. The depth scale from 0 to 10 Å is given for both P and Cl as indicated by the horizontal bars.

Figure 7-4 shows the deconvoluted profiles for the four systems studied. A small peak appears around 1759 eV which corresponds to the energy of zero depth for chlorine, while a larger structure appears at lower energies. This would suggest that the smaller peaks are owing to chloride, while the larger structures are phosphorus, which is further supported by the fact that the Cl peak only shows up for the two systems with the highest salt concentrations. The P peak has a similar shape for the concentrations 0, 0.1 and 1 mM NaCl, indicating that the structure of the surfactant at the surface of these films are not greatly affected by the presence of salt at these concentrations. The 10 mM NaCl film, however, also shows a change in the shape of the peak attributed to P. The area of the P peak has increased as well as the onset shifted to higher energies while the peak attributed to Cl has the same shape as that in the 1 mM NaCl spectrum and a somewhat higher intensity. An increase in the area of the P peak means that the amount of $C_{12}DMPO$ adsorbed at the surface has increased. A shift towards the surface would mean that the surfactant molecule reorients such that the P-group is moving closer to the outermost layer. It must be noted that the concentrations are determined by normalising the integral of the deconvoluted spectrum to the integral of the measured 'input' spectrum. Given that

the cross-section of Cl is larger than P, the concentration for the Cl peaks have been multiplied by a factor to reflect this difference in cross section.

The question arises whether the area of the P peak appearing at higher kinetic energy has in fact to be attributed to P or would have to be attributed to Cl. Based on the present measurement this question cannot be decided. Thus, only the qualitative conclusion that both P and Cl show an enhanced concentration at the surface for the 1 and 10 mM NaCl solution can be drawn. While the enhanced concentration of P at the surface is in agreement with the fact, that C_{12}DMPO is a surfactant known to stabilise foam films and thus expected to have an enhanced surface concentration, the adsorption of Cl^- is not necessarily expected because Cl^- is not known as a surfactant in a polar solvent. However, it cannot be excluded that Cl^- is present at a high concentration at the surface of a foam film because Cl^- could contribute this way to stabilising the foam film.

While the deconvolution has allowed for the separation of the P and Cl peaks, it must be noted that these deconvoluted profiles are not the real concentration depth profiles, as the effects of energy loss straggling were neglected for the evaluation.

7.4   Conclusions

NICISS provides an ideal technique for measuring the concentration depth profiles of the elements in foam films, thus determining the adsorption behaviours of surfactants and salts in these films. However in the case of evaluating the profiles of two elements of similar masses, it was found that the small separations of the onsets of the two profiles overlap in the measured spectra. Deconvoluting the measured profile yields concentration depth profiles of both elements, hence separating them for further analysis. The steps taken for deconvoluting the data for this case have been discussed, where the energy loss straggling has to be neglected from the deconvolution in order to obtain good fits for the deconvoluted spectra. However, the separation of P and Cl is not fully unambiguous and the adsorption of both P and Cl can be discussed only qualitatively and not fully quantitatively. While a full quantitative evaluation is not possible for the data, the deconvoluted profiles do give strong evidence towards the adsorption of chlorine to the surface, a result which could not be conclusively drawn from the convoluted profiles.

7.5   References

1   Bergeron, V. Forces and structure in thin liquid soap films. *Journal of Physics: Condensed Matter*, R215 (1999).

2   Stubenrauch, C. & Klitzing, R. v. Disjoining pressure in thin liquid foam and emulsion films - new concepts and perspectives. *Journal of Physics: Condensed Matter*, R1197 (2003).

3   Israelachvili, J. N. *Intermolecular and Surface Forces*. Second edn, (Academic Press, 2000).

4   Andersson, G. & Morgner, H. Investigations on solutions of tetrabutylonium salts in formamide with NICISS and ICISS: concentration depth profiles and composition of the outermost layer. *Surface Science* **445**, 89-99 (2000).

5   Schulze, K. D. & Morgner, H. Investigation of the electric charge structure and the dielectric permittivity at surfaces of solutions containing ionic surfactants. *Journal of Physics: Condensed Matter*, 9823 (2006).

6   Bökman, F., Bohman, O. & Siegbahn, H. O. G. Electric double layers at solution surfaces studied by means of electron spectroscopy: a comparison of potassium octanoate in formamide and ethylene glycol solution. *Chemical Physics Letters* **189**, 414-419 (1992).

7   Jungwirth, P. & Tobias, D. J. Ions at the Air/Water Interface. *J. Phys. Chem. B* **106**, 6361-6373 (2002).

8   Jungwirth, P. & Tobias, D. J. Surface Effects on Aqueous Ionic Solvation: A Molecular Dynamics Simulation Study of NaCl at the Air/Water Interface from Infinite Dilution to Saturation. *The Journal of Physical Chemistry B* **104**, 7702-7706 (2000).

9   Brown, E. C., Mucha, M., Jungwirth, P. & Tobias, D. J. Structure and vibrational spectroscopy of salt water/air interfaces: predictions from classical molecular dynamics simulations. *J. Phys. Chem. B* **109**, 7934-7940 (2005).

10   Cwiklik, L., Andersson, G., Dang, L. X. & Jungwirth, P. Segregation of inorganic ions at surfaces of polar nonaqeuous liquids. *ChemPhysChem* **8**, 1457-1463 (2007).

11   Andersson, G., Morgner, H., Cwiklik, L. & Jungwirth, P. Anions of Alkali Halide Salts at Surfaces of Formamide Solutions: Concentration Depth Profiles and Surface Topography. *The Journal of Physical Chemistry C* **111**, 4379-4387 (2007).

12   Hanni-Ciunel, K., Schelero, N. & von Klitzling, R. Negative charges at the air/water interface and their consequences for aqueous wetting films containing surfactans. *Faraday Discuss.* **141**, 41-53 (2009).

13   Schelero, N. & von Klitzing, R. Correlation between specific ion adsorption at the air/water interface and long-range interactions in colloidal systems. *Soft Matter* **7**, 2936-2942 (2011).

14   Schelero, N., Hedicke, G., Linse, P. & Klitzing, R. v. Effects of Counterions and Co-ions on Foam Films Stabilized by Anionic Dodecyl Sulfate. *The Journal of Physical Chemistry B* **114**, 15523-15529 (2010).

15   Andersson, G. & Morgner, H. Impact collision ion scattering spectroscopy (ICISS) and neutral impact collision ion scattering spectroscopy (NICISS) at surfaces of organic liquids. *Surface Science* **405**, 138-151 (1998).

16   Andersson, G., Krebs, T. & Morgner, H. Activity of surface active substances determined from their surface excess. *Physical Chemistry Chemical Physics* **7**, 136-142 (2005).

17   Andersson, G., Krebs, T. & Morgner, H. Angle resolved ion scattering spectroscopy reveals the local topography around atoms in a liquid surface. *Physical Chemistry Chemical Physics* **7**, 2948-2954 (2005).

18   Hammer, T., Reichelt, M. & Morgner, H. Influence of the aliphatic chain length of imidazolium based ionic liquids on the surface structure. *Physical Chemistry Chemical Physics* **12**, 11070-11080 (2010).

19   Krebs, T., Andersson, G. & Morgner, H. Chemical Potential of a Nonionic Surfactant in Solution. *The Journal of Physical Chemistry B* **110**, 24015-24020 (2006).

20   Ridings, C. & Andersson, G. Determining concentration depth profiles of thin foam films with neutral impact collision ion scattering spectroscopy. *Review of Scientific Instruments* **81**, 113907-113915 (2010).

21   Andersson, G., Morgner, H. & Pohl, H. Energy-loss straggling of helium projectiles at low kinetic energies: Deconvolution of concentration depth profiles of inorganic salt solutes in aqueous solutions. *Physical Review A (Atomic, Molecular, and Optical Physics)* **78**, 032904 (2008).

Chapter 8

Change of Surface Structure upon Foam Film Formation

8.1   Introduction

In foam films two liquid surfaces come into such close proximity that the presence of the one surface influences the structure of the other one. Foam films have a large surface area and are at least in a metastable state. Facilitating the stable or metastable state means that there must be an internal force which hinders the collapsing of the foam film. One of the contributions to this internal force results from the overlap of electric double layers which originate from the separation of charges at the surface of the foam film.[1,2] Such separation of charges plays a central role in the models describing the internal force in foam films. However, the separation of the charges has not yet been measured experimentally. The aim of this contribution is to show that charge separation at the surface of a foam film is different to that at the surface of the respective bulk solution. This finding has implications for the understanding of foam films and charges at liquid surfaces in general.

The overlap of the electric double layer can be described as an osmotic pressure or approximated as a surface charge or surface potential. The charge separation itself does not depend on the specific type of ions in the foam film, however specific ion effects have been shown to influence bubble coalescence[3,4] and the formation of wetting films,[5] and thus could influence the overlap of the electric double layer. Bubble coalescence has been found to depend on the combination of ions in solution and selection rules have been proposed to describe bubble coalescence. The thickness of wetting films also has been found to depend on the type of ions in the solution.[5]

The thickness of foam films is described with the concept of the disjoining pressure which treats the steric, van der Waals, and electrostatic repulsion (overlapping electric double layer) forces as separate, additive forces contributing to the total internal pressure that stabilises the film.[6] The concept of the disjoining pressure is based on DLVO theory. The

lack of experimental determination of the foam film surface structure limits these models to describing systems only within a narrow parameter range, such as low concentrations and minimum surface separations.[7] The most common technique for investigating the thickness of films is the thin film pressure balance (TFPB). This technique measures the disjoining pressure of films as a function of their thickness. The resulting curves can be fitted with the concept of the disjoining pressure, using the surface potential as a fitting parameter, to obtain the electrostatic contribution to the disjoining pressure.[8-13] The interpretation of the TFPB measurements is limited because the quantities describing the disjoining pressure are not measured directly but derived from fitting the measured data.[14] One example of this is the electrostatic double layer, and as a consequence of the double layer, the charge distribution in the near surface area. Additionally, the sign of the surface charge can only be inferred from measurements of the corresponding wetting films, not from the foam films themselves. Measuring the concentration depth profiles of the elements in foam films directly, however, allows for determining the charge distribution at the surface of foam films. The charge distribution in foam films has not yet been experimentally measured. The structure of foam films has been measured by neutron reflectivity[15] and x-ray reflectivity.[16,17] However, the large area requirement for the measurements meant the films were measured in a state of drainage and possibly had not reached an equilibrium thickness. The measurements were able to determine the aqueous core thickness of CBFs as well as allowing for conclusions on the orientation of the surfactant alkyl chains. From measurements x-ray and neutron reflectivity the charge distribution in the foam films could not be determined.

Neutral impact collision ion scattering spectroscopy (NICISS) is a low energy ion scattering method capable of determining the concentration depth profiles of elements at soft matter surfaces, with a resolution of 2 - 3 Å near the surface and a depth range of $10 - 20$ nm. An experimental setup using NICISS has previously been established that is capable of generating and holding foam films stable for measurement under vacuum conditions, allowing for the first experimentally determined concentration depth profiles form a foam film.[18] In that study the cationic surfactant hexadecyltrimethylammonium bromide ($C_{16}TAB$) was used in glycerol, but due to the low cross-section of nitrogen – representing the position of the cation – the position of the positive charge could not be determined with these measurements. As a consequence, the charge distribution could not

be evaluated with the measurements using C_{16}TAB. In the present study the surfactant is replaced with the analogous hexadecyltrimethylphosphonium bromide (C_{16}TPB) where the phosphorus (cation) has a larger cross section and can easily be detected at the required concentration.

8.2   Experimental

Glycerol (>99.5%, spectrophotometric grade) was purchased from Sigma-Aldrich (Australia) and used as received. C_{16}TPB was synthesised following the procedure detailed in ref [19] with 1-bromohexadecane (>97%, Aldrich) and trimethylphosphine solution (1.0 M in toluene, Aldrich) purchased from Sigma-Aldrich (Australia). The surfactant was re-crystalised, with the resulting HNMR spectrum conforming to literature.

8.3   Results and Discussion

The solution being investigated is 4 mmol/kg C_{16}TPB in glycerol with the concentration chosen to be below both the cmc and solubility limit in glycerol. The solvent glycerol was chosen for two reasons. Firstly, glycerol has a low vapour pressure allowing it to form stable films under the vacuum conditions (10^{-5} mbar). Secondly, glycerol has a low self-dissociation constant which is about 4 orders of magnitude lower than that of water.[20] As a consequence the presence of charges resulting from the self-dissociation of the solvent at the surface of the foam film can be neglected. Two different systems were investigated
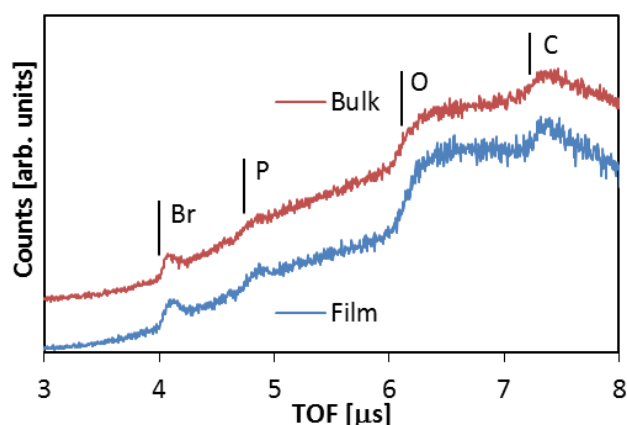

Figure 8-1. NICISS time-of-flight spectrum of the glycerol / C16TPB system from the liquid surface and foam film surface. The vertical lines indicate the onset of the step for the respective element, while the spectra have been vertically offset for clarity.

with this solution: a 'bulk liquid', and a foam film. The bulk liquid surface is generated using the established method of immersing a flat, rotating metal disc into a reservoir containing the solution,[21] with the foam film setup being described in a previous paper.[18] Given the bulk liquid lamella has a thickness of a few tenths of a millimetre, the surface being investigated is that of a typical bulk liquid surface that is not influenced by an opposing surface, which is in contrast to the surface of a foam film.

Figure 8-1 shows the measured NICISS spectra on the time of flight (TOF) scale for both the foam film and bulk liquid surface, where the spectra have been vertically offset for clarity. Apart from a broad background due to recoil hydrogen, the spectra contain four distinct features which are owing to the concentration depth profiles of the indicated elements. The appearance of carbon and oxygen as steps indicates the continuous profile of the solvent, glycerol, while the appearance of bromine and phosphorus (owing only to the surfactant) as peaks indicate that these elements are not detected at bulk concentration levels, but only as an excess in the near surface area. The profiles of each element must be extracted separately to reveal the concentration depth profiles. It must be noted that the profiles extracted in this way are convoluted due to inelastic effects of the back scattering process of He projectiles.[22]

The concentration depth profiles of the cation and the anion as well as the solvent can be determined from the profiles of bromide, phosphorous, and oxygen, respectively. Carbon is a constituent of both the solvent and the surfactant alkyl chain. Given that the oxygen profile is due only to glycerol, while carbon is due to both the surfactant and glycerol, the carbon profile for only the surfactant can be determined by subtracting the oxygen profile form the carbon profile, as shown in Figure 8-2. The carbon owing to the surfactant is named 'alkyl', although some of this carbon signal will also be due to the methyl groups as part of the surfactant headgroup. The shallow onset of the oxygen profile indicates a depletion of glycerol from the surface, which is compensated by the adsorption of surfactant. Similar to the P and Br peaks, the bulk concentration of surfactant is below the detection limits of the experiment, hence only the surface excess of surfactant is detected.
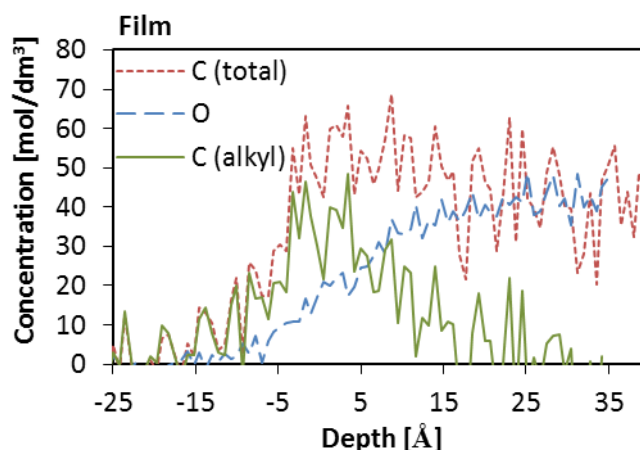
Figure 8-2. Concentration depth profiles of carbon and oxygen from the foam film. Subtracting the profile of oxygen from that of carbon leaves only the carbon due to the surfactant.

Knowing the profiles of the anion, surfactant alkyl chain, and cationic headgroup allows for the determination of the surface structure. Figure 8-3 gives the surface structure for both the bulk liquid surface (left) and foam film (right).

The amount of P and alkyl is equal within experimental uncertainty. However, the amount of bromide determined from the concentration depth profile is 20% lower, i.e. significantly lower than that of phosphorous. The fact that the number of C-alkyl chains is equal to the amount of P proves that there are no carbon-based impurities in the solution. Additionally, NMR of the surfactant is matched with that in the literature indicating a pure sample.[19] In a previous study it was found that a P impurity was present in a P containing surfactant similar to the one investigated here leading to unequal amounts of P and Br at the surface. The P impurity could be detected with NMR. After purification the impurity could not be detected with NMR and the Br and P signal in the NICIS spectra were equal.[23] Thus the unbalance in the P and Br data is attributed to a different effect, namely to the presence of a diffusive Br⁻ layer in the near-surface area. The measured NICIS spectrum shows that there is a diffusive Br⁻ layer. It is very difficult to separate quantitatively the diffusive Br⁻ layer from the recoil hydrogen background due to the low concentration of Br⁻ in the diffusive layer. The fact that there is a smaller amount of Br detected than expected (i.e. 1:1 ratio with P) is thus due to the diffusive layer whose
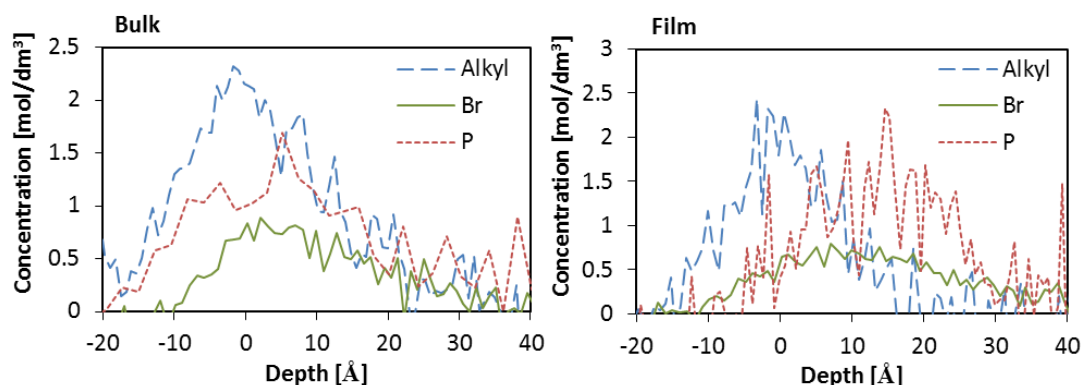
Figure 8-3. Concentration depth profiles of the anion, cation and surfactant alkyl chain of the C16TPB in glycerol for the surface of the bulk solution (left panel) and the foam film (right panel).

concentration decays towards the bulk levels over a range of several nanometres rather than the presence of a P impurity in the solution.

For both the bulk surface and the foam film surface the alkyl chains of the surfactant appear at the outermost layer. However the shift of P away from the surface of the film compared to the bulk as can be seen in Figure 8-3 indicates that the surfactant becomes orientated more parallel to the surface normal upon formation of a film, pushing the phosphonium headgroup further away from the surface. Given that the shift of the anion (Br) profile is much smaller than that of the cation, this indicates that the surface of the foam film becomes more negatively charged than the bulk surface. Figure 8-4 compares the alkyl, phosphorus, and bromine profile for the bulk liquid surface and foam film surface. The phosphorus profiles (middle) further highlights the shift of P away from the surface in the case of the foam film, while only a very slight shift is noticed for Br.

As described above, the measured concentration depth profiles can be described as a convolution of the real concentration depth profile with a function describing a broadening of the measurements due to the inelastic energy loss processes appearing in a NICISS experiment. These processes are the inelastic contributions to the backscattering process as well as the energy loss straggling of the projectiles travelling through the sample.[24] The backscattering energy distribution for each element, and the energy loss straggling of the
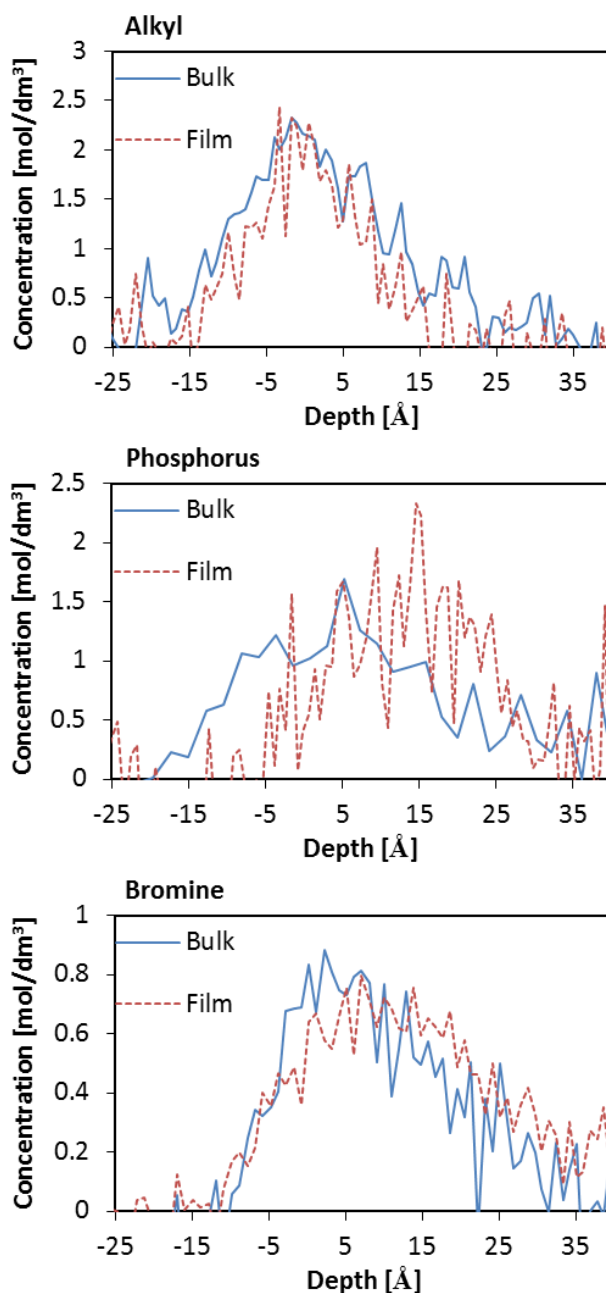
Figure 8-4. Comparing the concentration depth profiles between the 'bulk' and film surface for the surfactant 'alkyl' (top), phosphorus headgroup (middle), and bromide anion (bottom).

projectiles have been determined experimentally which allows for the measured profiles to be deconvoluted.[22] The deconvoluted Br and P profiles are given in Figure 8-5, where the bromine profiles have been adjusted by a factor such that they balance the positive charge from the P. The bromide distribution does not significantly change between the bulk liquid

Figure 8-5. Deconvoluted profiles for P at the bulk liquid and foam film surface (left) and Br at the bulk liquid and foam film surface (right). The Br profiles have been adjusted by a factor such that charge neutrality is observed between the cation and anion.
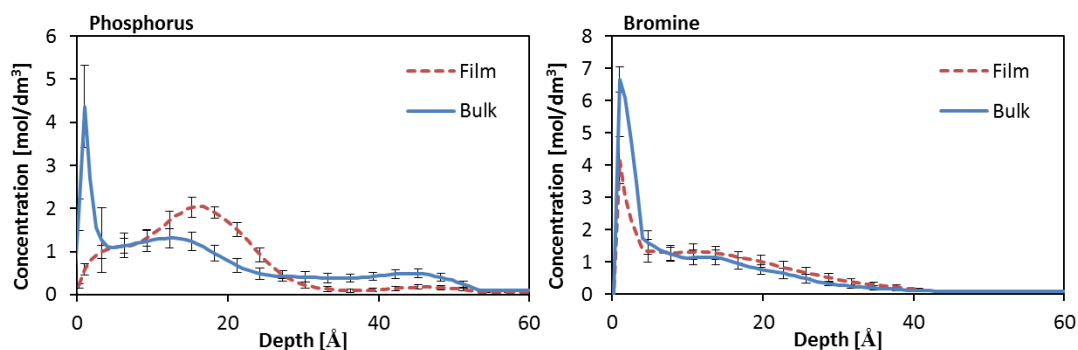
and foam film surface, while the phosphorus distribution is shifted away from the surface by several Å. The fact that P and Br shift independently between the bulk and foam film give good indication that the ionic surfactant is at least partly dissociated in solution, and that charge separation occurs at the foam film surface. This charge separation influences the osmotic pressure due to the overlapping electric double layer and contributes to the disjoining pressure stabilising the foam film.

8.4 Conclusions

Concentration depth profiles of elements in a foam film have been measured, showing the structure of the surfactant, cationic headgroup, and counterion. These measurements are the first directly determining the charge distribution at the surface of a foam film. The surface structure of the foam film is compared to that of the corresponding bulk solution. The data reveals that the cation is pushed away from the surface upon film formation due to surfactant orientation in the foam film while the anion profile is not significantly changed. This causes the surface of the foam film to become more negatively charged compared to the surface of the bulk liquid. Furthermore, the independent shifts of the cation and anion indicate charge separation at the surface of the foam film.

8.5 References

1   Bergeron, V. Forces and structure in thin liquid soap films. *Journal of Physics: Condensed Matter* **11**, R215-R238 (1999).

2   Hunter, R. J. *Foundation of Colloid Science* Vol. 1 (Oxford University Press, 1989).

3   Henry, C. L. & Craig, V. S. J. Ion-Specific Influence of Electrolytes on Bubble Coalescence in Nonaqueous Solvents. *Langmuir* **24**, 7979-7985 (2008).

4   Craig, V. S. J. Bubble coalescence and specific-ion effects. *Current Opinion in Colloid & Interface Science* **9**, 178-184 (2004).

5   Schelero, N. & von Klitzing, R. Correlation between specific ion adsorption at the air/water interface and long-range interactions in colloidal systems. *Soft Matter* **7**, 2936-2942 (2011).

6   Bergeron, V. Forces and structure in thin liquid soap films. *Journal of Physics: Condensed Matter*, R215 (1999).

7   Ninham, B. W. On progress in forces since the DLVO theory. *Advances in Colloid and Interface Science* **83**, 1-17 (1999).

8   Bergeron, V. Disjoining Pressures and Film Stability of Alkyltrimethylammonium Bromide Foam Films. *Langmuir* **13**, 3474-3482 (1997).

9   Andersson, G., Carey, E. & Stubenrauch, C. Disjoining Pressure Study of Formamide Foam Films Stabilized by Surfactants. *Langmuir* **26**, 7752-7760 (2010).

10   Kristen, N. *et al.* No Charge Reversal at Foam Film Surfaces after Addition of Oppositely Charged Polyelectrolytes? *The Journal of Physical Chemistry B* **113**, 7986-7990 (2009).

11   Schelero, N., Hedicke, G., Linse, P. & Klitzing, R. v. Effects of Counterions and Co-ions on Foam Films Stabilized by Anionic Dodecyl Sulfate. *The Journal of Physical Chemistry B* **114**, 15523-15529 (2010).

12   Stubenrauch, C. & Khristov, K. Foams and foam films stabilized by CnTAB: Influence of the chain length and of impurities. *Journal of Colloid and Interface Science* **286**, 710-718 (2005).

13   Todorov, R., Cohen, R. & Exerowa, D. Surface forces in foam films from DPPC and lung surfactant phospholipid fraction. *Colloids and Surfaces A: Physicochemical and Engineering Aspects* **310**, 32-38 (2007).

14   Attard, P. Recent advances in the electric double layer in colloid science. *Current Opinion in Colloid & Interface Science* **6**, 366-371 (2001).

15   Thomas, R. K. *et al.* Critical reflection of neutrons from a soap film. *Journal of Colloid and Interface Science* **97** (1984).

16   Cuvillier, N., Millet, F., Petkova, V., Nedyalkov, M. & Benattar, J.-J. Structure of Freestanding Phospholipidic Bilayer Films. *Langmuir* **16**, 5029-5035 (2000).

17   Bélorgey, O. & Benattar, J. J. Structural properties of soap black films investigated by x-ray reflectivity. *Physical Review Letters* **66**, 313 (1991).

18   Ridings, C. & Andersson, G. Determining concentration depth profiles of thin foam films with neutral impact collision ion scattering spectroscopy. *Review of Scientific Instruments* **81**, 113907-113915 (2010).

19   Pindzola, B. A. & Gin, D. L. Lyotropic Liquid-Crystalline Phase Behavior of Some Alkyltrimethylphosphonium Bromides. *Langmuir* **16**, 6750-6753 (2000).

20   Manfredi, A., Ranucci, E., Suardi, M. & Ferruti, P. Polymerization Kinetics of Poly(amidoamine)s in Different Solvents. *Journal of Bioactive and Compatible Polymers* **22**, 219-231 (2007).

21   Ridings, C., Lockett, V. & Andersson, G. Effect of the aliphatic chain length on electrical double layer formation at the liquid/vacuum interface in the [Cnmim][BF4] ionic liquid series. *Physical Chemistry Chemical Physics* **13**, 17177-17184 (2011).

22   Andersson, G., Morgner, H. & Pohl, H. Energy-loss straggling of helium projectiles at low kinetic energies: Deconvolution of concentration depth profiles of inorganic salt solutes in aqueous solutions. *Physical Review A (Atomic, Molecular, and Optical Physics)* **78**, 032904 (2008).

23   Andersson, G., Krebs, T. & Morgner, H. Activity of surface active substances determined from their surface excess. *Physical Chemistry Chemical Physics* **7**, 136-142 (2005).

24   Andersson, G. & Morgner, H. Impact collision ion scattering spectroscopy (ICISS) and neutral impact collision ion scattering spectroscopy (NICISS) at surfaces of organic liquids. *Surface Science* **405**, 138-151 (1998).

Chapter 9

Effect of sodium halides on the surface structure of foam films stabilized by a non-ionic surfactant

9.1   Introduction

Foam films consist of a liquid core with two opposing surfactant-loaded liquid/gas interfaces. As the liquid drains from the core, the two interfaces begin to approach one another until at some distance – around 100 nm – they begin to interact via overlapping surface forces. Given that these systems have a particularly high surface area to bulk ratio they are thermodynamically unstable, yet are able to exist in a metastable state.[1] This is most commonly described with the concept of the disjoining pressure, which is the sum of the long range repulsive electrostatic forces, Π_{el}, the long range attractive van der Waals forces, Π_{vdW}, and the short range repulsive steric forces, Π_{steric}.[1-3]

$$\Pi = \Pi_{el} + \Pi_{vdW} + \Pi_{steric}$$

Eq. 9-1

The thin film pressure balance (TFPB) is a technique that measures the disjoining pressure of foam films as a function of their thickness. These curves can then be fitted using the concept of the disjoining pressure to gain a quantitative assessment of the contribution of the individual forces towards the total disjoining pressure.[2] The interpretation of these results, however, is somewhat limited by the fact that the individual contributions giving rise to the disjoining pressure are not directly measured, but rather are derived from the data fitting. This is particularly the case for the electrostatic contribution to the disjoining pressure, where the fitting parameter is either the surface charge or the surface potential. Neither of these parameters are determined explicitly with the TFPB, and correlating the effective surface charge in a system to those measured with techniques like charge

titration is not a trivial matter.[4,5] These parameters could be quantified, however, if the concentration depth profiles of the charges were known.

Von Klitzing et al. have shown previously that the TFPB can be used to investigate the effect different anions have on the thickness of foam and wetting films.[6-8] Their results show that specific ion effects play a role in foam film thickness, with NaI films being thicker than the corresponding NaF films at the same salt concentration. The results are explained with the aid of theoretical simulations by Jungwirth and Tobias which show that the larger, more polarisable iodide has a stronger tendency to adsorb to the liquid surface compared to the smaller, less polarisable fluoride.[9,10] Neutral impact collision ion scattering spectroscopy (NICISS) is a low energy ion scattering technique capable of determining the concentration depth profiles of elements at soft matter surfaces. It has previously been established that this technique can be used to investigate foam films using a specialised setup that allows the foam films to be stabilised under vacuum,[11-13] as well as having been used in investigations into the adsorption of ions at liquids surfaces.[14-18] This technique can therefore be used to directly probe the surface structure of foam films, gaining information on the adsorption of the surfactant and the charge distribution at the surface. The aim of this work is to use NICISS to determine the effect of added electrolyte on the surface structure of foam films stabilised by the non-ionic surfactant dodecyldimethyl phosphine oxide (C_{12}DMPO). Varying the anion will allow the investigation as to whether the nature of the ions affects the foam film surface structure. Note that glycerol is used as solvent for NICISS measurements since its low vapour pressure allows forming foam films under vacuum.[12] C_{12}DMPO is used as the surfactant as it is a non-ionic surfactant whose head group, consisting of phosphorus, has a large enough cross-section for NICISS experiments to be detected easily. Additionally, the surfactant has been used extensively in the literature, where it has been shown that it is pH and temperature stable.[19-25] The results will be compared with TFPB measurements on the corresponding aqueous films to gain further insight on the effect of salts on film thicknesses.

9.2 **Experimental**

Glycerol (>99.5%, spectrophotometric grade), NaI (>99.5%, SigmaUltra) and NaCl (>99.5%, SigmaUltra) were purchased from Sigma-Aldrich (Australia). These materials were used as received. C_{12}DMPO was purchased from ABCR Chemicals (Germany) and re-crystallised twice from *n*-hexane prior to usage. The concentration of C_{12}DMPO in glycerol was 2.66 mM which corresponds to 0.5 cmc as determined by surface tension (see Figure 9-1). Solutions were sonicated for approximately 15 minutes at approximately 30 ^{o}C in order to dissolve the surfactant. The surfactant has not been observed to have precipitated out of solution even after several weeks.
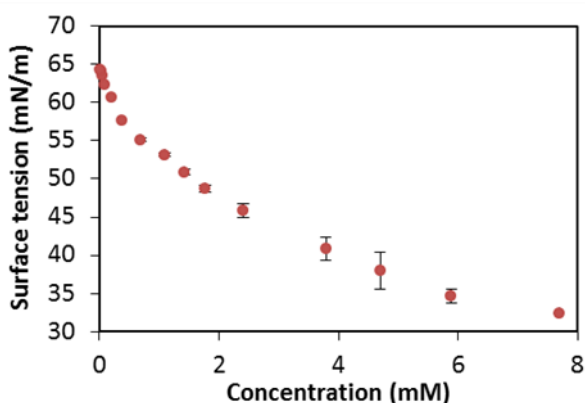
9.2.1 **Surface tension**

Figure 9-1. Surface tension as a function of concentration for the glycerol / C_{12}DMPO system.

The surface tensions were measured as a function of surfactant concentration at room temperature by the Du Noüy ring method using a STA1 tensiometer from Sinterface Technologies. A 100 mL flask of a stock solution at a concentration close to the maximum solubility was prepared. For each measurement 10-20 mL solution for washing the glassware was taken out, and 20 mL solution was used for the measurement. After each measurement the flask was filled up with glycerol .The platinum ring was washed with water and annealed. The diluted solution was then used for the next measurement. The resulting surface tension curve is shown in Figure 9-1.

9.3 Results and Discussion

The formation of the foam film surface and the addition of salts to the solution have various consequences for the structure of the bulk surface and the foam film surface. The results section is structured such that the observations are described in the following order:

- Effect of salt on surfactant adsorption
- Changes of the surface upon foam film formation
- Preferential adsorption of ions at the foam film surface
- Influence of salt on the thickness of foam films

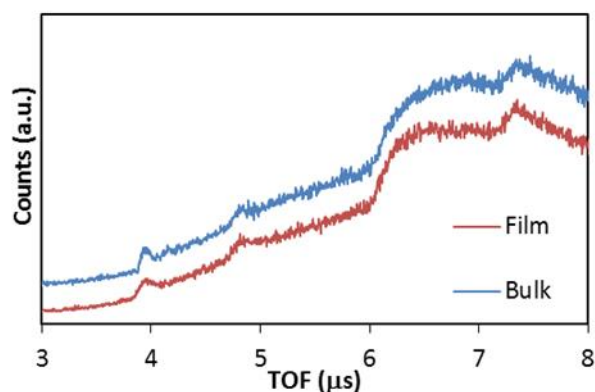### 9.3.1 Effect of salt on surfactant adsorption

Figure 9-2. NICISS spectra of glycerol / C12DMPO / 7.90 mM NaI for both the foam film and bulk liquid surface. Spectra are shown on the time of flight scale, and are vertically offset for clarity. The onsets for the steps of each element are indicated by the dashed lines.

NICISS spectra are measured on the time of flight (TOF) scale. Apart from the broad background due to recoil hydrogen, the spectra consist of features owing to the elements constituting the sample. Figure 9-2 shows the TOF spectra for the glycerol / C_{12}DMPO / 7.90 mM NaI solution for both the bulk liquid and foam film. The vertical lines indicate the onset for each element on the TOF scale, with increasing TOF indicating increased depth into the sample. A peak for P and I⁻ can be seen, while C and O are present as steps.
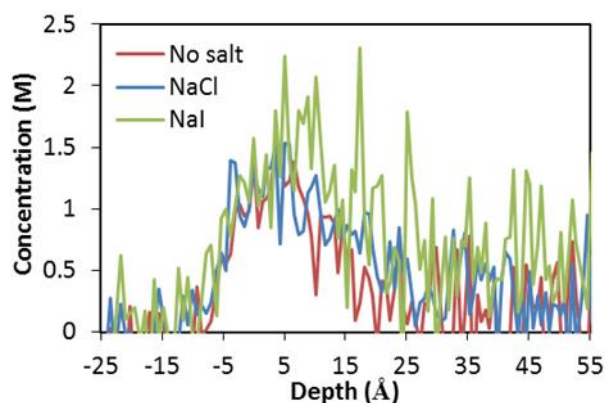
Figure 9-3. Concentration depth profiles of phosphorus at the glycerol / C_{12}DMPO bulk liquid surface with no added salt, added NaCl, and added NaI. Both salt concentrations are 7.90 mM.

The presence of a peak, rather than a step, indicates that P and I^- are detected as a surface excess, with the bulk concentration falling below the detection limits of the experiment.

The individual concentration depth profiles are isolated from the measured spectrum by subtracting the recoil hydrogen background and then converting the time of flight scale to the depth scale for the individual elements. Given that the relationship between energy loss and the depth scale is non-linear, the concentration depth profile for each element must be evaluated individually. Figure 9-3 compares the concentration depth profiles for P at the bulk liquid surface for the glycerol / C_{12}DMPO systems with no salt, added NaCl, and added NaI, with both salt concentrations at 7.90 mM. The P signals for no salt and added NaCl are the same within data scattering, while the P signal for NaI shows a slight increase in surface excess as well as a slight shift away from the surface. Figure 9-2 and Figure 9-3 therefore show that not only is the surfactant needed to encourage the I^- adsorption at the bulk liquid surface, but I^- also increases the amount of surfactant adsorbed at the bulk liquid surface.

Figure 9-4 compares the concentration depth profiles of P in the foam films. The left panel shows that the addition of NaI to the solutions increases the amount of P adsorbed to the film surface, although this amount does not change with increasing amount of salt. The right panel compares the P profiles for the films containing 7.90 mM NaCl and NaI. The

profiles show an increased intensity at 'negative depths' for NaCl, but this is due to Cl⁻ as will be described in the following section. The fact that both profiles are the same for depths ≥ 0 Å shows that P behaves the same regardless of the type of anion. This is in contrast to the bulk surface where only NaI induced an enhanced P adsorption while NaCl had no effect.
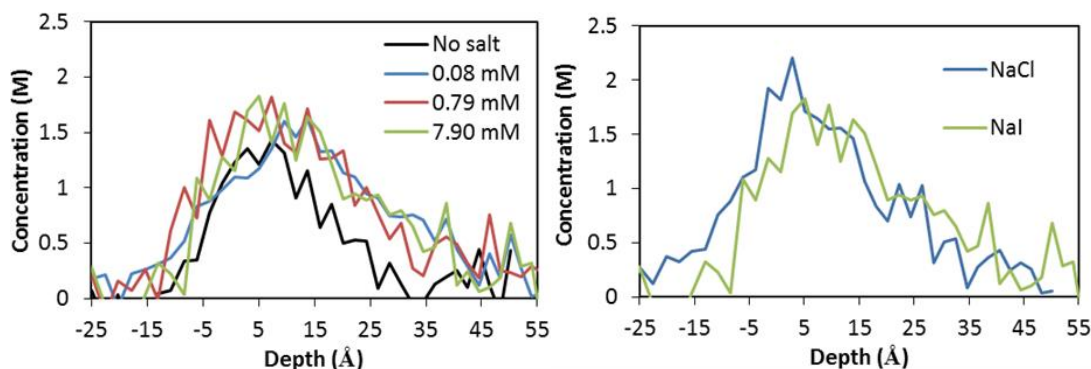

Figure 9-4. Concentration depth profiles of phosphorus as measured. Comparison of the P profiles of glycerol / C_{12}DMPO / NaI films with NaI concentrations as indicated (left), and of glycerol / C_{12}DMPO / 7.90 mM salt films with the salt as indicated (right).

9.3.2 Changes of the surface upon foam film formation

Figure 9-5 shows the carbon profile of the surfactant alkyl chain and the P profile of the surfactant head group for the foam film and the bulk liquid surface of the glycerol / C_{12}DMPO system. The P profile experiences a slight shift away from the surface in the foam film compared to the bulk, which is seen by the separation of the alkyl and P profiles in the left and right panel of Figure 9-5. This indicates that the surfactant changes orientation upon foam film formation, with the head group being pushed away from the surface, compensated by the alkyl chains of the surfactant arranging parallel to the surface normal. This trend of surfactant re-orientation upon film formation has been observed previously in NICISS experiments with the ionic surfactant hexadecyltrimethyl phosphonium bromide.[13]
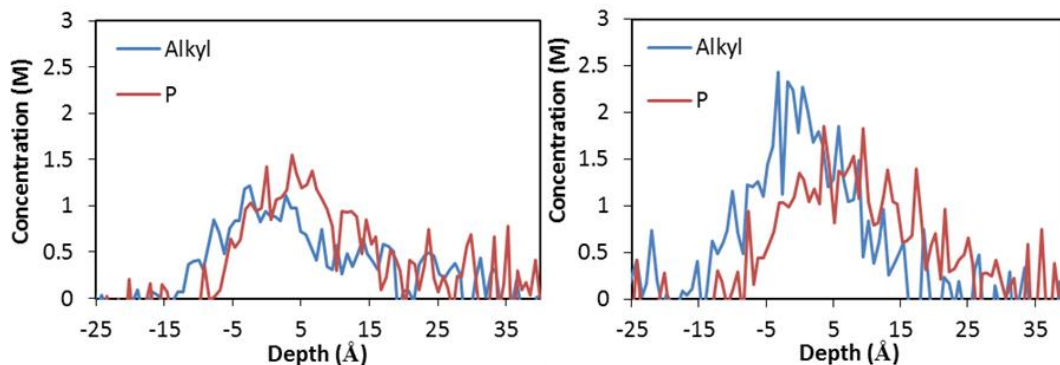
Figure 9-5. Comparison of the alkyl chain profile and P profile at the surface of the bulk liquid (left) and foam film (right) in the glycerol / C_{12}DMPO system. The shift of P away from the surface in the film compared to the bulk indicates a change in orientation of the surfactant in the foam film.

9.3.3   Preferential adsorption of ions at the foam film surface

Figure 9-6 shows the TOF spectra for the bulk liquid surfaces of pure glycerol, glycerol / NaI, and glycerol / C_{12}DMPO / NaI with both NaI concentrations at 7.90 mM. What is of initial interest is that iodide only becomes detected as a surface excess when C_{12}DMPO is present, with no I⁻ signal detected in the glycerol / NaI solution. This indicates that the
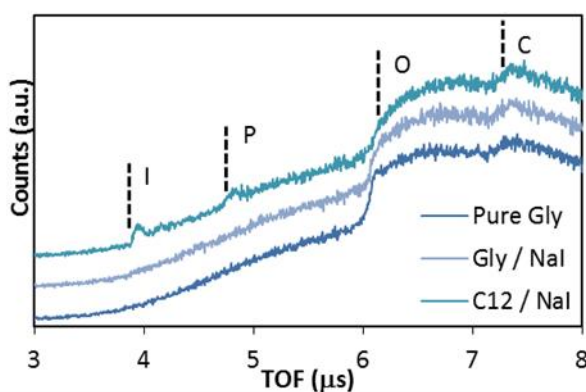

Figure 9-6. NICISS spectra of pure glycerol, glycerol / NaI, and glycerol / C_{12}DMPO / NaI with both NaI concentrations at 7.90 mM. Spectra are shown on the time of flight scale, and are vertically offset for clarity.
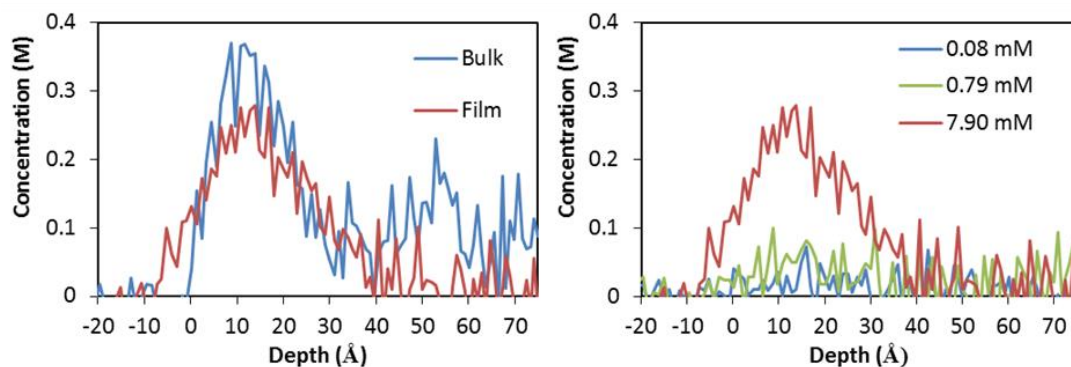
Figure 9-7. Comparison of the concentration depth profiles of iodide for the system glycerol / C$_{12}$DMPO / 7.90 mM NaI at the surface of the bulk liquid and the surface of the foam film (left). Concentration depth profiles of iodide at the foam film surface for three different NaI concentrations (right).

presence of surfactant draws additional iodide to the surface. This effect is not noticed for Cl$^-$, with no Cl$^-$ observed even with the addition of surfactant as will be discussed further below.

Figure 9-7 compares the concentration depth profiles of iodide at the surface of the bulk liquid and at the surface of the foam film for the glycerol / C$_{12}$DMPO / 7.90 mM NaI solution. Figure 9-7 (left) shows that the onset for the I$^-$ profile is shifted closer to the surface in the case of the foam film, compared to the bulk liquid. Additionally, the bulk liquid profile shows some additional structure for I$^-$ at around 55 Å that is not seen in the foam film. This indicates that I$^-$ is shifted closer to the surface in the case of the foam film compared to the bulk liquid surface. Figure 9-7 (right) shows the I$^-$ profiles for the foam films at three different NaI concentrations. While the peak for the 0.79 mM profile lies within the data scattering, the 7.90 mM profile can clearly be seen as a surface excess of I$^-$ which decays to bulk levels beyond 40 Å.

The separation of elements with similar masses becomes complicated in NICISS when the ratio between the mass of the projectile and target atoms becomes smaller. Hence while lighter elements such as C and O can be readily separated, heavier elements such as P and Cl$^-$ become more difficult to separate. This presents an issue with identifying Cl$^-$ when C$_{12}$DMPO is present due to the dominating P signal. As part of the data evaluation, the
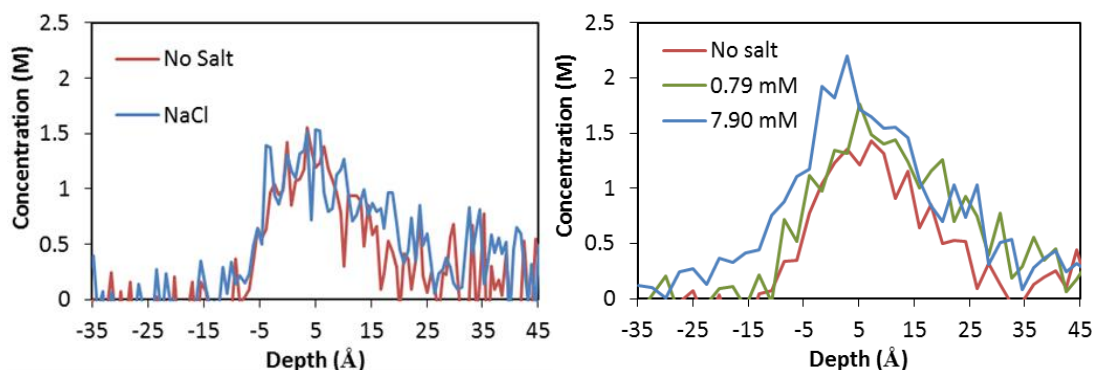
Figure 9-8. Concentration depth profile of P for the glycerol / C_{12}DMPO system at the bulk liquid surface (left) and foam film surface (right). Due to their similar masses, the signals for Cl^- and P are hardly distinguishable (see text for further details). Cl^- should appear at a slight negative depth on the P depth scale, which is seen in the foam film as the increased concentration at negative depths in the 7.90 mM system. This presence of Cl^- is not detected at the bulk liquid surface.

structure owing to each element is removed from the total spectrum, and that TOF range is converted to the depth for that element. Hence when two elements appear close on the TOF scale, they will then also appear on the each other's depth scales. Figure 9-8 shows the concentration depth profiles for P in the glycerol / C_{12}DMPO system. The left panel shows the bulk liquid surface, while the right panel shows the foam film surface. The Cl^- profile has its onset at a small negative depth on the P depth scale, and it can be noticed that an increased signal is seen for the high NaCl concentration in the foam film, but not the bulk liquid surface. This indicates that Cl^- is not adsorbed as a detectable surface excess at the bulk liquid surface, even with the presence of surfactant which is in contrast to iodide which is detected upon the addition of surfactant. However Cl^- can be seen to adsorb at the foam film surface at higher concentrations.

As outlined in the experimental section, the measured concentration depth profiles are a convolution of the actual profiles with factors relating to the ion scattering experiment. While the convoluted profiles still closely represent the actual concentration depth profiles, a deconvolution procedure can be applied to gain a more detailed profile, particularly relating to the profile in the near surface area. This procedure has been performed for the NaCl films in order to reveal further details about any Cl^- adsorption at

the surface. The specifics of this procedure for the given data have been discussed in a previous publication,[11] (Chapter 8 of this thesis) but will be described briefly here. The deconvolution procedure can only be performed on a specific energy scale for each element, so given the overlapping profiles of P and Cl⁻, the procedure needs to be modified to remove the effects of energy loss straggling (a depth dependent function) in the deconvolution. This allows for the profiles to be deconvoluted, however, leads to some uncertainty on the depth scale. Despite this constraint, the deconvolution does reveal that Cl⁻ is indeed present at the surface of the foam films, as shown in Figure 9-9. The lack of Na detected in either the bulk liquid surface or foam film indicates that its concentration is below the detection limits of NICISS. The presence of the counterion in a diffuse layer has been noticed before in investigations of the cationic surfactant hexadecyltrimethyl phosphonium bromide, where the detected Br⁻ surface excess was less than the cation surface excess.[13] The presence of the anion as a surface excess combined with the diffuse cation concentration profile indicates that these films have a negative surface charge.
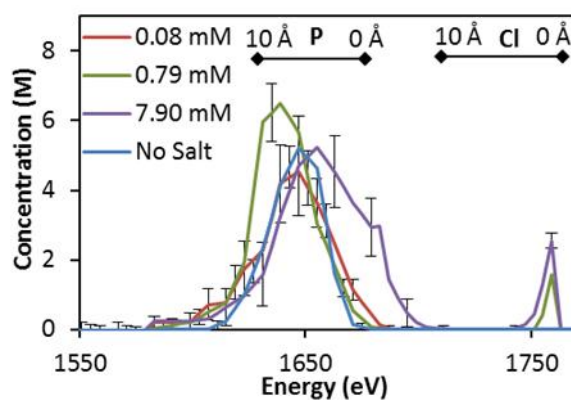
Figure 9-9. Deconvoluting the P/Cl⁻ profiles allows for the separation of the profiles of the two elements. This result shows that Cl⁻ is present as a detectable surface excess in the foam films.

9.3.4 Influence of salt on the thickness of foam films

Disjoining pressure curves have been measured for C_{12}DMPO films with no salt, NaCl, and NaI in water, glycerol, and a 1:1 mass ratio of glycerol and water. However, the high viscosity of glycerol made it difficult to obtain reliable disjoining pressure curves for the

glycerol containing systems. Disjoining pressure curves for water were relatively easy to obtain and were reproducible. For this reason, only the aqueous films will be presented here. It is expected that while the exact film thicknesses will not be the same for aqueous and glycerol films, respectively, the trends for salt effects should be similar given the similar polar nature of both solvents. Figure 9-10 shows the disjoining pressure curves for the water / C_{12}DMPO system without added electrolyte, as well as with 0.1 mM NaI, and 0.1 mM NaF. The DLVO fits to the data are shown as dotted lines, with the resulting surface charges given in the legend. The data shows a slight increase in film thickness for the NaI films compared to the NaF films, which is in agreement with previous results of Hanni-Ciunel et al.[8] The DLVO fitting interprets this as the NaI films having a higher surface charge, which could indicate an increased presence of I^- compared to Cl^- at the surface of the foam films. The charges in the films with no added electrolyte are due to the dissociation of water into H^+/OH^- at a concentration of 10^{-4} mM. This low concentration of charges leads to a weak contribution of the electrostatic force to the disjoining pressure
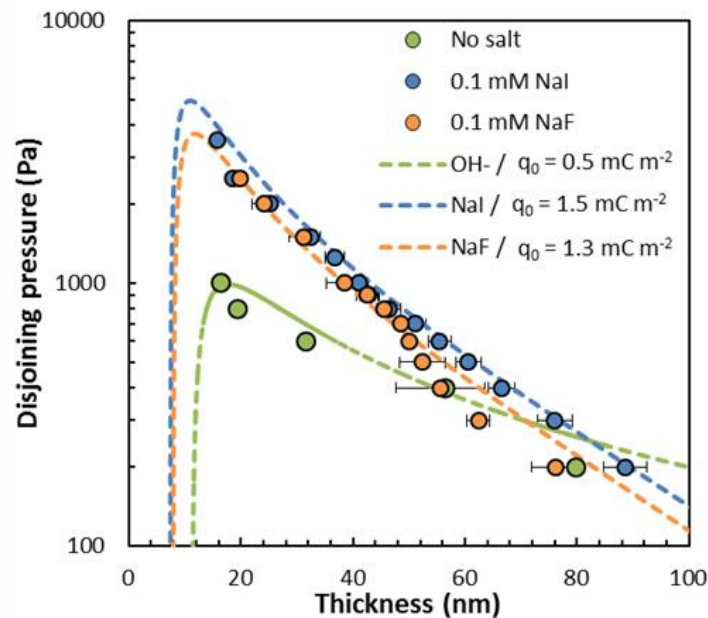

Figure 9-10. Disjoining pressure curves for the water / C_{12}DMPO system with no salt, 0.1 mM NaI, and 0.1 mM NaF. DLVO fits to the data are shown as dotted lines, with the resulting surface charge given in the legend.

and results in films with poorly-defined thicknesses. Carey and Stubenrauch have previously investigated aqueous C_{12}DMPO films, finding that increasing the surfactant concentration past the cmc leads to the formation of Newton black films (NBFs), even in the presence of 0.1 mM NaCl.[20] This result implies that the densely packed surfactant layer leaves no room for ions which would stabilise a common black film (CBF). Hence the disjoining pressure curves measured at $c = 0.5$ cmc (see Figure 9-1) provide evidence for the adsorption of ions at the surface of these films in the case of both NaI and NaF. This is confirmed by the NICISS data as seen in Figure 9-7 and Figure 9-9, which clearly show the presence of the anion as a surface excess in the foam films.

9.4   Conclusions

The surface structure of a glycerol / C_{12}DMPO solution was experimentally determined for both the bulk liquid surface and the foam film surface for two different added salts, NaCl and NaI, as well as for different salt concentrations. Firstly, the effect of salt on the surface structure can be seen by comparing between the bulk liquid and the foam film surfaces. NaI was found to increase the amount of P at the bulk liquid surface, while NaCl had no noticeable effect. However, both NaCl and NaI were found to increase the amount of surfactant adsorption at the surface of the foam film, where even 0.08 mM was enough to induce this effect. The adsorption of ions was compared between the bulk liquid surface and the foam film surface. It was seen that I^- was only present at the glycerol surface upon the addition of the surfactant, while Cl^- was not detected at all, even with added surfactant. However both Cl^- and I^- were seen to adsorb to the foam film surface. This leads to an interesting observation as to the preference of the anions sitting at the surface. Firstly, surfactant significantly increases the adsorption of I^- to the bulk liquid surface. Secondly, the presence of both Cl^- and I^- is enhanced in the foam film compared to the bulk liquid. Given that the adsorption of surfactant is increased in the foam film, along with the change in orientation of the surfactant, these results could indicate that the anions have a preference to sit among the alkyl chains of the surfactant, a result which has been seen previously.[11,17]

Additionally, comparing the I^- profiles between the bulk liquid and foam film surfaces, it could be seen that I^- is shifted closer to the outermost layer in the case of the foam film

compared to the bulk liquid. This results in an increasing negative surface charge for the foam film compared to the bulk liquid surface. The cation was not detected in the experiments, which indicates that it must be present as a diffuse layer below the surface with peak concentration laying beneath the detection limit of the experiment. This gives further evidence to the negative surface charge of the foam films. The TFPB was used to determine the thickness of the studied foam films and it was found that increasing the amount of salt lead to thicker films, with films containing NaI being thicker than films containing NaCl. While the adsorption of I^- and Cl^- could not be compared quantitatively at the foam film surface, the increased propensity for I^- to adsorb at the bulk liquid surface is expected to correlate to the behaviour in the foam film. This increased ion adsorption would lead to an increased surface charge and thus an increased repulsion between the surfaces of the film, resulting in thicker films.

9.5   References

1   Bergeron, V. Forces and structure in thin liquid soap films. *Journal of Physics: Condensed Matter*, R215 (1999).

2   Stubenrauch, C. & Klitzing, R. v. Disjoining pressure in thin liquid foam and emulsion films - new concepts and perspectives. *Journal of Physics: Condensed Matter*, R1197 (2003).

3   Israelachvili, J. N. *Intermolecular and Surface Forces*. Second edn, (Academic Press, 2000).

4   Attard, P. Recent advances in the electric double layer in colloid science. *Current Opinion in Colloid & Interface Science* **6**, 366-371 (2001).

5   Attard, P. Ion condensation in the electric double layer and the corresponding Poisson-Boltzmann effective surface charge. *The Journal of Physical Chemistry* **99**, 14174-14181 (1995).

6   Schelero, N., Hedicke, G., Linse, P. & Klitzing, R. v. Effects of Counterions and Co-ions on Foam Films Stabilized by Anionic Dodecyl Sulfate. *The Journal of Physical Chemistry B* **114**, 15523-15529 (2010).

7   Schelero, N. & von Klitzing, R. Correlation between specific ion adsorption at the air/water interface and long-range interactions in colloidal systems. *Soft Matter* **7**, 2936-2942 (2011).

8   Hanni-Ciunel, K., Schelero, N. & von Klitzling, R. Negative charges at the air/water interface and their consequences for aqueous wetting films containing surfactans. *Faraday Discuss.* **141**, 41-53 (2009).

9   Jungwirth, P. & Tobias, D. J. Molecular Structure of Salt Solutions: A New View of the Interface with Implications for Heterogeneous Atmospheric Chemistry. *The Journal of Physical Chemistry B* **105**, 10468-10472 (2001).

10   Jungwirth, P. & Tobias, D. J. Ions at the Air/Water Interface. *J. Phys. Chem. B* **106**, 6361-6373 (2002).

11   Ridings, C. & Andersson, G. G. Deconvolution of NICISS profiles involving elements of similar masses. *Nuclear Instruments and Methods in Physics Research Section B: Beam Interactions with Materials and Atoms*.

12   Ridings, C. & Andersson, G. Determining concentration depth profiles of thin foam films with neutral impact collision ion scattering spectroscopy. *Review of Scientific Instruments* **81**, 113907-113915 (2010).

13   Ridings, C. & Andersson, G. Change of Surface Structure upon Foam Film Formation. *Angewandte Chemie International Edition* **Under review** (2014).

14   Andersson, G. & Morgner, H. Investigations on solutions of tetrabutylonium salts in formamide with NICISS and ICISS: concentration depth profiles and composition of the outermost layer. *Surface Science* **445**, 89-99 (2000).

15   Andersson, G., Krebs, T. & Morgner, H. Activity of surface active substances determined from their surface excess. *Physical Chemistry Chemical Physics* **7**, 136-142 (2005).

16   Andersson, G., Morgner, H., Cwiklik, L. & Jungwirth, P. Anions of Alkali Halide Salts at Surfaces of Formamide Solutions: Concentration Depth Profiles and Surface Topography. *The Journal of Physical Chemistry C* **111**, 4379-4387 (2007).

17   Ridings, C., Lockett, V. & Andersson, G. Effect of the aliphatic chain length on electrical double layer formation at the liquid/vacuum interface in the [Cnmim][BF4] ionic liquid series. *Physical Chemistry Chemical Physics* **13**, 17177-17184 (2011).

18   Ridings, C., Lockett, V. & Andersson, G. Significant changes of the charge distribution at the surface of an ionic liquid due to the presence of small amounts of water. *Physical Chemistry Chemical Physics* **13**, 21301-21307 (2011).

19   Blunk, D., Tessendorf, R., Buchavzov, N., Strey, R. & Stubenrauch, C. Purification, Surface Tensions, and Miscibility Gaps of Alkyldimethyl and Alkyldiethylphosphine Oxides. *Journal of Surfactants and Detergents* **10**, 155-165 (2007).

20   Carey, E. & Stubenrauch, C. A disjoining pressure study of foam films stabilized by mixtures of a nonionic (C12DMPO) and an ionic surfactant (C12TAB). *Journal of Colloid and Interface Science* **343**, 314-323 (2010).

21   Claesson, P. M. *et al.* Forces between non-ionic surfactant layers. *Faraday Discussions of the Chemical Society* **90**, 129-142 (1990).

22   Lunkenheimer, K., Haage, K. & Miller, R. On the adsorption properties of surface-chemically pure aqueous solutions of n-alkyl-dimethyl and n-alkyl-diethyl phosphine oxides. *Colloids and Surfaces* **22**, 207-214 (1987).

23   Herder, C. E. Interaction between phosphine oxide surfactant layers adsorbed on hydrophobed mica. *Journal of Colloid and Interface Science* **143**, 1-8 (1991).

24   Herder, C. E. Adsorption of dimethyldodecylphosphine oxide on mica and the interaction between the adsorbed layers. *Journal of Colloid and Interface Science* **143**, 573-580 (1991).

25   Lunkenheimer, K., Haage, K. & Hirte, R. Novel Results on the Adsorption Properties of n-Alkyldimethylphosphine Oxides at the Air/Water Interface. *Langmuir* **15**, 1052-1058 (1999).

Chapter 10

Conclusions

This thesis presents the results of investigations into the surface structure of liquids containing ionic species. Liquid surfaces were investigated by two main techniques: NICISS and MIES, while the types of liquids investigated were surfactant solutions and ionic liquids.

While the investigation of volatile liquids such as water using vacuum based techniques is problematic, liquids with relatively low vapour pressures allow these investigations to be carried out. Ionic liquids are one such example, given their ionic nature lead to negligible vapour pressures. Given the often complex molecular nature of these ions, the effect of changing the molecular structure of these ions on their resulting behaviour at the surface becomes of interest. The effect of increasing the cation aliphatic chain length was investigated in the $[C_nmim][BF_4]$ IL series (n = 6, 8, 10) using NICISS, while the effect of modifying the cation chain in the R-ammonium nitrate series (R = ethyl, propyl, ethanol) was investigated using a combination of NICISS and MIES. In both cases it was seen that increasing the cation aliphatic chain length resulted in an increased adsorption of the cation to the surface, with subsequent re-alignment to be more parallel to the surface normal in the case of the $[C_nmim][BF_4]$ series. This cation surface behaviour did not necessarily lead to an increased positive surface charge. In the case of the $[C_nmim][BF_4]$ series, the change in cation change orientation with increasing chain length resulted in the centre of charge for the cation being pushed further away from the surface than the anion, thus resulting in a decreasing positive surface charge with increasing chain length. The advantage of MIES to be sensitive to solely the outermost layer of the target was used to confirm that neither the cation nor anion in the R-ammonium nitrate IL series was exclusively adsorbed at the surface.

Given the highly hygroscopic nature of many ILs, the effect of water a surface impurity was investigated for $[C_6mim][Cl]$. A known quantity of water was added to the IL, which was subsequently exposed to vacuum for a period of time after which a NICIS spectrum was taken. After recording of the NICIS spectrum, the final water content in the IL sample

was determined via Karl Fisher titration. The surface structure of the IL-water mixture was determined at water contents of 0.25%, 0.60%, and 1.00%. It was found that increasing the water content lead to an increased surface excess of the anion, with the anion only present as a shallow surface excess in the case of the lowest water content. This result was described in terms of the chloride anion forming clusters with the water molecules which drew the anion to the surface, which demonstrates how the surface structure of these ILs is determined by many other factors apart from the Coulombic interaction of ions.

The surface structure of surfactant solutions was investigated using both ionic and non-ionic surfactants with glycerol as the solvent. Glycerol is a polar solvent, with a suitably low vapour pressure which allows it to be handled under vacuum conditions. A unique setup was developed that allowed for a thin foam film to be investigated using a vacuum based technique for the first time. This setup involved placing a specially designed film holder inside an enclosed cell, where the only opening was an aperture positioned in front of where the film is held. The small size of this aperture reduces the loss of solvent vapour, thus maintaining the inside of the cell at the vapour pressure of the solvent, reducing further evaporation from the film. Concentration depth profiles were obtained from a system of glycerol / hexadecyltrimethylphosphonium bromide, below the cmc. The surface of the bulk liquid for this solution was compared to the surface of the corresponding foam film. This study was the first time the charge distribution had been experimentally observed for a foam film. It was seen that the phosphorus was pushed further away from the surface in the foam film compared to the corresponding bulk liquid surface, with little change seen in the position of the anion. This was interpreted as being due to the surfactant orienting to lie more parallel to the surface normal in the case of the foam film which pushes the cation headgroup further from the surface. This leads to a decreasing positive surface charge upon formation of the foam film. Additionally, it was concluded that while a surface excess of the anion was detected, the low concentrations observed must indicate that the anion is present as a diffuse layer whose concentration falls below the detection limits of the experiment.

The effect of added electrolyte on foam film thickness and surface structure was investigated using the non-ionic surfactant, dodecyldimethylphophine oxide. Additionally, the influence of specific ion effects was investigated by comparing sodium chloride and sodium iodide as the salt. It was seen that the anion was not detected at the bulk liquid

surface until surfactant was added, upon which iodide is adsorbed as a significant surface excess. Chloride was not seen to adsorb to the bulk liquid surface even with surfactant. For the foam films, it was seen that the addition of salt increased the amount of phosphorus at the surface, where phosphorus is due only to the headgroup of the surfactant. Additionally, it could be seen that both chloride and iodide were adsorbed to the foam film surface. Due to the data evaluation procedure required for the sodium chloride films, it was not possible to quantitatively compare the iodide and chloride distribution at the foam film surface. It was also seen that the cation, sodium, was not detected which indicates that in this case the cation must be present as a diffuse layer below the detection limits of the experiment.

The outcomes for the investigations into foam films highlight the importance of understanding the surface structure of the foam films in order to understand their stability. The change of surface structure upon foam film formation, in particular the reorientation of the surfactant molecules and change in surface charge may not be fully accommodated for in models which correlate the surface structure of foam films to the surface structure of their respective bulk liquids. Additionally, understanding the surface structure of the foam films could help to explain foam film stability in terms of the entropy change due to the surfactant orientation, as well as the osmotic pressure due to the surface excess of ions.

These studies highlight in particular the influence of the non-polar alkyl chains that may form part of an ion. The study of the $[C_n mim][BF_4]$ series directly showed that increasing the cation aliphatic chain length led to a significant decrease in the surface charge, due to the orientation of the cation. Similar effects are seen in the study of $C_{16}TPB$ foam films, where the change in orientation of the surfactant (cation) upon foam film formation leads to a decrease in the positive surface charge. While the counterions (anions) in these cases remained in close proximity to the cations, they were not shifted to the same extent, preferring to sit above the cation centre of charge, amongst the alkyl chains. The alkyl chains prefer to orient parallel to the surface normal in order to optimise the surface energy, and this is seen to have a direct impact on anion adsorption in the study of $[C_6 mim][X]$, $X = BF_4^-$ and Cl^-. The BF_4^- anion is observed to adsorb at the surface in a significantly higher amount than Cl^-, where in the latter case the depletion of anions from the surface is compensated by the increased presence of alkyl chains of the cations.

This thesis has demonstrated the ability of vacuum based surface analytical techniques, in particular NICISS, to be a powerful tool in the investigation of liquid surface structure. The effect of molecular structure on surface structure of ionic liquids was investigated by systematic investigations, while specialised equipment was developed for the first investigations of foam films under vacuum. There is still plenty of scope for further research, particularly in the area of foam films where the NICISS setup provides a particularly powerful technique which can reveal the strengths and weaknesses of the assumptions used in the existing models for surface forces.